1 Gene age predicts the transcriptional landscape of sexual morphogenesis in
2 multicellular fungi

3 Zsolt Merényi[1], Máté Virágh[1], Emile Gluck-Thaler[2], Jason C. Slot[3], Brigitta Kiss[1], Torda Varga[1], András Geösel[4], Botond
4 Hegedüs[1], Balázs Bálint[1], László G. Nagy[1,5,*]

5 *[1] Synthetic and Systems Biology Unit, Biological Research Center, Szeged, 6726, Hungary*
6 *[2] Department of Biological Sciences, University of Pittsburgh, 4249 Fifth Avenue, Pittsburgh, PA 15260, USA*
7 *[3] College of Food, Agricultural, and Environmental Sciences, Department of Plant Pathology, The Ohio State University,*
8 *Columbus, USA*
9 *[4] Institute of Horticultural Science, Department of Vegetable and Mushroom Growing, Hungarian University of Agriculture*
10 *and Life Sciences, Budapest, 1118, Hungary*
11 *[5] Department of Plant Anatomy, Institute of Biology, Eötvös Loránd University, Budapest, 1117, Hungary*

12 *Author for correspondence: lnagy@fungenomelab.com

13 Key words: developmental hourglass, oyster mushroom, allelic imbalance, mushroom development, Agaricomycetes,
14 *Cryptococcus neoformans*

15 Abstract

16 Multicellularity has been one of the most important innovations in the history of life. The role of regulatory evolution in
17 driving transitions to multicellularity is being increasingly recognized; however, patterns and drivers of transcriptome
18 evolution are poorly known in many clades. We here reveal that allele-specific expression, natural antisense transcripts
19 and developmental gene expression, but not RNA editing or a developmental hourglass act in concert to shape the
20 transcriptome of complex multicellular fruiting bodies of fungi. We find that transcriptional patterns of genes are strongly
21 predicted by their evolutionary age. Young genes showed more expression variation both in time and space, possibly
22 because of weaker evolutionary constraint, calling for partially non-adaptive interpretations of evolutionary changes in
23 the transcriptome of multicellular fungi. Gene age also correlated with function, allowing us to separate fruiting body
24 gene expression related to simple sexual development from that potentially underlying complex morphogenesis. Our
25 study highlighted a transcriptional complexity that provides multiple speeds for transcriptome evolution, but also that
26 constraints associated with gene age shape transcriptomic patterns during transitions to complex multicellularity in fungi.

Introduction

The emergence of multicellularity has been one of the most influential transitions in evolution (Knoll, 2011; Smith and Szathmary, 1995). However, while simple multicellular aggregations evolved several times and evidence is accumulating that these transitions may not have had as many genetic obstacles as originally thought (Abedin and King, 2008; Kiss et al., 2019; Nagy et al., 2018; Sebé-Pedrós et al., 2017), origins of complex multicellularity (CM) seem to be rare evolutionary events. Simple multicellularity refers to cell aggregations, colonies or filaments, whereas CM comprise 3-dimensional organisms in which not all cells are in direct contact with the environment and necessitated the evolution of mechanisms for transport, cell adhesion and complex developmental programs (Knoll, 2011). Recent research suggests that besides changes in gene content or protein sequence, the evolution of gene expression and genome regulation are also important in the transition to CM (King et al., 2003; Merényi et al., 2020; Sebé-Pedrós et al., 2018). However, much of the changes underlying to origins of CM remain unknown.

Uniquely across life on Earth, fungi show evidence for multiple evolutionary origins of CM (Nagy, 2018; Nguyen et al., 2017) as well as for transitions between simple hyphae and 3-dimensional organization during the development of sexual fruiting bodies. The latter allows real-time transcriptomic readout of changes in complexity level, which make fungi an ideal model system to investigate CM. Fungi reached highest multicellular complexity in fruiting bodies of mushroom-forming fungi (Agaricomycetes, Kües & Navarro-González, 2015; Nagy, 2018) which includes most industrially cultivated edible and medicinal mushrooms. CM fruiting bodies in the Agaricomycetes have been widely studied by transcriptomic approaches, however, the interpretation of transcriptomes has been complicated by the lack of an understanding of the general principles of transcriptome evolution. This has impeded a general synthesis on the genetics of CM in fungi. Recent studies of fruiting body development reported species-specific and conserved genes (Krizsán et al., 2019; Nguyen et al., 2017), long non-coding RNA (Kim et al., 2018a), natural antisense transcripts (Muraguchi et al., 2015; Ohm et al., 2010; Shao et al., 2017), allele specific expression (Gehrmann et al., 2018), RNA-editing (Wu et al., 2019, 2018), small RNA (Lau et al., 2018), alternative splicing (Krizsán et al., 2019), chromatin remodelling (Vonk and Ohm, 2021) as well as transcriptome conservation patterns predicted by the developmental hourglass hypothesis (Cheng et al., 2015) however, how these contribute to CM is not known.

Similarly, several genes and cellular processes have been identified in fruiting bodies. Fruiting bodies are composite structures in which structural cell types enclose reproductive ones (basidia, meiospores) into a protective environment. Basidium and spore development are evolutionarily significantly older than CM fruiting bodies. The underlying genes show up in developmental transcriptomes, which, if not properly accounted for, can blur signals for real CM-related genes. Accordingly, while some hitherto identified genes can be linked to CM functions (e.g. defense of fruiting bodies Künzler, 2018), most fruiting body-expressed genes, including those related to cell wall remodeling (Liu et al., 2021), transcriptional regulation, selective protein degradation (Krizsán et al., 2019), complex secretomes (Almási et al., 2019) may relate either to CM or more general functions.

The goal of this study was to systematically tease apart the components and driving forces of transcriptome evolution in CM fungi. To this end, we compared the transcriptomes of eight CM fungi and that of a simple yeast-like species (*Cryptococcus neoformans*). We examined natural antisense transcripts, allele-specific expression and RNA-editing and found that evolutionary age predicts, to a large extent, the behaviour of a gene in the CM transcriptome. Because the simple vegetative (hyphal) and complex reproductive (fruiting body) stages are distinct, we expect morphogenetic genes specifically expressed in the complex multicellular stage to exist (Krizsán et al., 2019), in contrast to animals and plants, where such sharp separation cannot be expected. Fruiting body transcriptomes showed a clear gene-age related stratification, allowing the separation of genes related to general sexual processes from those likely linked to sculpting CM fruiting bodies. These data will help understanding both complex multicellular and simple, sexual morphogenesis in fungi.

Results and Discussion

Overview of new RNA-Seq data

We present the first highly resolved developmental transcriptome data for *Pleurotus ostreatus* (oyster mushroom), one of the three most widely cultured species worldwide (Zhu et al., 2019), as well as for *Pterula gracilis*, a closely related species with a simple fruiting body morphology (Fig. 1/a). In *P. ostreatus* we sampled six developmental stages and up to four tissue types within a stage, whereas in *Pt. gracilis*, tissues could not be separated, therefore we sampled four developmental stages (Fig. S1-2). Strand-specific RNA-Seq yielded 15.9-34.0 million reads per sample (Table S1). Multidimensional scaling of the normalized transcriptome data accurately identified sample groups with biological replicates being tightly positioned together (Fig. S3). For uniformity in downstream analyses, we reanalysed data from former studies (Almási et al., 2019; Gehrmann et al., 2018; Ke et al., 2020; Krizsán et al., 2019; Liu et al., 2018; Sipos et al., 2017), yielding data for eight species in the order Agaricales, which comprises a single origin of complex fruiting body morphologies (Marisol et al., 2020; Varga et al., 2019). *P. ostreatus* and *Pt. gracilis* had 4,294 and 474 developmentally expressed genes (≥4FC), respectively, within the range reported earlier (Almási et al., 2019; Krizsán et al., 2019; Sipos et al., 2017) (Fig. S4).

Developmental hourglass

Previously, an hourglass concept has been proposed to explain the incorporation of genetic novelty into the developmental programs of CM eukaryotes (Domazet-Lošo and Tautz, 2010; Drost et al., 2017), including fungi (Cheng et al., 2015). This concept posits that evolutionarily older genes are expressed at mid-development, while younger genes are expressed at early and late stages (Domazet-Lošo and Tautz, 2010). To test this hypothesis, we analyzed the transcriptomes of the nine species based on transcriptome age indexes, which measure transcriptome conservation. We obtained hourglass-like patterns only in *P. ostreatus, M. kentingensis* and *A. bisporus*, whereas in other species no clear-cut signal for a developmental hourglass was found (Fig. 1/b, Fig. S5). We observed that, in each species, the highest level of transcriptome conservation coincided with mitotic/meiotic gene upregulation (Fig. 1/d), a well-known signal for cell proliferation and sporulation-related meiosis. This suggests that in fungi, transcriptome conservation patterns are merely driven by expression peaks of ultra-conserved genes related to the cell cycle, and may not reflect mechanisms for incorporating genetic novelty, as hypothesised for metazoans (Domazet-Lošo and Tautz, 2010).

Developmental gene clusters

We found evidence for the grouping of developmentally expressed genes into hotspots in the genomes (see Methods) (Table S2, Fig. S6). Altogether 153 hotspots were detected in eight genomes; however, most of these were species-specific and not conserved across species (e.g. the luciferase cluster in the bioluminescent *A. ostoyae,* Ke et al., 2020b).

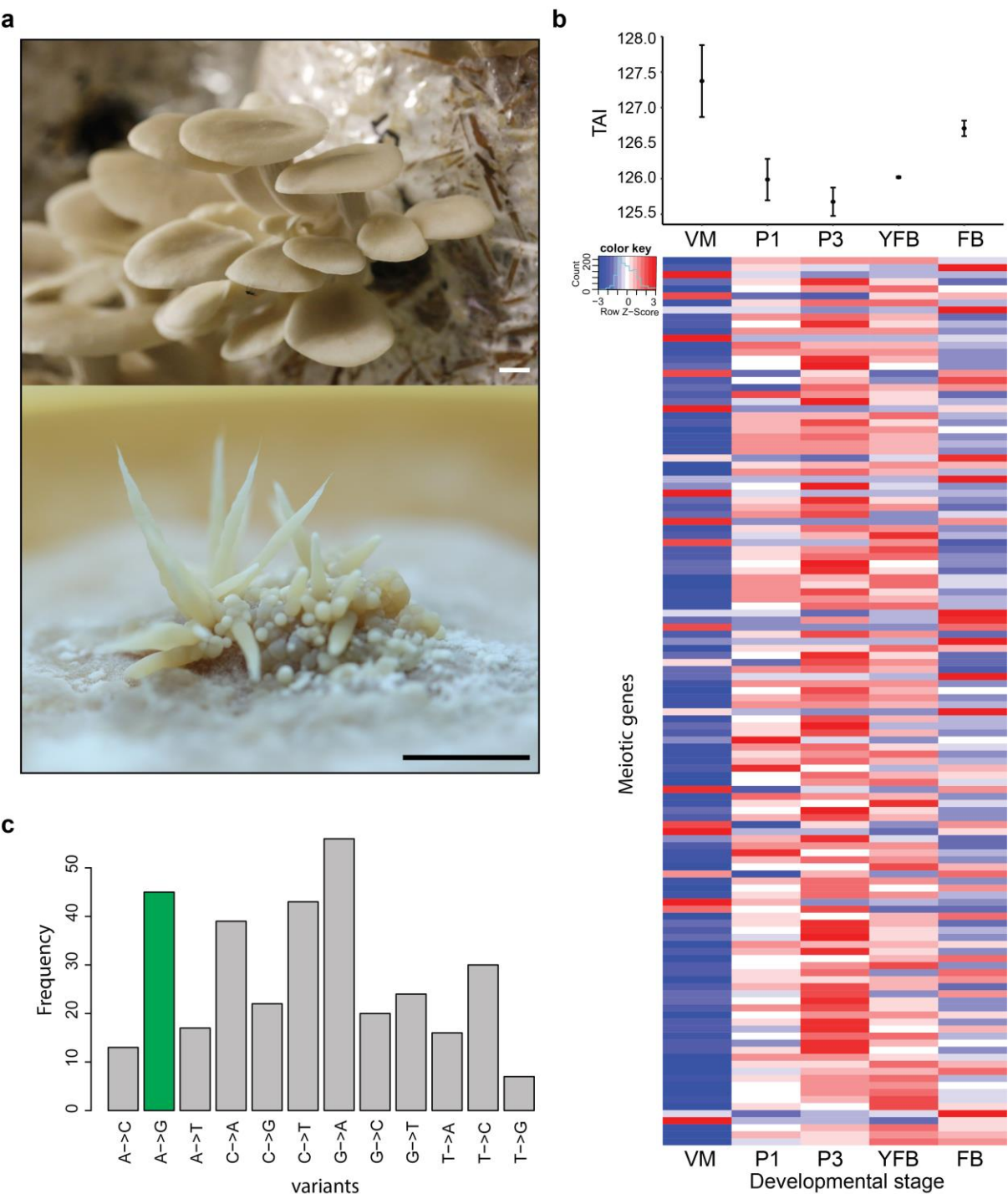**Figure 1 Overview of developmental transcriptomes. a)** Fruiting bodies of *Pleurotus ostreatus* (upper) and *Pterula gracilis* (lower). **b)** Transcriptome conservation in *P. ostreatus* based on transcriptome age index (TAI) and its correlation with meiotic gene expression **c)** distribution of variant types retained in the RNA editing specific pipeline with A-to-I variants being marked with green. Abbreviations as follows: 'VM' vegetative mycelium; 'P1' stage 1 primordium; 'P3' stage3 primordium; 'YFB' young fruiting body, 'FB' fruiting body; 'H' cap (entire); 'C' cap trama (only the inner part, without Lamellae, or skin); 'L' lamellae; 'S' stipe; 'V' cuticle; 'D' dedifferentiated tissue of cap.

Allele-specific expression but not RNA editing is abundant in fruiting body transcriptomes

P. ostreatus is a good model to distinguish the contributions of RNA editing and Allele-Specific Expression (ASE) because both parental genomes are sequenced, and sufficiently differ from each other to classify variants either as ASE (variants differing from one parental genome) or RNA editing (variants differing from both parental genomes).

4

112   Overall, 2,244,348 variants were input to the ASE analysis and were used to decide which haploid nucleus the
113   reads originated from (Table S3). We inferred that 31.2% and 32.2% of the reads derive from PC15 and PC9 nuclei,
114   respectively, while 36.5% of reads were not able to be assigned to either parental genomes (Table S3). This allowed us to
115   characterize 9,948 PC15 genes (80.7% of all genes and 95.1% of expressed genes) for ASE. Similar to gene expression,
116   allele specific expression levels showed clear stage- and tissue-specific patterns (Fig. S7-8).
117   At the scale of the entire genome or scaffolds, the two parental genomes expressed almost equally (Fig. S9-10),
118   whereas at the gene level 7,793 (74,8%) of the 10,419 expressed genes were assigned as Equally Expressed genes (EE
119   genes, hereafter) in all stages and tissue types and 2,626 genes (25.2%) was biased towards the same nucleus in all
120   biological replicates of at least one stage or tissue (referred to as ASE genes, Fig. 2/c). Of these, 1,560 genes showed 2 <
121   FC < 4-fold expression imbalance (hereafter referred to as S2 genes; 15%) and 1,066 (S4 genes; 10.2%) showed over
122   four-fold difference between the two nuclei in at least one stage (averaged across replicates, Table S4). In comparison, in
123   *A. bisporus* ASE was reported for 411 genes (~4% of the genome), perhaps due to fewer SNPs between and, accordingly,
124   lower power in assigning reads, to parents (Gehrmann et al., 2018).
125   Enrichment analysis based on InterPro domains and GO terms of ASE genes highlighted a significant
126   overrepresentation of some well-known fruiting-related gene families (Krizsán et al., 2019), such as hydrophobins,
127   glycoside hydrolase families, aquaporins and fungal type protein kinases (Table S5-6, Fig. S11). Notably, all of these
128   families are volatile, characterized by frequent duplications.
129   In the RNA-editing pipeline (Fig. S12), 627,093 of the 1,999,221 input variants remained after filtering for
130   extreme low frequency (< 0.1%). We chose this permissive threshold (as opposed to 1/3/10% in other protocols (Liu et
131   al., 2017; Wu et al., 2018), to avoid discarding any signal in the early steps. As many as 546,790 sites were located in
132   gene regions, of which 346,105 possibly corresponded to erroneous mapping around splice sites (Fig. S13), while
133   218,685 were retained for further analysis. Surprisingly, only 1.2% of these (2,701 sites) were consistent between at least
134   two of the three biological replicates. After eliminating potential sequencing errors (Wilcoxon signed-rank test, p-
135   value<0.01), we obtained 1,179 variants. Requiring at least 1% mean variant frequency in at least 1 stage left 332
136   potential RNA editing sites, with 6 to 62 in each variant type. (Table S7). Among these A-to-I and C-to-U transitions
137   were not enriched (Fig. 1/c), consistent with previous Basidiomycota studies (Bian et al., 2019; Teichert, 2020). Wu et al.
138   (2018) hypothesized that the lack of A-to-I enrichment indicates a greater diversity of editing sites and novel mechanisms
139   of RNA editing in Basidiomycetes. To explore other explanations, we examined what, other than RNA-editing, our
140   remaining variants could potentially correspond to. By examining motifs around the 332 sites, we detected solely an
141   enrichment of adenines 1-2 nucleotides downstream of C-to-A sites (Fig. S14/b). However, because 69% (20 of 29) of
142   these were within +/-20nt from the 3' end of the last exon of genes, we think that adenine enrichment corresponds to the
143   polyadenylation sequence. Together, we interpret these results as limited or no evidence for RNA editing, but abundant
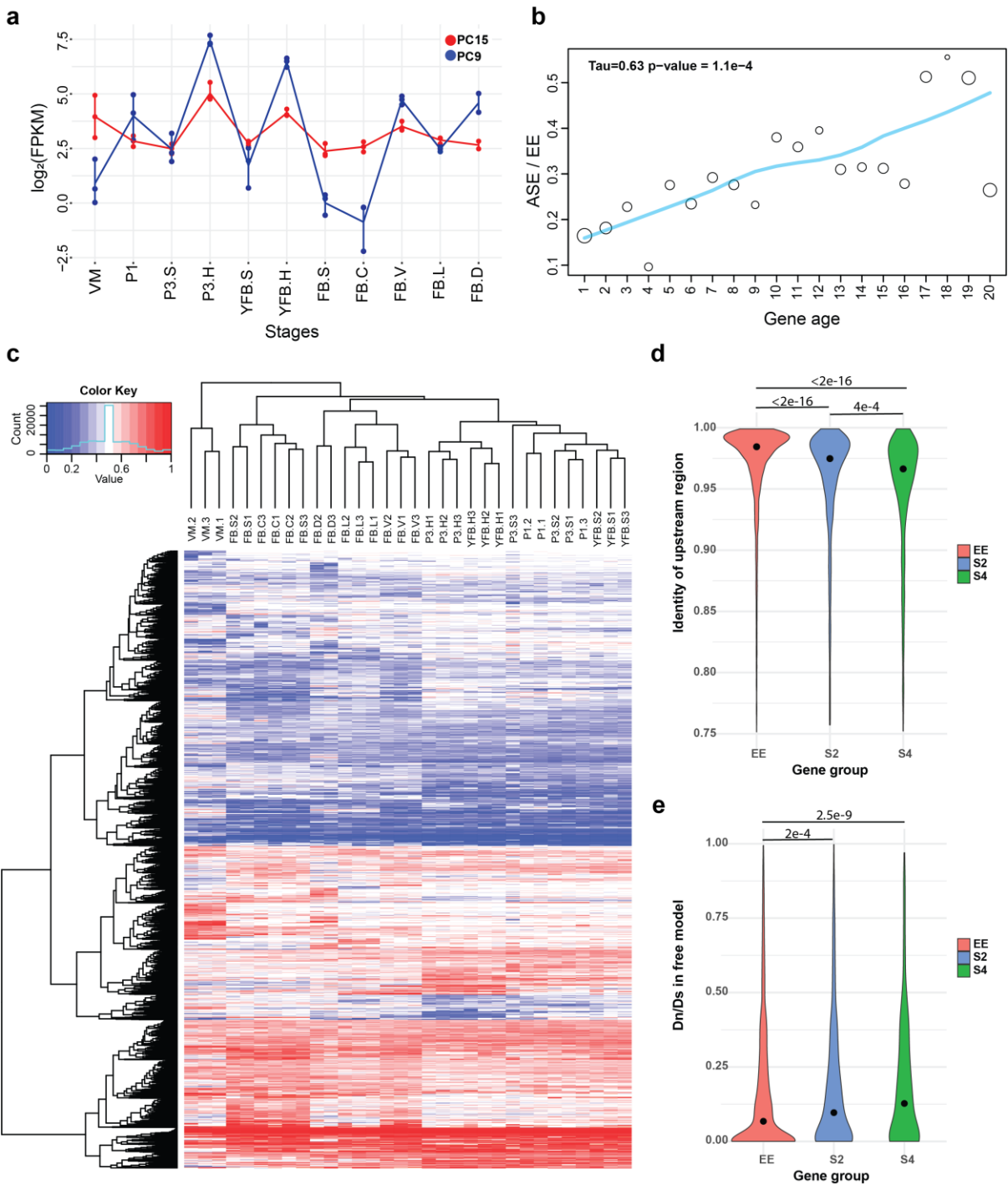144   occurrence of allele-specific expression in *P. ostreatus*.

Figure 2 Transcriptome patterns correlate with gene age in *Pleurotus*. a) allele specific expression (ASE) of Mycotoxin biosynthesis protein UstYa-like domain containing protein (PleosPC15_2_159921) **b)** Proportion of ASE shows a significant increasing tendency (Mann-Kendall statistics) across gene ages. Size of circles represents the number of proteins ($\log_{10}$ transformed). **c)** Heatmap based on AS ratio (expression contribution of PC15 relative to the sum of PC15 and PC9) of genes that showed at least two-fold ASE in at least one stage. **d)** percent sequence identity between the upstream regions of PC15 and PC9 genes **e)** dN/dS distribution for three gene groups under the free (fb) model in CODEML. Abbreviations as follows: 'VM' vegetative mycelium; 'P1' stage 1 primordium; 'P3' stage3 primordium; 'YFB' young fruiting body, 'FB' fruiting body; 'H' cap (entire); 'C' cap trama; 'L' lamellae; 'S' stipe; 'V' cuticle; 'D' dedifferentiated tissue of cap.

Allele-specific expression is enriched in young genes

We next asked what mechanisms could give rise to ASE. Gehrmann et al. (2018) found that DNA methylation can explain at most 10% of ASE, which is consistent with the negligible role of gene body methylation in fungi (Montanini et al., 2014), suggesting other mechanisms. Following reports of divergent cis-regulatory alleles causing allelic gene expression imbalance (Gaur et al., 2013; Chen et al., 2016; Cowles et al., 2002; McManus et al., 2010; M. Wang et al., 2017), we hypothesised that ASE may arise from cis-regulatory divergence between nuclei of *P. ostreatus*. Indeed, upstream 1.2 kb regions, which probably comprise cis-regulatory elements, of S2 and S4 genes are significantly more different (Kruskal-Wallis with Nemenyi post hoc test $P < 2e-16$) between the two parents than those of EE genes (Fig. 2/d). This is consistent with divergent cis-regulatory elements in the same trans-regulatory cellular environment causing differential binding of transcription factors, thus causing biased gene expression in the two nuclei. Protein sequences of S4 and S2 genes are also significantly more different between the two parents (Kruskal-Wallis test with Nemenyi post hoc test $P<2.2e-16$ and 2.7e-14 Fig. S15/a) than that of EE genes, and dN/dS also showed an increased level among ASE genes (Kruskal-Wallis test with Nemenyi post hoc test $P=2.5e-9$ and 2.0e-4 Fig. 2/e, Fig. S15/b). Together, these observations indicate that ASE in *P. ostreatus* may arise from the divergence of cis-regulatory alleles, possibly in fast-evolving genes that are released from selection constraints.

A well-known group of genes under relaxed selection are evolutionarily young genes, therefore, we tested whether ASE is correlated with relative gene age in our dataset (gene ages were assigned based on time since last duplication, see Methods). ASE genes showed a strong and significant overrepresentation in the three youngest gene ages (Fisher's exact test P=2.6e-7 - 4.8e-44), with clear trends (Fig. 2/b, Mann-Kendall test P= 1.1e-4), which together contain 51,2% of ASE genes. At the same time, they are significantly underrepresented in the three oldest age categories (gene age 1-3: $P=2.9e-3$ to 1.5e-49, Fisher's exact test, Fig. 2/b). These observations are consistent with recently duplicated genes tolerating expression imbalance better than conserved genes, probably due to relaxed constraint (Dong et al., 2011; Gu et al., 2005; Kondrashov et al., 2002).

If genes under weak selection can tolerate expression variation, and developmental expression is considered an adaptively or neutrally arising expression variation then ASE genes and developmentally expressed genes should overlap to some extent. Indeed, half of the ASE genes (S4: 52.7% and S2: 49.1%) were also developmentally regulated (FC>4), significantly more than in EE genes (31.8%, Fisher's Exact Test p=8.2e-58). We observed that as we move towards younger genes, the proportion of developmentally expressed ASE genes increase, as compared to non-ASE genes (Fig. S16-S17). The strongest overrepresentation of ASE genes can be observed among developmentally expressed genes that arose in the last common ancestor of *Pleurotus* (gene age 18, $P_{S4/EE}=7.8e-16$, Fisher's Exact Test).

Natural Antisense Transcripts show fast turnover

Natural antisense transcripts (NATs) are abundantly transcribed from fungal genomes and can include important regulatory RNAs that influence, among others, sexual development (Donaldson et al., 2017; Donaldson and Saville, 2012; Faghihi and Wahlestedt, 2009; Kim et al., 2018a). We analysed NATs in *P. ostreatus* and *Pt. gracilis* based on strand-specific RNA-seq data, and we identified 2,043 and 763 *de novo* transcripts as NATs (Fig. S18), corresponding to 17.6% and 6.3% of protein coding genes, respectively. Lengths, exon structures and coding potentials of the assembled NATs were similar to those in earlier reports (Borgognone et al., 2019; Kim et al., 2018a; Wang et al., 2019) (Fig. S18-S19).

NATs showed developmentally dynamic expressions with NAT expression patterns reflecting stage and tissue identity, with tight grouping of biological replicates (Fig. S20). As many as 1173 (57.4%) and 126 (16.5%) NATs of *P. ostreatus* and *Pt. gracilis* were developmentally expressed, respectively. These may expand the space of developmentally regulated transcripts in fruiting bodies, thus, irrespective of their exact mechanism of action, can contribute to CM. In *P. ostreatus* we identified 166 NATs (8.1%) that showed at least 2-fold higher expression in all fruiting body stages than in vegetative mycelium, comparatively more than genes (4.8%). Such transcripts may regulate the transition from simple multicellularity in VM to complex multicellularity in FB, one of the most significant transcriptomic reprogramming events in the fungal life cycle (Krizsán et al., 2019). Kim et al. (2018) found a similar proportion (21.3%, 547 of 2,574) of

200   lncRNA that might have a role in sexual development of *Fusarium graminearum*. Nevertheless, only 39.1% of *P.*
201   *ostreatus* and 4.1% of *Pt. gracilis* of the NAT-possessing genes show developmental regulation.

202   The detected NATs displayed low sequence conservation. Of the 2,043 NATs of *P. ostreatus*, 1,815 (89%)
203   showed homology in the closest sequenced species (*P. eryngii*) and only 177 (8.7%) in other species (Fig. 3). In *Pt.*
204   *gracilis* only 15 (2.0 %) NATs showed homology in other species (Fig. S21). We find that low overlap with gene exons
205   can explain the lack of sequence conservation in NATs. In *P. ostreatus*, only 596 of the 2,043 NATs (29%) showed at
206   least 75% total exon-exon overlap. This suggests that, even if located in conserved genes, NATs mostly overlap with
207   introns or intergenic regions, which may allow rapid sequence turnover, as reported in vertebrates (Kapusta and
208   Feschotte, 2014). We also failed to detect conservation of sense gene identity: of the 6,232 co-orthologous genes between
209   *P. ostreatus* and *Pt. gracilis*, only 70 showed evidence for NAT in both species. All of these observations imply low
210   conservation of NATs at the sequence level, consistent with the view that NAT homology is detectable only among
211   closely related species (Donaldson and Saville, 2013; Rhind et al., 2011).

212   In *P. ostreatus* 263 NATs (12.8%) showed significant positive (Pearson r > 0.7, P < 0.05, Fig. S22 twice as many
213   as expected by chance P<0.01, Fig. S23) while 33 showed significant negative expression correlation (Pearson r < -0.7, P
214   <0.05, Fig. S24) with their sense genes. An enrichment of positive over negative correlation between lncRNA/gene pairs
215   was noted previously in *Fusarium* and in *Ganoderma lucidum* (Kim et al., 2018b; Shao et al., 2017). Positively
216   correlating pairs may be co-regulated via chromatin accessibility, or be stabilized via dsRNA formation (Donaldson and
217   Saville, 2013), whereas negative correlation can be explained by transcriptional interference, antisense mediated
218   chromatin remodelling or RNA masking (reviewed in Donaldson & Saville, 2012).

219   Together, the developmentally relevant expression, the lack of functional clues (Fig. S25) and the low
220   conservation of NATs suggests that antisense transcription is a fast-evolving component of CM transcriptomes with
221   potential functions in modulating gene expression. Nevertheless, as above, non-adaptive explanations should not be ruled
222   out, such as some NATs being transcriptional noise or leakage (Dahary et al., 2005; Lloréns-Rico et al., 2016).
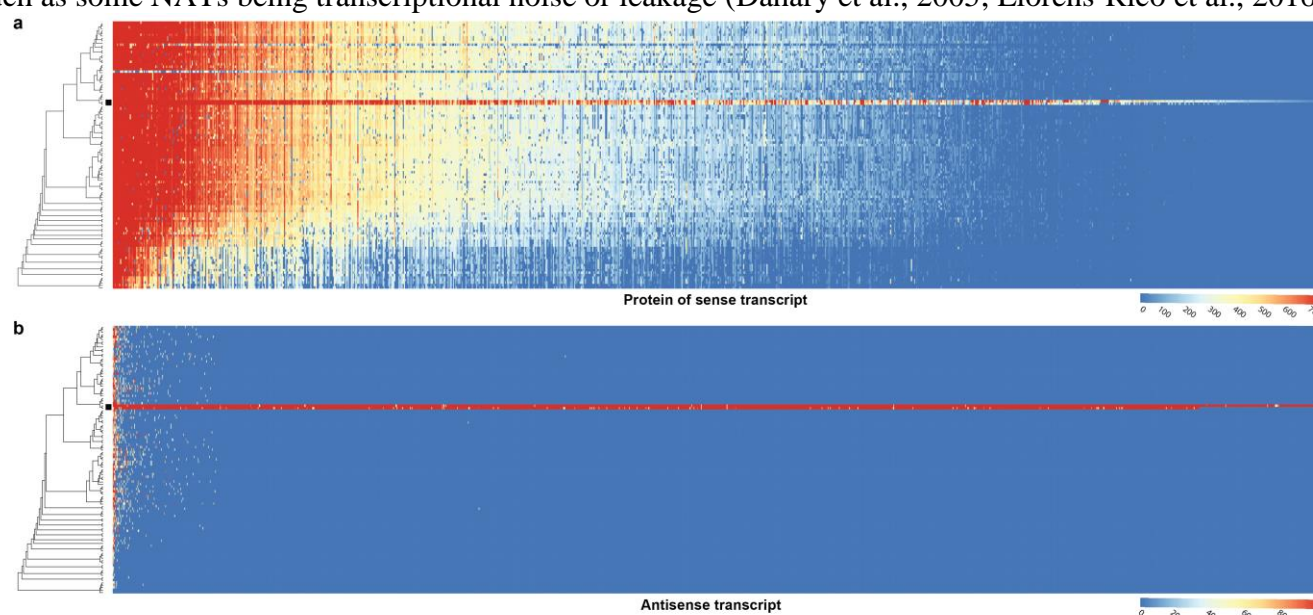
223
224   **Figure 3 Conservation of sense genes and their antisense transcripts (NAT) in *Pleurotus ostreatus*. a**) similarity of
225   sense transcripts measured with –log$_{10}$(e-value) from MMSeqs search **b**) mapping score of antisense transcripts based on
226   Minimap2. Warmer colour represents a higher similarity according to the scales. Black square denotes *P. ostreatus*. Rows
227   represents the species while columns represent the antisense query transcripts (b) or proteins from sense transcripts (a).
228   For a larger species tree and the same plot in *Pt. gracilis*, see Figs. S29 and S21, respectively.

Sexual and CM development recruit genes of different ages

230   After we asserted/contended that transcriptome patterns may be affected by gene age and constraint (or lack thereof), we
231   examined age distributions of developmentally expressed genes. We found that developmental transcriptomes are

232 dominated by old and young genes in all species, creating 'U' shaped distributions (Fig. 4/c, Fig. S26). While this shape
233 mirrors the genome-wide gene age figures, most species displayed an enrichment of developmental expression (at fold
234 change>4) among young genes (Fisher's exact test, FDR corrected $P<0.05$, Fig. 4/c, Fig. S26), indicating that, like in the
235 case of ASE, young genes have a disproportionately high share in fruiting bodies. To eliminate young genes and focus on
236 key CM functions, we first looked for 1-to-1 orthologous genes, hereafter called 'orthogroups' (1 gene per species),
237 which show developmentally dynamic expression in most species (FC>2/4, see Methods). This yielded 1,781
238 orthogroups, considered hereafter as conserved developmental orthogroups.
239   To distinguish genes related to basic sexual processes (sporulation, meiosis) from those related to CM, we
240 reanalysed transcriptome data for sexual sporulation and basidium development of *Cryptococcus neoformans* (Liu et al.,
241 2018)*. This species has a simple, non-CM development and we used it here as a minimal model of sexual development
242 (Fig. 4/a/b). Of the 1,781 conserved orthogroups, 913 and 868 were developmentally expressed both in *C. neoformans*
243 and CM species and only in CM species (Fig. 4/e), and are referred to as shared and CM-specific orthogroups,
244 respectively. Of the 868 CM-specific orthogroups, 754 were completely missing in *C. neoformans* whereas 114 were
245 present but not developmentally regulated (Fig 4/e, Table S8). Phylostratigraphic analyses showed that, on average,
246 shared orthogroups contain evolutionarily old genes that predate the origin of Dikarya, while CM-specific orthogroups are
247 younger (Fig. 5). Shared orthogroups included more housekeeping gene functions, such as mitosis/meiosis, general
248 transcription factors or ribosomal proteins, whereas CM-specific orthogroups contained more genes encoding sequence
249 specific transcription factors, cell wall remodelling, oxylipin biosynthesis, protein ubiquitination (F-box, BTB/POZ and
250 RING zinc finger domain proteins) as well as functionally unclassified proteins (Fig. 4/d/f-g).
251   Cell division related (DNA replication, meiosis, mitosis, DNA repair, etc.) and ribosomal protein encoding genes
252 comprised the most frequent annotations in shared orthogroups (Fig 4/g). Meiosis happens in the basidia in both *C.*
253 *neoformans* and CM fungi and associated genes showed clear peaks in their expression (Fig. S27). *C. neoformans* showed
254 a single peak in meiotic/mitotic gene expression, whereas higher fungi like *P. ostreatus* showed two peaks, one
255 corresponding to meiosis in gills and another to intense hyphal cell division (mitosis) in primordia. Ribosomal protein
256 gene expression, as a proxy for the activity of protein synthesis, has been widely associated with cell growth and
257 proliferation (Jorgensen et al., 2002; Kraakman et al., 1993). Ribosomal proteins showed an early peak in all species,
258 while in CM species a second peak was also observed, coincident with meiosis and spore production in gills, possibly
259 reflecting the requirement for increased protein synthesis (Fig. S28). We infer that the first ribosomal gene expression
260 peak corresponds to an early, proliferative phase of development followed by the transition to growth by cell expansion
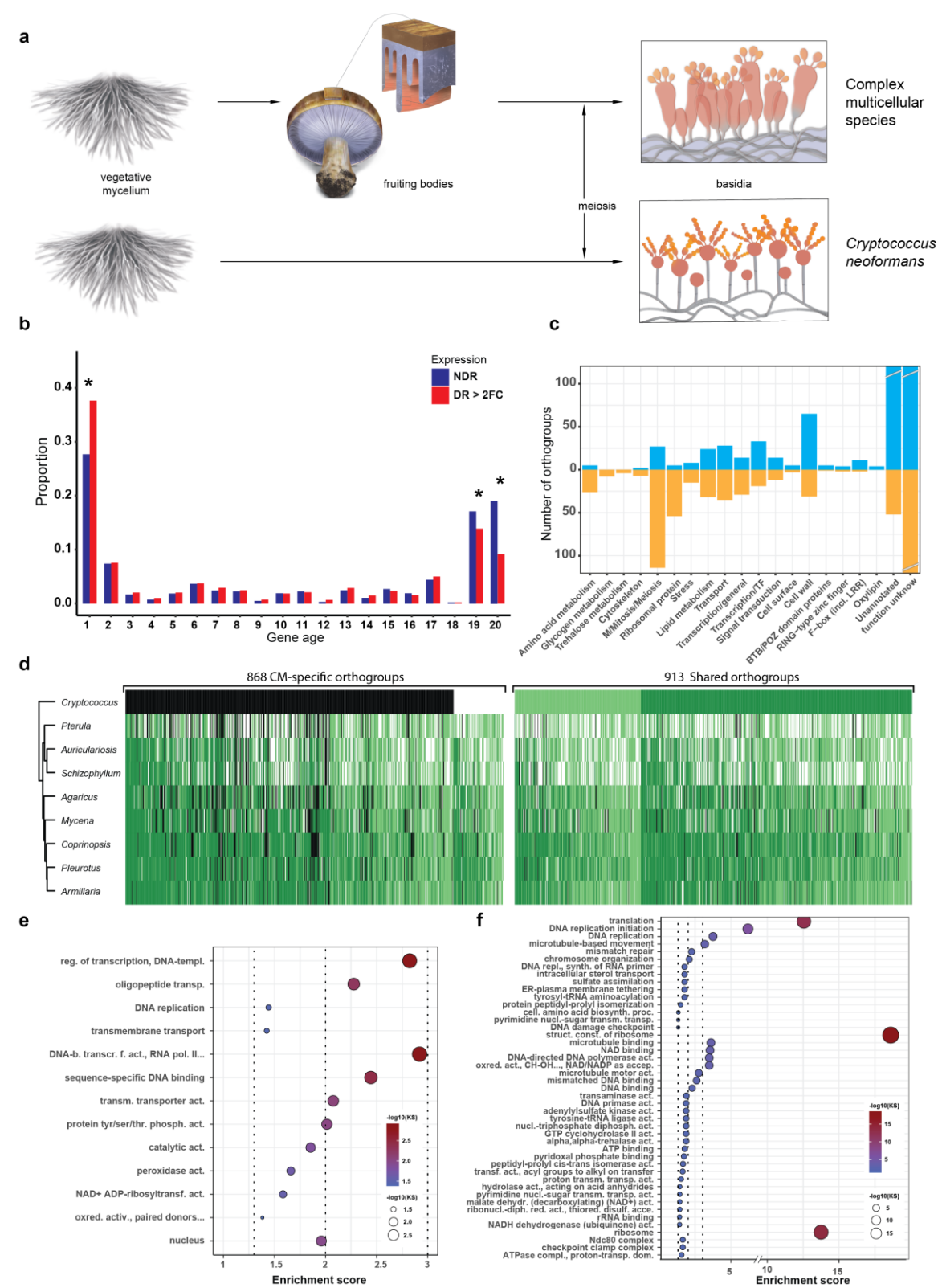261 (Krizsán et al., 2019), which gives the final shape and size of fruiting bodies before spore release.

Figure 4 Conserved developmental expression in CM fungi a) schematic representation of complex multicellular and simple development and the use of *C. neoformans* as a minimal model of sexual development in the Basidiomycota **b)** Enrichment analysis of developmentally regulated genes in different gene ages. **c)** Number of conserved orthogroups in different functional categories **d)** distribution of genes and their developmental expression in the nine species. Dark and light green refers to genes with developmental regulation at fold change > 4 and 2, respectively, whereas white and black denoted non-developmentally regulated and missing genes, respectively. Gene Ontology (GO) enrichment for **e)** CM-

269   specific and **f)** Shared orthogroups. KS means the p-value of Kolmogorov-Smirnov test implemented in the R package
270   'topGO'. On panels e and f, cutoff lines (dashed line) are drawn at enrichment scores corresponding to p=0.05, p=0.01
271   and p=0.001 (from left to right). GO terms are ordered by Kolmogorov-Smirnov p-values. See also Table S12 for GO
272   enrichment details.

273   Several cell surface proteins (fasciclins, ricin-B lectins and the PriA family) and putative cell wall remodelling
274   enzymes (e.g. chitin- and glucan- active glycoside hydrolases, expansins, CE4 chitooligosaccharide deacetylases,
275   laccases) previously linked to fruiting body morphogenesis (Pezzella et al., 2013; Xie et al., 2018) were shared between
276   *C. neoformans* and CM species (Table S8), suggesting that these families are important for sexual morphogenesis in
277   general, not restricted to CM. Cell wall remodeling enzymes have been hypothesised to produce fruiting body-specific
278   cell wall architectures (Buser et al., 2010; Krizsán et al., 2019; Liu et al., 2021; Ohga, 2000); the upregulation of these in
279   *C. neoformans* suggests a role during non-CM sexual processes as well, possibly in generating aerial hypha- or basidium-
280   specific cell walls. Most genes related to glycogen metabolism also showed shared expression (Table S8). Glycogen has
281   been known as a storage material in CM fruiting bodies, but our observations indicate that it may serve that role in *C.*
282   *neoformans* too and possibly in sexual development in general. Notable transcription factors in share orthogroups
283   included the light sensing white collar complex member WC-1, orthologs of *S. cerevisiae* sexual reproduction-related
284   Ste12, a Basidiomycota-specific velvet factor as well as orthologs of the carbon catabolite repressor CreA (*A. nidulans*).

285   CM-specific orthogroups showed a phylostratigraphic enrichment in early mushroom-forming fungi (FDR<0.01,
286   Fisher's exact test, Fig. 5) and may correspond to innovations related to CM fruiting bodies, or, to a smaller extent,
287   conserved genes lost in *C. neoformans* (e.g. hydrophobins and cerato-platanins). This observation complements our
288   previous analysis (Krizsán et al., 2019) that could not resolve a clear signal of genetic innovation related to CM, possibly
289   because of confounding effects of very conserved genes. In comparison to shared orthogroups, CM-specific orthogroups
290   contained more transcription factors, genes related to cell wall biosynthesis/modification and defense (Table S9).
291   Hydrophobins (probably the best-known fruiting body expressed genes) and cerato-platanins, as well as fatty acid
292   desaturases and linoleate-diol synthases putatively related to biosynthesis of the signal molecule oxylipin were
293   exclusively found in CM-specific orthogroups (Fig. 4/d). Hydrophobins and cerato-platanins are completely missing and
294   defense-related genes are strongly underrepresented (1/4th that of CM species) in the genome of *C. neoformans*, probably
295   as a consequence of the adaptation to a primarily yeast-like lifestyle (Nagy et al., 2014). The large number of conserved
296   unannotated genes among CM-specific orthogroups underscore the still cryptic nature of CM development in fungi.
297   Detailed descriptions of all conserved developmental genes will be given in a separate publication (Nagy et al in prep).
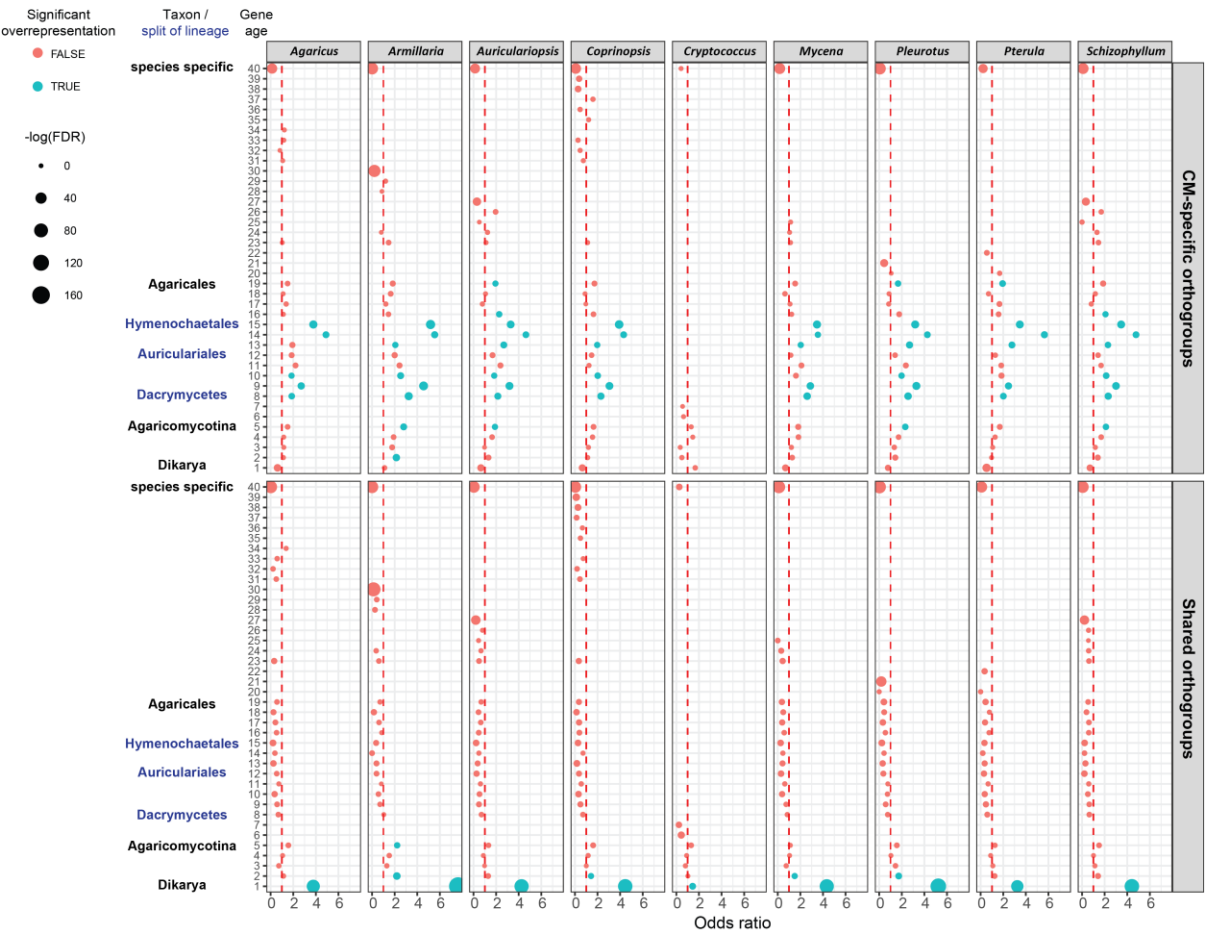
Figure 5 Gene age enrichment for shared and CM-specific conserved developmentally regulated orthogroups. CM-specific orthogroups are significantly enriched in the most recent common ancestors of lineages in which the first complex structures emerged. Y axis of the scatterplot represents relative gene age (see Fig. S29 for definition of ages). X-axis displays the odds ratio of Fisher's exact test. If the odds ratio exceeds 1 (red dotted line) orthogroups are overrepresented in that gene age. Non-significant and significant (FDR p< 0.05) overrepresentation are marked with red and blue, respectively. The size of circles corresponds to the FDR corrected p-value.

Conclusions

In this study, we disentangled developmental transcriptomes of complex multicellular fungi, both in terms of mechanisms and function, using a comparative dataset that included the first developmental gene expression profiling data for *Pleurotus ostreatus* (oyster mushroom), the second most widely cultured fungus worldwide (Grimm and Wösten, 2018; Royse et al., 2017).

The availability of the genomes of both parental monokaryons (Alfaro et al., 2016; Riley et al., 2014) as well as new strand-specific RNA-Seq data allowed bioinformatic deconvolution of RNA editing, allele-specific expression and antisense transcription in the *P. ostreatus* transcriptome. We found virtually no evidence for RNA editing, whereas allele specific expression was abundant, which supports the only previously available report of ASE in CM fungi (Gehrmann et al., 2018). RNA editing has been recently reported in the Agaricomycetes (Wu et al., 2019, 2018; Zhu et al., 2014), however, in contrast to the Ascomycota (Lau et al., 2020; Liu et al., 2016; Teichert et al., 2017), it displayed no clear-cut enrichment of A-to-I compatible variants in three previous studies (Bian et al., 2019; Teichert, 2020; Zhu et al., 2014) or in this study. Rather, our final candidate RNA-editing sites merely alluded to potential polyA site- and/or read alignment inaccuracies leading us to conclude that RNA editing is not abundant in *P. ostreatus*. On the other hand, ASE was detected in thousands of genes in *P. ostreatus*, In *A. bisporus* ASE was interpreted as a regulated and adaptive mechanism

12

320 that could, for example, aid the division of labour between nuclei (Gehrmann et al., 2018). We found that in *P. ostreatus*
321 ASE is characteristic of young genes and likely arises from promoter divergence, which creates a cellular environment
322 with divergent cis-regulatory alleles but identical trans-regulatory elements. Young genes are known to be under weaker
323 evolutionary constraint than conserved ones, raising the possibility that ASE might arise neutrally in the transcriptome.
324 This would be consistent with the neutral model of expression evolution (Fay and Wittkopp, 2008) and non-adaptive
325 explanations, such as leaky regulation or transcriptional noise (Cheng et al., 2017; Khan et al., 2012; Shih and Fay, 2021;
326 Wainer-Katsir and Linial, 2019). Under this interpretation, ASE may be a tolerated, rather than an adaptive phenomenon
327 in CM fungi. However, even if neutral at the level of the individual, ASE may generate gene expression variation that can
328 serve as substrate for adaptive evolution, similar to how transcription from random promoters can facilitate de novo gene
329 birth (Van Oss and Carvunis, 2019). ASE may have important implications in mushroom breeding, where intraspecific
330 hybrids harbouring cis-regulatory alleles with various levels of divergence may show differences in industrially relevant
331 traits (Gehrmann et al., 2018).
332   Fruiting bodies integrate several distinct processes, some of which are conserved across all organisms
333 (mitosis/meiosis), fungi (spore production), or specific to CM species (fruiting body morphogenesis). Analysing the
334 evolutionary stratification of developmentally expressed genes helped us distinguish conserved genes related to basic
335 sexual development from those putatively related to CM morphogenesis. As in the case of ASE, young genes might
336 display more expression variance and noise across development, whereas genes with conserved developmental expression
337 more likely provide clues about key CM functions. While our transcriptome-based approach has limitations as far as
338 conservation of expression versus that of function is concerned, it proved relevant for understanding the evolution of CM.
339 This may help for establishing a minimal model of sexual development (e.g. for pathogens like *C. neoformans*) in the
340 Basidiomycota, that include several genes previously considered specific to fruiting bodies. Notable examples include
341 fasciclins, which have been implicated in cell adhesion (Nagy et al., 2018), and the *PriA* family of secreted cell surface
342 proteins (including *C. neoformans* cfl1 and dha1 Gyawali et al., 2017) with unknown function. Our strategy also
343 identified regulatory genes which are developmentally expressed only in CM species, including certain transcription
344 factors reported in mushrooms (e.g. hom1, fst3, fst4, wc1; Hou et al., 2020; Kamada et al., 2010; Ohm et al., 2011) but
345 also novel ones, such as a velvet factor that is widely conserved in Agaricomycetes and showed stipe-specific expression
346 in CM species.
347   Taken together, this study emphasises the complexity of transcriptome evolution in the transition to complex
348 multicellularity in fungi. Our results suggest that CM transcriptomes are likely shaped by both adaptive and neutral
349 processes and encourage non-adaptationist views of transcriptome evolution and analysis. We anticipate that the
350 dissection of shared and CM-specific genes as well as allele-specific expression and natural antisense transcripts will help
351 understanding the intricate gene regulatory networks governing development in both pathogenic and CM Basidiomycota
352 and will contribute to the growth of mushroom developmental biology.

Materials & Methods

Growth condition, sampling and RNA-Sequencing

355 For fruiting the dikaryotic strain N001 (CECT-20600) of *Pleurotus ostreatus* (recently interpreted as *P. cf. floridanus* J.
356 Li et al., 2019) we first prepared spawn by inoculating sterilized rye and incubating for 10 days. Pasteurized straw-based
357 commercial oyster compost (95 vol%) and the colonized spawn (5 vol%) were mixed gently and three kilograms were
358 filled into polyethylene bags. Bags were incubated in the dark at 27 °C and 85-90% relative humidity for 17 days. Next,
359 bags were transferred to the growing room for fruiting at 18-19 °C, relative humidity 80-85% and 8/16h light/dark period
360 (with approximately 1200 lux light intensity). We sampled vegetative mycelium (VM), six developmental stages and five
361 tissue types, each in three biological replicates as explained in Fig. S1. VM was collected from the sawdust culture. In the
362 case of stage 1 and 2 primordia (P1 and P2) the whole tissue was collected containing both stipe and cap initials. In the
363 stage 3 primordium (P3) and the young fruiting body (YFB) stages, stipes and caps were sampled separately. We divided

364   mature fruiting bodies (FB) into stipe (S), cap trama (C), cap cuticle (V). We defined cap (H) as the whole upper part of
365   the fruiting body (in P3 and YFB) while cap trama (C) refers to just the inner part of cap without lamellae or cuticule (in
366   FB). The last stage was the dedifferentiated cap trama (D), a dissection from inner cap tissue which was inoculated for
367   24h on a sterile PDA-agar plate, until the emergence of new hyphae. Tissue from 3-8 individual fruiting bodies was
368   pooled for each replicate of each sample type.
369   *Pterula gracilis* CBS 309.79 was inoculated onto Malt Extract Agar plates with cellophane, and incubated at 25
370   °C for 25-27 days. For fruiting, plates were moved to a growth chamber at 15 °C under 10/14h light/dark period (light
371   intensity: 11 $\mu E\ m^{-2}\ s^{-1}$). VM samples were scraped off the cellophane after three days. We defined primordia (P) as small
372   (<1mm) globose structures, young fruiting bodies as ~5 mm long awl-shaped structures, while structures longer than
373   10mm were considered mature fruiting bodies (Fig. S2).
374   Three biological replicates of each sample type were stored at -80 °C until RNA extraction. Tissue samples were
375   homogenized with micropestles using liquid N_2, and RNA was extracted by using the Quick-RNA Miniprep Kit (Zymo
376   Research) according to the manufacturer's instructions. Strand-specific cDNA libraries were constructed from poly(A)-
377   captured RNA, using the Illumina TruSeq Stranded RNA-Seq library preparation kit, and sequenced on the Illumina
378   HiSeq 4000/x platform in PE 2x150 format with 40 million reads per sample at OmegaBioservices (USA).

379   Bioinformatic analyses of RNA-Seq data

380   New data for *P. ostreatus* and *Pt. gracilis* was reanalysed together with previously published transcriptomes of seven
381   Basidiomycota species (Table S10). To remove adaptors, ambiguous nucleotides and any low quality read end parts,
382   reads were trimmed using bbduk.sh and overlapping read pairs were merged with bbmerge.sh tools (part of
383   BBMap/BBTools; http://sourceforge.net/projects/bbmap/) with the following parameters: qtrim=rl trimq=25 minlen=40.
384   A two-pass STAR alignment (Veeneman et al., 2015) was performed against reference genomes with the same
385   parameters as in our previous study (Krizsán et al., 2019) except that the maximal intron length was reduced to 3000 nt.
386   Read count data was normalized using EdgeR (Robinson et al., 2010) as in our previous study (Krizsán et al., 2019).
387   Expression levels were calculated as fragments per kilobase of transcript per million mapped reads (FPKM). Samples,
388   such as FBCL and FBS of *Coprinopsis cinerea from* Krizsán et al. (2019), and stage 2 primordia (P2) of *P. ostreatus* were
389   excluded from our analysis to avoid the signs of fruiting body autolysis and for quality reasons, respectively. Raw RNA-
390   Seq reads have been deposited to NCBI's GEO archive (GSE176181).

391   Identification of developmentally regulated genes

392   Developmentally regulated genes were defined as in Krizsán et al. (2019). Genes with both two- and four-fold expression
393   change were considered developmentally regulated and analyzed separately.
394   We checked if developmentally regulated genes physically clustered together and if they overlapped with
395   predicted biosynthetic gene clusters in eight Basidiomycota species, including *P. ostreatus* and *Pt. gracilis* (Table S10).
396   To this end, we first considered all developmentally regulated genes separated by six or less intervening genes to be
397   clustered, and then calculated the probability of observing a cluster of that size using a binomial test, based on the
398   expected number of developmentally regulated genes that would be found in the same sized gene window as the cluster if
399   all developmentally regulated genes randomly distributed across the genome. Clusters with a probability of observation <
400   0.01 were designated 'hotspots'. We then checked hotspots for overlap with predicted biosynthetic gene clusters using *de*
401   *novo* antiSMASH v5 annotations (Medema et al., 2011). Conservation of hotspots between different fungal species was
402   assessed by BLASTp (Altschul et al., 1990) using two metrics: percent gene content similarity, which is the number of
403   genes in the query hotspot that are clustered together in the target genome; and percent FDBR similarity, which is the
404   number of developmentally regulated genes in the query hotspot that are also developmentally regulated and clustered
405   together in the target genome, using the same clustering criteria as above.
406
407   Species tree and relative gene age estimation

408   Protein sequences of 109 whole genomes (Table S11) across Basidiomycota and Ascomycota (as outgroup) were
409   downloaded from the JGI genome portal (Sep. 2019; Grigoriev et al., 2014; Nordberg et al., 2014). All-vs-all similarity

410   search was carried out with MMseqs2 (Steinegger and Söding, 2017) using three iterations, and setting sensitivity to 5.7,
411   max-seqs to 20,000, e-profile to 1e-4, a preliminary coverage cut-off to 0.2 and an e-value cut-off to 0.001. Then, an
412   asymmetrical coverage filtering was performed where we required >=0.2 pairwise alignment coverage from the longer
413   protein and >=0.8 from the shorter one, with the aim to omit aspecific partial hits while retaining gene fragments. Then
414   Markov Chain Clustering with an inflation parameter 2.0 was performed using the ratio of 'number of identical matches'
415   (Nident) and 'query sequence length' (qlen) as weight in the matrix. After clustering we removed contaminating proteins
416   from gene families following the logic of Richter et al. (2018).
417   For species tree reconstruction we used 115 single copy gene families, which were present in >= 50% of the 109
418   species. Multiple sequence alignments were inferred using PRANK v.170427 (Löytynoja, 2014) and trimmed with
419   TrimAL v.1.2 (-strict) (Capella-Gutierrez et al., 2009). Trimmed MSA-s shorter than 100 amino acid (AA) residues were
420   discarded. Best partitioning schemes, substitution models and species tree reconstruction were performed under
421   Maximum Likelihood (ML) in IQ-TREE v1.6.12 (Minh et al., 2020).
422   For gene tree reconstructions, gene families which contained at least four proteins were aligned with MAFFT
423   LINSI v7.313 (Katoh and Standley, 2013) algorithm or with FAMSA v1.5.12 (Deorowicz et al., 2016) and trimmed with
424   TrimAL (gt-0.4). We inferred gene trees for each of the alignments in RAxmlHPC-PTHREADS-AVX2 under the
425   PROTGAMMAWAG model of sequence evolution and assessed branch robustness using the SH-like support
426   (Stamatakis, 2014). Rooting and gene tree/species tree reconciliation were performed with NOTUNG v2.9. (Darby et al.,
427   2016) using an edge-weight threshold of 90. Then, a modified version of COMPARE (Nagy et al., 2014) was used to
428   delineate orthogroups within gene trees.
429   Orthogroups were used to define relative gene ages (hereafter: gene age) as the species tree node to which the
430   Most Recent Common Ancestor (MRCA) of species represented in the orthogroup mapped. Enrichment of gene sets in
431   gene age categories were analysed with Fisher's exact test (R core team 2020).
432
433   **Transcriptome age index**
434   Transcriptome age index for each developmental stage of the nine investigated species was computed as described
435   previously (Domazet-Lošo and Tautz, 2010) with slight modifications, using the following formula: $TAI = \frac{\sum_{i=1}^{n} RA_i e_i}{\sum_{i=1}^{n} e_i}$,
436   where RA_i represents the relative age of gene i, e_i is the log2 FPKM value of gene i at the given stage and n is the total
437   number of genes. If available, tissue specific expression values were averaged for each developmental stage. The TAI
438   values of the investigated developmental stages were computed for each replicate, then averaged.
439
440   **Orthology based on reciprocal best hits**
441   To characterize the conservation of developmental genes, we defined single copy orthologs from the nine species based
442   on reciprocal best hits between proteins. This strategy was stricter than the above-mentioned orthogroup definition, and
443   was required to obtain functionally highly similar protein sets for comparing developmentally regulated genes. Proteins of
444   each species were searched against the proteomes of other eight species using the RBH module of MMSeqs2 with an e-
445   value cut-off of 1e-5. To remove spurious reciprocal best hits, we excluded a protein from the RBH group if its bit score
446   was at least three times lower than the mean bit score of other hits of that query (self-hit excluded) and it shared <50 % of
447   its hits with those of the query. The orthogroups obtained this way comprised considerably more focused gene sets than
448   the approach used in Krizsán et al. (2019).
449
450   **Annotation of genes, gene families**
451   We detected conserved domains in proteins using InterProScan-5.47-82.0 (Jones et al., 2014). Enrichment analysis on
452   IPR domains was performed with Fisher's exact test (R Core Team, 2020), while enrichment analysis on gene ontology
453   categories was carried out using the R package topGO 2.44.0 (Alexa and Rahnenfuhrer, 2020). Proteins were further
454   characterized by the best bidirectional hits to proteins of the model organisms *Saccharomyces cerevisiae* (Engel et al.,
455   2014), *Schizosaccharomyces pombe* (Wood et al., 2012), *Neurospora crassa* (Galagan et al., 2003) and *Aspergillus*
456   *nidulans* (Cerqueira et al., 2014).
457

Identification of Natural Antisense Transcripts

Natural antisense transcripts (NAT) were defined as *de novo* assembled transcripts located antisense to a gene >200 nucleotide (nt) long, not showing similarity to structural RNA species, not overlapping with UTRs of neighbouring genes, and showing an expression above a given cut-off (Fig. S18). For *de novo* transcript assembly, quality filtered reads were first mapped to the reference genome using STAR_2.6.1a_08-27 (Veeneman et al., 2015). After identifying splice sites, a second mapping was performed. StringTie version 2.0.3 (Pertea et al., 2015) was used to generate a genome-guided *de novo* transcriptome assembly and annotation. Transcripts shorter than 200 nt or supported by <5 reads in a single sample were excluded. Output GTF files from each sample were merged, compared to the reference annotation with gffcompare v0.11.2 (Pertea and Pertea, 2020) and transcripts with exonic overlap on the opposite strand (i.e. antisense; class_code x) were retained. To exclude transcripts mapped to repeats, RepeatModeler v2.0 (Flynn et al., 2020) was used to identify repeat regions of genomes. Conserved structural RNA transcripts (tRNAs, U2 spliceosome, ribosomal RNAs, Hammerhead ribozymes) were identified with Infernal 1.1.3 (Nawrocki and Eddy, 2013) based on the Rfam database (Kalvari et al., 2021) and were removed. Fungal genomes are densely packed with genes, raising the possibility that a detected transcript is actually the UTR region of the closest gene (Rhind et al., 2011). To avoid identifying UTR regions as NATs, candidate NATs showing a strongly correlated expression (Pearson's P-value < 0.05) and located <500 nt from the closest coding genes on the same strand were discarded from further analysis. Coding potential of NATs were characterized based on the default cut-off of the Coding Potential Calculator CPC2 (Kang et al., 2017).

Expression level of NATs was quantified with the FeatureCounts R package (Liao et al., 2014) based on the union of the exons per transcript. FPKM calculations were carried out as mentioned above, only transcripts with at least five mapped reads in at least three samples were retained. Developmental regulation of potential NATs was calculated as for genes. To assess conservation of NATs we mapped the transcripts on the genomes of the 109 species with minimap2 v 2.17 (options: -k15 -w5 --splice -g2000 -G200k -A1 -B1 -O1,20 -E1,0 -C9 -z500 -ub --junc-bonus=9 --splice-flank=yes) (Li, 2018).

RNA editing and allele specific expression

To estimate the importance of RNA editing and Allele Specific Expression (ASE) during fruiting body formation of *P. ostreatus* we evaluated mismatches in Illumina reads according to their potential origin (RNA-editing, ASE, noise). A custom pipeline (Fig. S12) was constructed to first classify mismatches either as candidates for "RNA editing" or "allele-specific". Then, these mismatches were analysed further in more specialized pipelines. First, we hard trimmed 10-10 nucleotides from both the 3' and 5' end of already quality trimmed reads to decrease the impact of sequencing errors during variant calling. A two-round STAR alignment was performed against both parental genomes (PC15 and PC9) as references, with the above mentioned parameters. Variants were identified with a custom awk script excluding bases with a Phred quality value below 30. Nucleotides differing the same way from both parental alleles were considered technical errors (caused by PCR amplification, sequencing or alignment), somatic mutations or RNA editing. Therefore, such mismatches were transferred to the RNA editing specific pipeline. In contrast, variants which differed only from one of the parental genomes were attributed to allele specific expression. The first part of the pipeline yielded lists of variants which were further analysed either in the RNA editing specific pipeline or in allele specific expression pipeline, as follows.

In the RNA editing pipeline (Fig. S12) we re-called variants for sites with pysamstats 1.0.1 (https://github.com/alimanfoo/pysamstats; min-base quality 30 and max depth to 500,000) that were input to the RNA editing pipeline. We continued the analysis with only those variants which had >=3 supporting reads, mapped to both reference genomes and the total read support did not differ more than five times between the two parental mappings, in order to avoid signal coming purely from the differential mapping to the two reference genomes (e.g. erroneous alignment). Further, we removed variants where read coverage was <10, a single variant was supported by <3 reads, or the proportion of the variant was below 0.1% in order to reduce the effect of technical errors, but retain editing sites. Because erroneous alignment around splice sites can produce variants indistinguishable from editing events, we discarded variants in which multiple sites with mismatches grouped within 3 nt distance of each other and in which the proportion of gaps exceeded 80% of the read coverage. After this step we kept only variants which were present in at least two

505 biological replicates. In addition, for a variant to be considered an RNA editing site, it had to be significantly more
506 frequent across all samples (Wilcoxon rank sum test with $p<0.01$) than any other nucleotide at that site (except reference).
507 Finally, we considered a site an RNA editing site, if the geometric mean of its frequencies across the three replicates
508 exceeded 1%. Relative to the editing site, -3 upstream and +3 downstream surrounding sequences were extracted with
509 rtracklayer package (Lawrence et al., 2009) and motifs were searched with the seqlogo package (Bembom and Ivanek,
510 2020).
511 　　　In the allele specific expression pipeline (Fig. S12), only previously assigned candidate allele specific SNPs were
512 considered. All reads were assigned to the parental genome to which it exhibited a smaller Hamming distance
513 (Hd=number of SNPs). We assigned a read as indecisive if i) Hd>1 from both reference genomes ii) Hd>15 from any of
514 the reference genomes (too divergent read) or, iii) if the Hd was equal to both parental genomes. FPKM values were
515 calculated as described above.
516 　　　To describe the relative expression between the two parental nuclei (AS ratio) the number of PC15 reads was
517 divided by the sum of parental specific reads (PC15 + PC9) for each gene (g) in each sample (s): $AS = \frac{PC15_{gs}}{PC15_{gs}+PC9_{gs}}$. An
518 AS ratio close to 1 means dominant expression from the PC15 nucleus, whereas an AS ratio close to 0 means dominant
519 expression from the PC9 nucleus. An AS ratio ~0.5 indicates equal expression from both nuclei. AS ratios were
520 considered equal (set to 0.5) if i) the expression was too low (FPKM<2), ii) the number of decisive reads was <16, iii) the
521 proportion of indecisive reads was greater than 80%. We calculated two further measures, Chromosome Read Ratio
522 (CRR) and Nuclear Read Ratio (NRR) introduced by Gehrmann et al., (2018), which represent the FPKM values of PC15
523 nucleus divided by the FPKM values of PC9 summed over chromosomes, and over all genes, respectively.
524 　　　We identified genes with two- (S2) and four-fold (S4) shifted expression between the two nuclei at AS cut-off
525 values of AS<0.31 or AS>0.68 (corresponding to 5% quantile of all AS ratio values) and AS<0.2 or AS>0.8, respectively.
526 For passing through these filters and geometric means of replicates had to reach the upper limits (0.68 or 0.8) for PC15
527 specific ASE or less than lower limits (0.31 or 0.2) for PC9 specific ASE.
528 　　　In order to understand how ASE may arise mechanistically, we compared putative promoters of ASE genes
529 among parents, defined as the region from spanning 1000 nt upstream to 200 nt downstream of the transcription start site.
530 Differences between the two parental regions were expressed as percent identity. For this analysis the meanwhile
531 released, improved version of PC9 was used (Lee et al., 2021). Protein sequences of parents were aligned with PRANK
532 and a ML distance was calculated under WAG model (dist.ml function from phangorn R package Schliep, 2011). Gene
533 pairs with putative promoters <75% similar or where protein ML distances were >0.5 and alignment coverage <0.7 were
534 removed to avoid potential orthology assignment errors. To identify the strength of selection for these genes we inferred
535 ω (dN/dS ratios) under two evolutionary models using CodeML, a program from PAML 4.4 (Yang, 2007). For this, CDSs
536 from the genomes of species in the Pluteoid clade (Table S11) were extracted using GenomicFeatures packages
537 (Lawrence et al., 2013). 1:1 orthologs were detected with MMSeqs RBH function and codon aligned using –code option
538 of PRANK. Reference tree for CodeML was extracted from the species tree, and ω values were calculated under one-ratio
539 (M0) model assuming that ω has been constant throughout the tree and free-ratio model (fb) allowing an independent ω
540 for each branch in the tree. For statistical comparisons the Kruskal-Wallis rank-sum test with Nemenyi post hoc test or
541 paired Wilcoxon signed-rank test and Fisher's exact test were implemented in R (R Core Team, 2020).

References

543   Abedin M, King N. 2008. The premetazoan ancestry of cadherins. *Science (80-)* **319**:946–948. doi:10.1126/science.1151084

544   Alexa A, Rahnenfuhrer J. 2020. topGO: Enrichment Analysis for Gene Ontology.

545   Alfaro M, Castanera R, Lavín JL, Grigoriev I V, Oguiza JA, Ramírez L, Pisabarro AG. 2016. Comparative and transcriptional
546   analysis of the predicted secretome in the lignocellulose-degrading basidiomycete fungus Pleurotus ostreatus. *Environ*
547   *Microbiol* **18**:4710–4726. doi:10.1111/1462-2920.13360

548   Almási É, Sahu N, Krizsán K, Bálint B, Kovács GM, Kiss B, Cseklye J, Drula E, Henrissat B, Nagy I, Chovatia M, Adam C, LaButti
549   K, Lipzen A, Riley R, Grigoriev I V., Nagy LG. 2019. Comparative genomics reveals unique wood-decay strategies and
550   fruiting body development in the Schizophyllaceae. *New Phytol* **224**:902–915. doi:10.1111/nph.16032

551   Altschul SF, Gish W, Miller W, Myers EW, Lipman DJ. 1990. Basic local alignment search tool. *J Mol Biol* **215**:403–410.
552   doi:10.1016/S0022-2836(05)80360-2

553   Bembom O, Ivanek R. 2020. seqLogo: Sequence logos for DNA sequence alignments.

554   Bian Z, Ni Y, Xu JR, Liu H. 2019. A-to-I mRNA editing in fungi: occurrence, function, and evolution. *Cell Mol Life Sci* **76**:329–
555   340. doi:10.1007/s00018-018-2936-3

556   Borgognone A, Sanseverino W, Cigliano RA, Castanera R. 2019. Distribution, characteristics, and regulatory potential of long
557   noncoding RNAs in brown-rot fungi. *Int J Genomics* **2019**. doi:10.1155/2019/9702342

558   Buser R, Lazar Z, Käser S, Künzler M, Aebi M. 2010. Identification, characterization, and biosynthesis of a novel N-glycan
559   modification in the fruiting body of the basidiomycete Coprinopsis cinerea. *J Biol Chem* **285**:10715–10723.
560   doi:10.1074/jbc.M109.076075

561   Capella-Gutierrez S, Silla-Martinez JM, Gabaldon T. 2009. trimAl: a tool for automated alignment trimming in large-scale
562   phylogenetic analyses. *Bioinformatics* **25**:1972–1973. doi:10.1093/bioinformatics/btp348

563   Cerqueira GC, Arnaud MB, Inglis DO, Skrzypek MS, Binkley G, Simison M, Miyasato SR, Binkley J, Orvis J, Shah P, Wymore F,
564   Sherlock G, Wortman JR. 2014. The *Aspergillus* Genome Database: multispecies curation and incorporation of RNA-Seq data
565   to improve structural gene annotations. *Nucleic Acids Res* **42**:D705–D710. doi:10.1093/nar/gkt1029

566   Chen J, Rozowsky J, Galeev TR, Harmanci A, Kitchen R, Bedford J, Abyzov A, Kong Y, Regan L, Gerstein M. 2016. A uniform
567   survey of allele-specific binding and expression over 1000-Genomes-Project individuals. *Nat Commun* **7**:1–13.
568   doi:10.1038/ncomms11101

569   Cheng J, Maier KC, Avsec Ž, Petra RUS, Gagneur J. 2017. Cis-regulatory elements explain most of the mRNA stability variation
570   across genes in yeast. *RNA* **23**:1648–1659. doi:10.1261/rna.062224.117

571   Cheng X, Hui JHL, Lee YY, Wan Law PT, Kwan HS. 2015. A "developmental hourglass" in fungi. *Mol Biol Evol* **32**:1556–1566.
572   doi:10.1093/molbev/msv047

573   Cowles CR, Hirschhorn JN, Altshuler D, Lander ES. 2002. Detection of regulatory variation in mouse genes. *Nat Genet* **32**:432–437.
574   doi:10.1038/ng992

575   Dahary D, Elroy-Stein O, Sorek R. 2005. Naturally occurring antisense: Transcriptional leakage or real overlap? *Genome Res*
576   **15**:364–368. doi:10.1101/gr.3308405

577   Darby CA, Stolzer M, Ropp PJ, Barker D, Durand D. 2016. Xenolog classification. *Bioinformatics* **33**:btw686.
578   doi:10.1093/bioinformatics/btw686

579   Deorowicz S, Debudaj-Grabysz A, Gudys A. 2016. FAMSA: Fast and accurate multiple sequence alignment of huge protein
580   families. *Sci Rep* **6**:1–13. doi:10.1038/srep33964

581   Domazet-Lošo T, Tautz D. 2010. A phylogenetically based transcriptome age index mirrors ontogenetic divergence patterns. *Nature*
582   **468**:815–819. doi:10.1038/nature09632

583   Donaldson ME, Ostrowski LA, Goulet KM, Saville BJ. 2017. Transcriptome analysis of smut fungi reveals widespread intergenic

584   transcription and conserved antisense transcript expression. *BMC Genomics* **18**:1–14. doi:10.1186/s12864-017-3720-8

585 Donaldson ME, Saville BJ. 2013. Ustilago maydis natural antisense transcript expression alters mRNA stability and pathogenesis.
586   *Mol Microbiol* **89**:29–51. doi:10.1111/mmi.12254

587 Donaldson ME, Saville BJ. 2012. Natural antisense transcripts in fungi. *Mol Microbiol* **85**:405–417. doi:10.1111/j.1365-
588   2958.2012.08125.x

589 Dong D, Yuan Z, Zhang Z. 2011. Evidences for increased expression variation of duplicate genes in budding yeast: From cis- to
590   trans-regulation effects. *Nucleic Acids Res* **39**:837–847. doi:10.1093/nar/gkq874

591 Drost HG, Janitza P, Grosse I, Quint M. 2017. Cross-kingdom comparison of the developmental hourglass. *Curr Opin Genet Dev*.
592   doi:10.1016/j.gde.2017.03.003

593 Engel SR, Dietrich FS, Fisk DG, Binkley G, Balakrishnan R, Costanzo MC, Dwight SS, Hitz BC, Karra K, Nash RS, Weng S, Wong
594   ED, Lloyd P, Skrzypek MS, Miyasato SR, Simison M, Cherry JM. 2014. The Reference Genome Sequence of Saccharomyces
595   cerevisiae: Then and Now. *G3 Genes, Genomes, Genet* **4**:389–398. doi:10.1534/g3.113.008995

596 Faghihi MA, Wahlestedt C. 2009. Regulatory roles of natural antisense transcripts. *Nat Rev Mol Cell Biol*. doi:10.1038/nrm2738

597 Fay JC, Wittkopp PJ. 2008. Evaluating the role of natural selection in the evolution of gene regulation. *Heredity (Edinb)*.
598   doi:10.1038/sj.hdy.6801000

599 Flynn JM, Hubley R, Goubert C, Rosen J, Clark AG, Feschotte C, Smit AF. 2020. RepeatModeler2 for automated genomic
600   discovery of transposable element families. *Proc Natl Acad Sci U S A* **117**:9451–9457. doi:10.1073/pnas.1921046117

601 Galagan JE, Calvo SE, Borkovich KA, Selker EU, Read ND, Jaffe D, FitzHugh W, Ma L-J, Smirnov S, Purcell S, Rehman B, Elkins
602   T, Engels R, Wang S, Nielsen CB, Butler J, Endrizzi M, Qui D, Ianakiev P, Bell-Pedersen D, Nelson MA, Werner-Washburne
603   M, Selitrennikoff CP, Kinsey JA, Braun EL, Zelter A, Schulte U, Kothe GO, Jedd G, Mewes W, Staben C, Marcotte E,
604   Greenberg D, Roy A, Foley K, Naylor J, Stange-Thomann N, Barrett R, Gnerre S, Kamal M, Kamvysselis M, Mauceli E,
605   Bielke C, Rudd S, Frishman D, Krystofova S, Rasmussen C, Metzenberg RL, Perkins DD, Kroken S, Cogoni C, Macino G,
606   Catcheside D, Li W, Pratt RJ, Osmani SA, DeSouza CPC, Glass L, Orbach MJ, Berglund JA, Voelker R, Yarden O, Plamann
607   M, Seiler S, Dunlap J, Radford A, Aramayo R, Natvig DO, Alex LA, Mannhaupt G, Ebbole DJ, Freitag M, Paulsen I, Sachs
608   MS, Lander ES, Nusbaum C, Birren B. 2003. The genome sequence of the filamentous fungus Neurospora crassa. *Nature*
609   **422**:859–868. doi:10.1038/nature01554

610 Gaur U, Li K, Mei S, Liu G. 2013. Research progress in allele-specific expression and its regulatory mechanisms. *J Appl Genet*
611   **54**:271–283. doi:10.1007/s13353-013-0148-y

612 Gehrmann T, Pelkmans JF, Ohm RA, Vos AM, Sonnenberg ASM, Baars JJP, Wösten HAB, Reinders MJT, Abeel T. 2018. Nucleus-
613   specific expression in the multinuclear mushroom-forming fungus Agaricus bisporus reveals different nuclear regulatory
614   programs. *Proc Natl Acad Sci U S A* **115**:4429–4434. doi:10.1073/pnas.1721381115

615 Grigoriev I V., Nikitin R, Haridas S, Kuo A, Ohm R, Otillar R, Riley R, Salamov A, Zhao X, Korzeniewski F, Smirnova T,
616   Nordberg H, Dubchak I, Shabalov I. 2014. MycoCosm portal: Gearing up for 1000 fungal genomes. *Nucleic Acids Res* **42**.
617   doi:10.1093/nar/gkt1183

618 Grimm D, Wösten HAB. 2018. Mushroom cultivation in the circular economy. *Appl Microbiol Biotechnol*. doi:10.1007/s00253-018-
619   9226-8

620 Gu X, Zhang Z, Huang W. 2005. Rapid evolution of expression and regulatory divergences after yeast gene duplication. *Proc Natl*
621   *Acad Sci U S A* **102**:707–712. doi:10.1073/pnas.0409186102

622 Gyawali R, Upadhyay S, Way J, Lin X. 2017. A family of secretory proteins is associated with different morphotypes in
623   Cryptococcus neoformans. *Appl Environ Microbiol* **83**. doi:10.1128/AEM.02967-16

624 Hou Z, Chen Q, Zhao M, Huang C, Wu X. 2020. Genome-wide characterization of the Zn(II)2Cys6 zinc cluster-encoding gene
625   family in Pleurotus ostreatus and expression analyses of this family during developmental stages and under heat stress. *PeerJ*
626   **2020**:e9336. doi:10.7717/peerj.9336

627 Jones P, Binns D, Chang H-Y, Fraser M, Li W, McAnulla C, McWilliam H, Maslen J, Mitchell A, Nuka G, Pesseat S, Quinn AF,

628 Sangrador-Vegas A, Scheremetjew M, Yong S-Y, Lopez R, Hunter S. 2014. InterProScan 5: genome-scale protein function
629   classification. *Bioinformatics* **30**:1236–40. doi:10.1093/bioinformatics/btu031

630 Jorgensen P, Nishikawa JL, Breitkreutz BJ, Tyers M. 2002. Systematic identification of pathways that couple cell growth and
631   division in yeast. *Science (80-)* **297**:395–400. doi:10.1126/science.1070850

632 Kalvari I, Nawrocki EP, Ontiveros-Palacios N, Argasinska J, Lamkiewicz K, Marz M, Griffiths-Jones S, Toffano-Nioche C,
633   Gautheret D, Weinberg Z, Rivas E, Eddy SR, Finn RD, Bateman A, Petrov AI. 2021. Rfam 14: Expanded coverage of
634   metagenomic, viral and microRNA families. *Nucleic Acids Res* **49**:D192–D200. doi:10.1093/nar/gkaa1047

635 Kamada T, Sano H, Nakazawa T, Nakahori K. 2010. Regulation of fruiting body photomorphogenesis in Coprinopsis cinerea.
636   *Fungal Genet Biol*. doi:10.1016/j.fgb.2010.05.003

637 Kang YJ, Yang DC, Kong L, Hou M, Meng YQ, Wei L, Gao G. 2017. CPC2: A fast and accurate coding potential calculator based
638   on sequence intrinsic features. *Nucleic Acids Res* **45**:W12–W16. doi:10.1093/nar/gkx428

639 Kapusta A, Feschotte C. 2014. Volatile evolution of long noncoding RNA repertoires: Mechanisms and biological implications.
640   *Trends Genet*. doi:10.1016/j.tig.2014.08.004

641 Katoh K, Standley DM. 2013. MAFFT Multiple Sequence Alignment Software Version 7: Improvements in Performance and
642   Usability. *Mol Biol Evol* **30**:772–780. doi:10.1093/molbev/mst010

643 Ke HM, Lee HH, Chan-Yi Ivy Lin, Liu YC, Lu MR, Hsieh JWA, Chang CC, Wu PH, Lu MJ, Li JY, Shang G, Lu RJH, Nagy LG,
644   Chen PY, Kao HW, Tsai IJ. 2020. Mycena genomes resolve the evolution of fungal bioluminescence. *Proc Natl Acad Sci U S A*
645   **117**:31267–31277. doi:10.1073/pnas.2010761117

646 Khan Z, Bloom JS, Amini S, Singh M, Perlman DH, Caudy AA, Kruglyak L. 2012. Quantitative measurement of allele-specific
647   protein expression in a diploid yeast hybrid by LC-MS. *Mol Syst Biol* **8**:602. doi:10.1038/msb.2012.34

648 Kim W, Miguel-Rojas C, Wang J, Townsend JP, Trail F. 2018a. Developmental dynamics of long noncoding RNA expression
649   during sexual fruiting body formation in Fusarium graminearum. *MBio* **9**. doi:10.1128/mBio.01292-18

650 Kim W, Miguel-Rojas C, Wang J, Townsend JP, Trail F. 2018b. Developmental dynamics of long noncoding RNA expression
651   during sexual fruiting body formation in Fusarium graminearum. *MBio* **9**:1–17. doi:10.1128/mBio.01292-18

652 King N, Hittinger CT, Carroll SB. 2003. Evolution of key cell signaling and adhesion protein families predates animal origins.
653   *Science (80-)* **301**:361–363. doi:10.1126/science.1083853

654 Kiss E, Hegedüs B, Virágh M, Varga T, Merényi Z, Kószó T, Bálint B, Prasanna AN, Krizsán K, Kocsubé S, Riquelme M,
655   Takeshita N, Nagy LG. 2019. Comparative genomics reveals the origin of fungal hyphae and multicellularity. *Nat Commun* **10**.
656   doi:10.1038/s41467-019-12085-w

657 Knoll AH. 2011. The Multiple Origins of Complex Multicellularity. *Annu Rev Earth Planet Sci* **39**:217–239.
658   doi:10.1146/annurev.earth.031208.100209

659 Kondrashov FA, Rogozin IB, Wolf YI, Koonin E V. 2002. Selection in the evolution of gene duplications. *Genome Biol* **3**:1–9.
660   doi:10.1186/gb-2002-3-2-research0008

661 Kraakman LS, Griffioen G, Zerp S, Groeneveld P, Thevelein JM, Mager WH, Planta RJ. 1993. Growth-related expression of
662   ribosomal protein genes in Saccharomyces cerevisiae. *MGG Mol Gen Genet* **239**:196–204. doi:10.1007/BF00281618

663 Krizsán K, Almási É, Merényi Z, Sahu N, Virágh M, Kószó T, Mondo S, Kiss B, Bálint B, Kües U, Barry K, Cseklye J, Hegedüs B,
664   Henrissat B, Johnson J, Lipzen A, Ohm RA, Nagy I, Pangilinan J, Yan J, Xiong Y, Grigoriev I V., Hibbett DS, Nagy LG. 2019.
665   Transcriptomic atlas of mushroom development reveals conserved genes behind complex multicellularity in fungi. *Proc Natl*
666   *Acad Sci U S A* **116**:7409–7418. doi:10.1073/pnas.1817822116

667 Kües U, Navarro-González M. 2015. How do Agaricomycetes shape their fruiting bodies? 1. Morphological aspects of development.
668   *Fungal Biol Rev* **29**:63–97. doi:10.1016/j.fbr.2015.05.001

669 Künzler M. 2018. How fungi defend themselves against microbial competitors and animal predators. *PLoS Pathog*.
670   doi:10.1371/journal.ppat.1007184

Lau AYT, Cheng X, Cheng CK, Nong W, Cheung MK, Chan RH-F, Hui JHL, Kwan HS. 2018. Discovery of microRNA-like RNAs during early fruiting body development in the model mushroom Coprinopsis cinerea. *PLoS One* **13**:e0198234. doi:10.1371/journal.pone.0198234

Lau AYT, Xie Y, Cheung MK, Cheung PCK, Kwan HS. 2020. Genome-wide mRNA and miRNA analysis in the early stages of germ tube outgrowth in Coprinopsis cinerea. *Fungal Genet Biol* **142**:103416. doi:10.1016/j.fgb.2020.103416

Lawrence M, Gentleman R, Carey V. 2009. rtracklayer: An R package for interfacing with genome browsers. *Bioinformatics* **25**:1841–1842. doi:10.1093/bioinformatics/btp328

Lawrence M, Huber W, Pagès H, Aboyoun P, Carlson M, Gentleman R, Morgan MT, Carey VJ. 2013. Software for Computing and Annotating Genomic Ranges. *PLoS Comput Biol* **9**:1003118. doi:10.1371/journal.pcbi.1003118

Lee YY, de Ulzurrun GVD, Schwarz EM, Stajich JE, Hsueh YP. 2021. Genome sequence of the oyster mushroom Pleurotus ostreatus strain PC9. *G3 Genes, Genomes, Genet* **11**. doi:10.1093/G3JOURNAL/JKAA008

Li H. 2018. Minimap2: Pairwise alignment for nucleotide sequences. *Bioinformatics* **34**:3094–3100. doi:10.1093/bioinformatics/bty191

Li J, Liu X Bin, Zhao ZW, Yang ZL. 2019. Genetic diversity, core collection and breeding history of Pleurotus ostreatus in China. *Mycoscience* **60**:14–24. doi:10.1016/j.myc.2018.07.002

Liao Y, Smyth GK, Shi W. 2014. FeatureCounts: An efficient general purpose program for assigning sequence reads to genomic features. *Bioinformatics* **30**:923–930. doi:10.1093/bioinformatics/btt656

Liu C, Bi J, Kang L, Zhou J, Liu X, Liu Z, Yuan S. 2021. The molecular mechanism of stipe cell wall extension for mushroom stipe elongation growth. *Fungal Biol Rev*. doi:10.1016/j.fbr.2020.11.001

Liu H, Li Y, Chen D, Qi Z, Wang Q, Wang J, Jiang C, Xu JR. 2017. A-to-I RNA editing is developmentally regulated and generally adaptive for sexual reproduction in Neurospora crassa. *Proc Natl Acad Sci U S A* **114**:E7756--E7765. doi:10.1073/pnas.1702591114

Liu H, Wang Q, He Y, Chen L, Hao C, Jiang C, Li Y, Dai Y, Kang Z, Xu JR. 2016. Genome-wide A-to-I RNA editing in fungi independent of ADAR enzymes. *Genome Res* **26**:499–509. doi:10.1101/gr.199877.115

Liu L, He GJ, Chen L, Zheng J, Chen Y, Shen L, Tian X, Li E, Yang E, Liao G, Wang L. 2018. Genetic basis for coordination of meiosis and sexual structure maturation in cryptococcus neoformans. *Elife* **7**. doi:10.7554/eLife.38683

Lloréns-Rico V, Cano J, Kamminga T, Gil R, Latorre A, Chen WH, Bork P, Glass JI, Serrano L, Lluch-Senar M. 2016. Bacterial antisense RNAs are mainly the product of transcriptional noise. *Sci Adv* **2**:e1501363. doi:10.1126/sciadv.1501363

Löytynoja A. 2014. Phylogeny-aware alignment with PRANKMethods in Molecular Biology (Clifton, N.J.). pp. 155–170. doi:10.1007/978-1-62703-646-7_10

Marisol S-G, Martin R, Faheema K, Torda V, László G. N, David S. H. 2020. Macroevolutionary dynamics of fruiting body forms and nutritional modes in mushroom-forming fungi based on an 8400 species phylogeny.

McManus CJ, Coolon JD, Duff MO, Eipper-Mains J, Graveley BR, Wittkopp PJ. 2010. Regulatory divergence in Drosophila revealed by mRNA-seq. *Genome Res* **20**:816–825. doi:10.1101/gr.102491.109

Medema MH, Blin K, Cimermancic P, De Jager V, Zakrzewski P, Fischbach MA, Weber T, Takano E, Breitling R. 2011. AntiSMASH: Rapid identification, annotation and analysis of secondary metabolite biosynthesis gene clusters in bacterial and fungal genome sequences. *Nucleic Acids Res* **39**:W339--W346. doi:10.1093/nar/gkr466

Merényi Z, Prasanna AN, Wang Z, Kovács K, Hegedüs B, Bálint B, Papp B, Townsend JP, Nagy LG. 2020. Unmatched Level of Molecular Convergence among Deeply Divergent Complex Multicellular Fungi. *Mol Biol Evol* **37**:2228–2240. doi:10.1093/molbev/msaa077

Minh BQ, Schmidt HA, Chernomor O, Schrempf D, Woodhams MD, Von Haeseler A, Lanfear R, Teeling E. 2020. IQ-TREE 2: New Models and Efficient Methods for Phylogenetic Inference in the Genomic Era. *Mol Biol Evol* **37**:1530–1534. doi:10.1093/molbev/msaa015

714 Montanini B, Chen PY, Morselli M, Jaroszewicz A, Lopez D, Martin F, Ottonello S, Pellegrini M. 2014. Non-exhaustive DNA
715   methylation-mediated transposon silencing in the black truffle genome, a complex fungal genome with massive repeat element
716   content. *Genome Biol* **15**:1–16. doi:10.1186/s13059-014-0411-5

717 Muraguchi H, Umezawa K, Niikura M, Yoshida M, Kozaki T, Ishii K, Sakai K, Shimizu M, Nakahori K, Sakamoto Y, Choi C, Ngan
718   CY, Lindquist E, Lipzen A, Tritt A, Haridas S, Barry K, Grigoriev I V., Pukkila PJ. 2015. Strand-specific RNA-seq analyses of
719   fruiting body development in Coprinopsis cinerea. *PLoS One* **10**:1–23. doi:10.1371/journal.pone.0141586

720 Nagy LG. 2018. Many roads to convergence. *Science (80-)* **361**:125–126. doi:10.1126/science.aau3144

721 Nagy LG, Kovács GM, Krizsán K. 2018. Complex multicellularity in fungi: evolutionary convergence, single origin, or both? *Biol
722   Rev* **93**:1778–1794. doi:10.1111/brv.12418

723 Nagy LG, Ohm RA, Kovács GM, Floudas D, Riley R, Gácser A, Sipiczki M, Davis JM, Doty SL, de Hoog GS, Lang BF, Spatafora
724   JW, Martin FM, Grigoriev I V, Hibbett DS. 2014. Latent homology and convergent regulatory evolution underlies the repeated
725   emergence of yeasts. *Nat Commun* **5**:4471. doi:10.1038/ncomms5471

726 Nawrocki EP, Eddy SR. 2013. Infernal 1.1: 100-fold faster RNA homology searches. *Bioinformatics* **29**:2933–2935.
727   doi:10.1093/bioinformatics/btt509

728 Nguyen TA, Cissé OH, Yun Wong J, Zheng P, Hewitt D, Nowrousian M, Stajich JE, Jedd G. 2017. Innovation and constraint
729   leading to complex multicellularity in the Ascomycota. *Nat Commun* **8**:14444. doi:10.1038/ncomms14444

730 Nordberg H, Cantor M, Dusheyko S, Hua S, Poliakov A, Shabalov I, Smirnova T, Grigoriev I V., Dubchak I. 2014. The genome
731   portal of the Department of Energy Joint Genome Institute: 2014 updates. *Nucleic Acids Res* **42**. doi:10.1093/nar/gkt1069

732 Ohga S. 2000. Transcriptional regulation of laccase and cellulase in relation to fruit body formation in the mycelium of Lentinula
733   edodes on a sawdust-based substrate. *Mycoscience* **41**:149–153. doi:10.1007/BF02464324

734 Ohm RA, de Jong JF, de Bekker C, Wösten HAB, Lugones LG. 2011. Transcription factor genes of Schizophyllum commune
735   involved in regulation of mushroom formation. *Mol Microbiol* **81**:1433–1445. doi:10.1111/j.1365-2958.2011.07776.x

736 Ohm RA, De Jong JF, Lugones LG, Aerts A, Kothe E, Stajich JE, De Vries RP, Record E, Levasseur A, Baker SE, Bartholomew
737   KA, Coutinho PM, Erdmann S, Fowler TJ, Gathman AC, Lombard V, Henrissat B, Knabe N, Kües U, Lilly WW, Lindquist E,
738   Lucas S, Magnuson JK, Piumi F, Raudaskoski M, Salamov A, Schmutz J, Schwarze FWMR, Vankuyk PA, Horton JS,
739   Grigoriev I V., Wösten HAB. 2010. Genome sequence of the model mushroom Schizophyllum commune. *Nat Biotechnol
740   ***28**:957–963. doi:10.1038/nbt.1643

741 Pertea G, Pertea M. 2020. GFF Utilities: GffRead and GffCompare. *F1000Research* **9**:304. doi:10.12688/f1000research.23297.2

742 Pertea M, Pertea GM, Antonescu CM, Chang TC, Mendell JT, Salzberg SL. 2015. StringTie enables improved reconstruction of a
743   transcriptome from RNA-seq reads. *Nat Biotechnol* **33**:290–295. doi:10.1038/nbt.3122

744 Pezzella C, Lettera V, Piscitelli A, Giardina P, Sannia G. 2013. Transcriptional analysis of Pleurotus ostreatus laccase genes. *Appl
745   Microbiol Biotechnol* **97**:705–717. doi:10.1007/s00253-012-3980-9

746 R Core Team. 2020. R: A language and environment for statistical computing. R Foundation for Statistical Computing. *Vienna,
747   Austria*. https://www.r-project.org/.

748 Rhind N, Chen Z, Yassour M, Thompson DA, Haas BJ, Habib N, Wapinski I, Roy S, Lin MF, Heiman DI, Young SK, Furuya K,
749   Guo Y, Pidoux A, Chen HM, Robbertse B, Goldberg JM, Aoki K, Bayne EH, Berlin AM, Desjardins CA, Dobbs E, Dukaj L,
750   Fan L, FitzGerald MG, French C, Gujja S, Hansen K, Keifenheim D, Levin JZ, Mosher RA, Müller CA, Pfiffner J, Priest M,
751   Russ C, Smialowska A, Swoboda P, Sykes SM, Vaughn M, Vengrova S, Yoder R, Zeng Q, Allshire R, Baulcombe D, Birren
752   BW, Brown W, Ekwall K, Kellis M, Leatherwood J, Levin H, Margalit H, Martienssen R, Nieduszynski CA, Spatafora JW,
753   Friedman N, Dalgaard JZ, Baumann P, Niki H, Regev A, Nusbaum C. 2011. Comparative functional genomics of the fission
754   yeasts. *Science (80-)* **332**:930–936. doi:10.1126/science.1203357

755 Richter DJ, Fozouni P, Eisen MB, King N. 2018. Gene family innovation, conservation and loss on the animal stem lineage. *Elife* **7**.
756   doi:10.7554/eLife.34226

757 Riley R, Salamov AA, Brown DW, Nagy LG, Floudas D, Held BW, Levasseur A, Lombard V, Morin E, Otillar R, Lindquist EA,

758 Sun H, LaButti KM, Schmutz J, Jabbour D, Luo H, Baker SE, Pisabarro AG, Walton JD, Blanchette RA, Henrissat B, Martin
759   F, Cullen D, Hibbett DS, Grigoriev I V. 2014. Extensive sampling of basidiomycete genomes demonstrates inadequacy of the
760   white-rot/brown-rot paradigm for wood decay fungi. *Proc Natl Acad Sci U S A* **111**:9923–9928. doi:10.1073/pnas.1400592111

761 Robinson MD, McCarthy DJ, Smyth GK. 2010. edgeR: a Bioconductor package for differential expression analysis of digital gene
762   expression data. *Bioinformatics* **26**:139–140. doi:10.1093/bioinformatics/btp616

763 Royse DJ, Baars J, Tan Q. 2017. Current Overview of Mushroom Production in the WorldEdible and Medicinal Mushrooms. John
764   Wiley & Sons, Ltd. pp. 5–13. doi:10.1002/9781119149446.ch2

765 Schliep KP. 2011. phangorn: Phylogenetic analysis in R. *Bioinformatics* **27**:592–593. doi:10.1093/bioinformatics/btq706

766 Sebé-Pedrós A, Degnan BM, Ruiz-Trillo I. 2017. The origin of Metazoa: a unicellular perspective. *Nat Rev Genet* **18**:498–512.
767   doi:10.1038/nrg.2017.21

768 Sebé-Pedrós A, Saudemont B, Chomsky E, Plessier F, Mailhé MP, Renno J, Loe-Mie Y, Lifshitz A, Mukamel Z, Schmutz S,
769   Novault S, Steinmetz PRH, Spitz F, Tanay A, Marlow H. 2018. Cnidarian Cell Type Diversity and Regulation Revealed by
770   Whole-Organism Single-Cell RNA-Seq. *Cell* **173**:1520-1534.e20. doi:10.1016/j.cell.2018.05.019

771 Shao J, Chen H, Yang D, Jiang M, Zhang H, Wu B, Li J, Yuan L, Liu C. 2017. Genome-wide Identification and Characterization of
772   Natural Antisense Transcripts by Strand-specific RNA Sequencing in Ganoderma lucidum. *Sci Rep* **7**:1–15.
773   doi:10.1038/s41598-017-04303-6

774 Shih C-H, Fay JC. 2021. Cis-regulatory variants affect gene expression dynamics in yeast. *bioRxiv* 2021.03.16.435665.
775   doi:10.1101/2021.03.16.435665

776 Sipos G, Prasanna AN, Walter MC, O'Connor E, Bálint B, Krizsán K, Kiss B, Hess J, Varga T, Slot J, Riley R, Bóka B, Rigling D,
777   Barry K, Lee J, Mihaltcheva S, LaButti K, Lipzen A, Waldron R, Moloney NM, Sperisen C, Kredics L, Vágvölgyi C,
778   Patrignani A, Fitzpatrick D, Nagy I, Doyle S, Anderson JB, Grigoriev I V., Güldener U, Münsterkötter M, Nagy LG. 2017.
779   Genome expansion and lineage-specific genetic innovations in the forest pathogenic fungi Armillaria. *Nat Ecol Evol* **1**:1931–
780   1941. doi:10.1038/s41559-017-0347-8

781 Smith JM, Szathmary E. 1995. The Major Transitions in Evolution. New York:W. H. Freeman and Company.

782 Stamatakis A. 2014. RAxML version 8: a tool for phylogenetic analysis and post-analysis of large phylogenies. *Bioinformatics*
783   **30**:1312–3. doi:10.1093/bioinformatics/btu033

784 Steinegger M, Söding J. 2017. MMseqs2 enables sensitive protein sequence searching for the analysis of massive data sets. *Nat*
785   *Biotechnol*. doi:10.1038/nbt.3988

786 Teichert I. 2020. Fungal RNA editing: who, when, and why? *Appl Microbiol Biotechnol*. doi:10.1007/s00253-020-10631-x

787 Teichert I, Dahlmann TA, Kück U, Nowrousian M. 2017. RNA editing during sexual development occurs in distantly related
788   filamentous ascomycetes. *Genome Biol Evol* **9**:855–868. doi:10.1093/gbe/evx052

789 Van Oss SB, Carvunis AR. 2019. De novo gene birth. *PLoS Genet* **15**:e1008160. doi:10.1371/journal.pgen.1008160

790 Varga T, Krizsán K, Földi C, Dima B, Sánchez-García M, Sánchez-Ramírez S, Szöllősi GJ, Szarkándi JG, Papp V, Albert L,
791   Andreopoulos W, Angelini C, Antonín V, Barry KW, Bougher NL, Buchanan P, Buyck B, Bense V, Catcheside P, Chovatia M,
792   Cooper J, Dämon W, Desjardin D, Finy P, Geml J, Haridas S, Hughes K, Justo A, Karasiński D, Kautmanova I, Kiss B,
793   Kocsubé S, Kotiranta H, LaButti KM, Lechner BE, Liimatainen K, Lipzen A, Lukács Z, Mihaltcheva S, Morgado LN,
794   Niskanen T, Noordeloos ME, Ohm RA, Ortiz-Santana B, Ovrebo C, Rácz N, Riley R, Savchenko A, Shiryaev A, Soop K,
795   Spirin V, Szebenyi C, Tomšovský M, Tulloss RE, Uehling J, Grigoriev I V., Vágvölgyi C, Papp T, Martin FM, Miettinen O,
796   Hibbett DS, Nagy LG. 2019. Megaphylogeny resolves global patterns of mushroom evolution. *Nat Ecol Evol* **3**:668–678.
797   doi:10.1038/s41559-019-0834-1

798 Veeneman BA, Shukla S, Dhanasekaran SM, Chinnaiyan AM, Nesvizhskii AI. 2015. Two-pass alignment improves novel splice
799   junction quantification. *Bioinformatics* **32**:btv642. doi:10.1093/bioinformatics/btv642

800 Vonk PJ, Ohm RA. 2021. H3K4me2 ChIP-Seq reveals the epigenetic landscape during mushroom formation and novel
801   developmental regulators of Schizophyllum commune. *Sci Rep* **11**:8178. doi:10.1038/s41598-021-87635-8

802 Wainer-Katsir K, Linial M. 2019. Allele specific expression in human - Genomic makeup and phenotypic implications. *bioRxiv*.
803   doi:10.1101/757997

804 Wang M, Uebbing S, Ellegren H. 2017. Bayesian inference of allele-specific gene expression indicates abundant Cis-regulatory
805   variation in natural flycatcher populations. *Genome Biol Evol* **9**:1266–1279. doi:10.1093/gbe/evx080

806 Wang Z, Jiang Y, Wu H, Xie X, Huang B. 2019. Genome-Wide Identification and Functional Prediction of Long Non-coding RNAs
807   Involved in the Heat Stress Response in Metarhizium robertsii. *Front Microbiol* **10**:1–11. doi:10.3389/fmicb.2019.02336

808 Wood V, Harris MA, McDowall MD, Rutherford K, Vaughan BW, Staines DM, Aslett M, Lock A, Bähler J, Kersey PJ, Oliver SG.
809   2012. PomBase: A comprehensive online resource for fission yeast. *Nucleic Acids Res* **40**:D695–D699. doi:10.1093/nar/gkr853

810 Wu B, Gaskell J, Held BW, Toapanta C, Vuong T, Ahrendt S, Lipzen A, Zhang J, Schilling JS, Master E, Grigoriev I V, Blanchette
811   RA, Cullen D, Hibbett DS. 2018. Substrate-Specific Differential Gene Expression and RNA Editing in the Brown Rot Fungus
812   Fomitopsis pinicola . *Appl Environ Microbiol* **84**:991–1009. doi:10.1128/aem.00991-18

813 Wu B, Gaskell J, Zhang J, Toapanta C, Ahrendt S, Grigoriev I V, Blanchette RA, Schilling JS, Master E, Cullen D, Hibbett DS.
814   2019. Evolution of substrate-specific gene expression and RNA editing in brown rot wood-decaying fungi. *ISME J* **13**:1391–
815   1403. doi:10.1038/s41396-019-0359-2

816 Xie C, Gong W, Zhu Z, Yan L, Hu Z, Peng Y. 2018. Comparative transcriptomics of Pleurotus eryngii reveals blue-light regulation
817   of carbohydrate-active enzymes (CAZymes) expression at primordium differentiated into fruiting body stage. *Genomics*
818   **110**:201–209. doi:10.1016/j.ygeno.2017.09.012

819 Yang Z. 2007. PAML 4: Phylogenetic analysis by maximum likelihood. *Mol Biol Evol* **24**:1586–1591. doi:10.1093/molbev/msm088

820 Zhu W, Hu J, Li Y, Yang B, Guan Y, Xu C, Chen F, Chi J, Bao Y. 2019. Comparative proteomic analysis of pleurotus ostreatus
821   reveals great metabolic differences in the cap and stipe development and the potential role of ca2+ in the primordium
822   differentiation. *Int J Mol Sci* **20**:6317. doi:10.3390/ijms20246317

823 Zhu Y, Luo H, Zhang X, Song J, Sun C, Ji A, Xu J, Chen S. 2014. Abundant and selective RNA-editing events in the medicinal
824   mushroom ganoderma lucidum. *Genetics* **196**:1047–1057. doi:10.1534/genetics.114.161414

Acknowledgements

Data Availability Statement

The RNA-Seq data was deposited in the NCBI's Gene Expression Omnibus (GEO) Archive at www.ncbi.nlm.nih.gov/geo (accession no. GSE176181). Other data used in this study are available on request from the corresponding author.

Supplementary Materials:

Figures S1-S29

Tables S1-S12

837 **Supplementary Figures for**

838 # Gene age predicts the transcriptional landscape of sexual morphogenesis in
839 # multicellular fungi

840

841 Zsolt Merényi, Máté Virágh, Emile Gluck-Thaler, Jason C. Slot, Brigitta Kiss, Torda Varga, András Geösel, Botond
842 Hegedüs, Balázs Bálint, László G. Nagy

843

844 Correspondence to: lnagy@fungenomelab.com

845

846

847 **This PDF file includes:**

848 Figures S1 to S29

849 Captions for Table S1 to S12

850

851 **Other Supplementary Materials for this manuscript include the following:**

852 Tables S1 to S12

853

Figure S1 Sampled developmental stages and tissue types during fruiting body formation of *Pleurotus ostreatus*. a) 'VM' vegetative mycelium b) 'P1' stage 1 primordium; c) 'P3' stage 3 primordium; d) 'YFB' young fruiting body; e) 'FB' fruiting body; f) dashed areas and black arrows show different tissue types 'S' stipe, 'C' cap trama, 'D' dedifferentiated tissue of cap trama, 'L' lamellae, 'V' cuticle. Bars represent 1 mm in a and b, 5 mm in c and d while 1 cm in e-g.
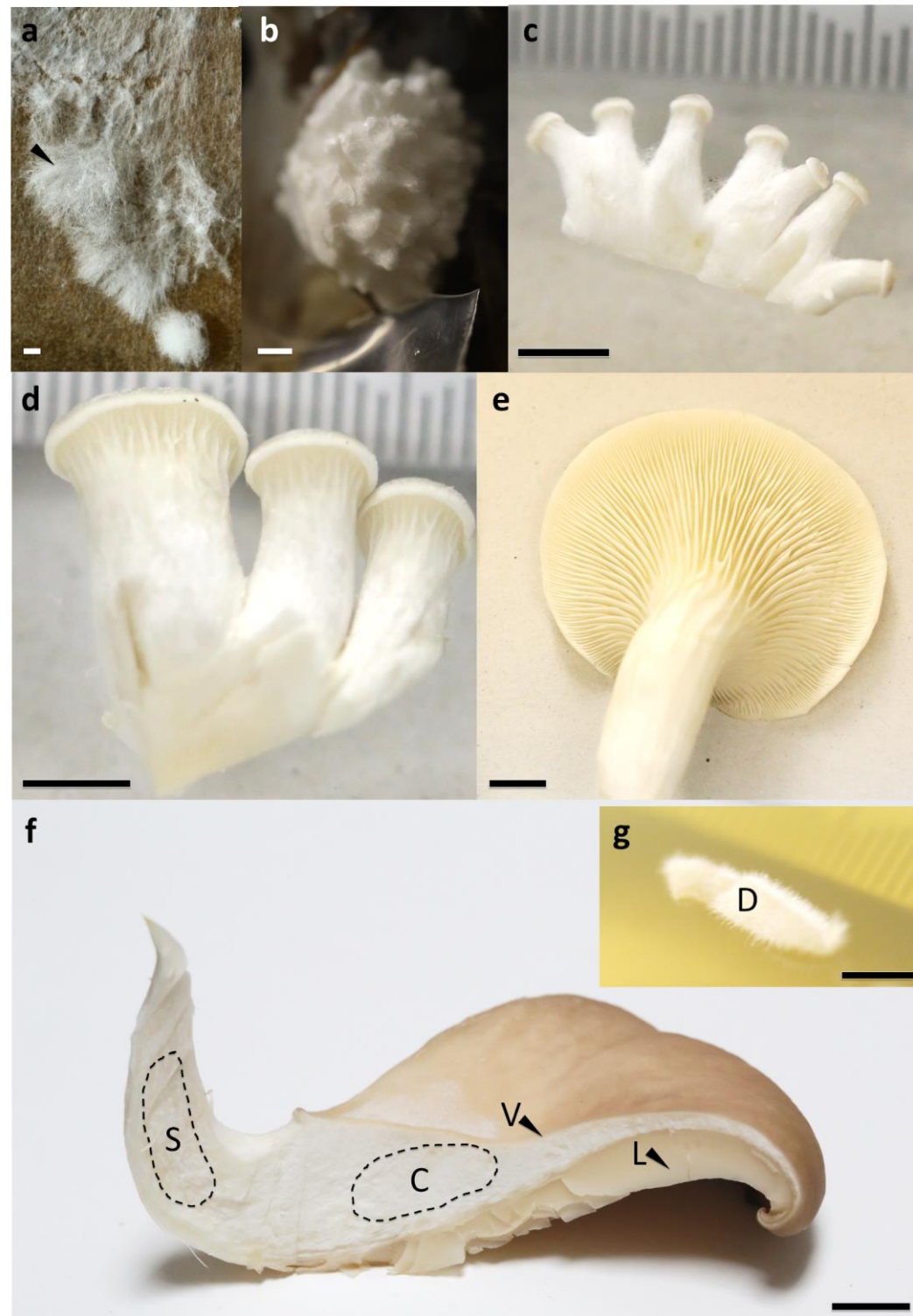
859 **Figure S2** Sampled developmental stages during fruiting body formation of *Pterula gracilis*. a) 'VM' vegetative
860 mycelium; b) 'P' primordium; c) 'YFB' young fruiting body; e) 'FB' fruiting body; Bars represent 1 mm in b-c 5mm in d
861 while 1 cm in a.
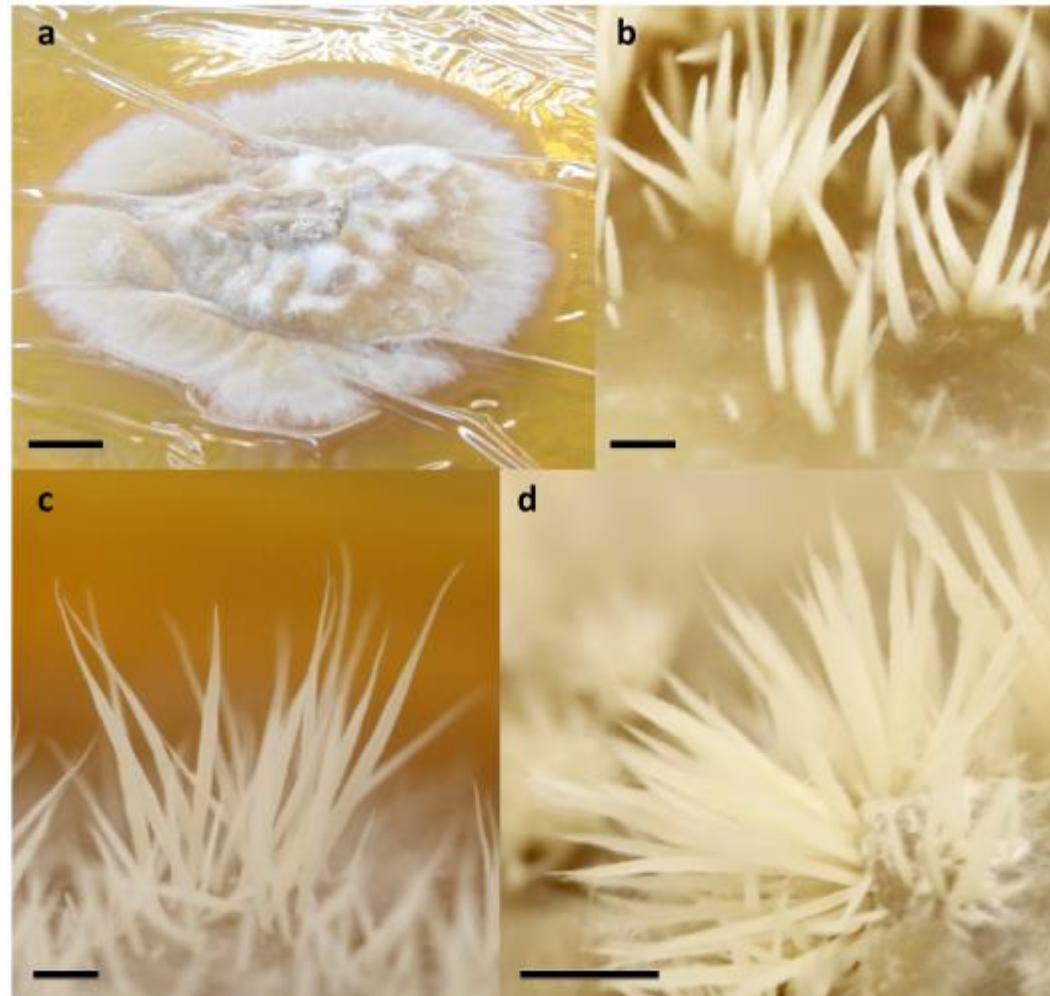
862

863 **Figure S3**: MDS plot based on the expression of genes in a) *Pleurotus ostreatus* and b) *Pterula gracilis*. Abbreviations as
864 follows: 'VM' vegetative mycelium; 'P1' stage 1 primordium; 'P3' stage3 primordium; 'YFB' young fruiting body, 'FB'
865 fruiting body; 'H' cap (entire); 'C' cap trama (only the inner part, without Lamellae, or skin); 'L' lamellae; 'S' stipe; 'V'
866 cuticle; 'D' dedifferentiated tissue of cap.

867
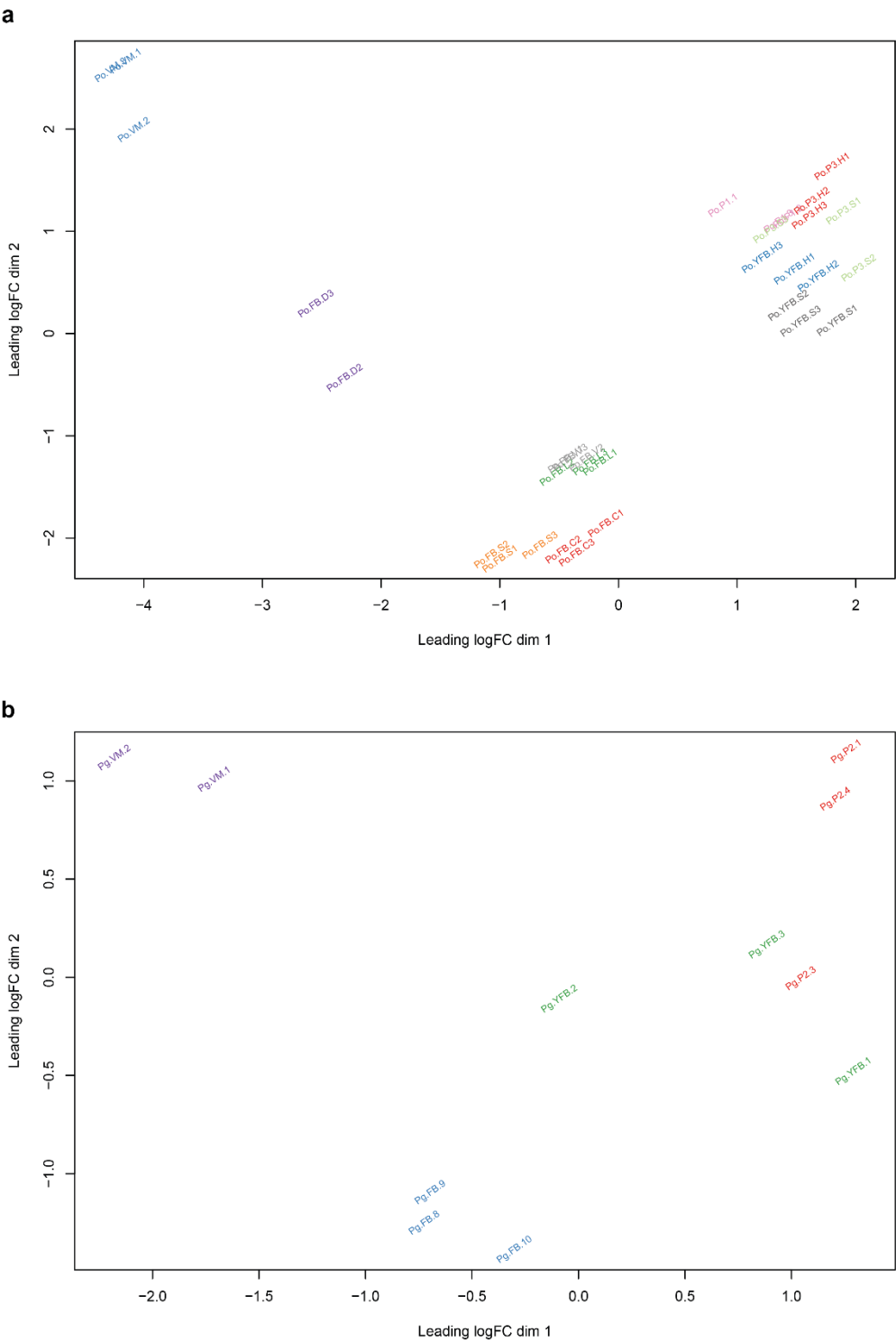
868   **Figure S4**: The distribution of developmentally regulated genes in each species. Abbreviations: NDR not
869   developmentally regulated; >DR2 Developmentally regulated with at least 2 Fold Change; >DR4 Developmentally
870   regulated with at least 4 Fold Change.

871

872
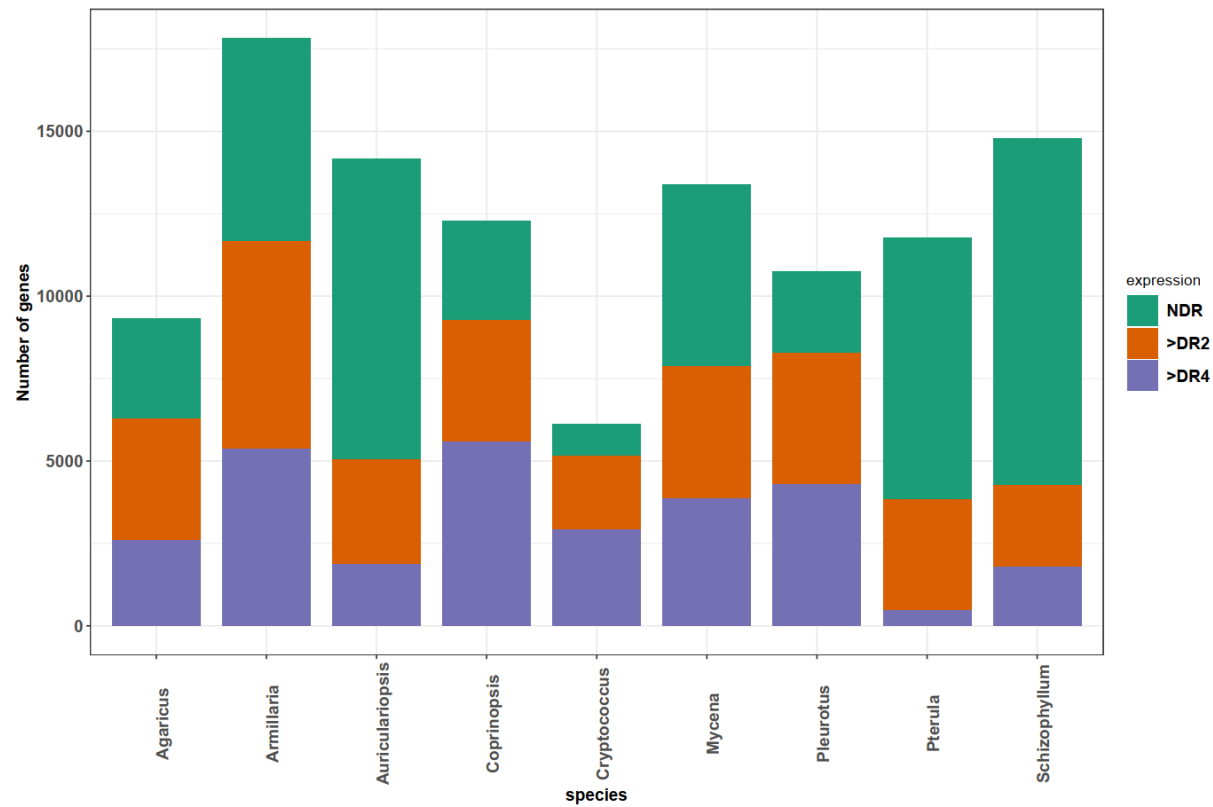
873 **Figure S5**: Transcriptome age index of the different developmental stages of the nine studied fungal species. The mean
874 values of the transcriptome age indexes from three replicates were plotted throughout the development of eight fruiting
875 body forming fungi and through the process of the basidium differentiation of *C. neoformans*. Lower TAI values
876 represent older transcriptomes. We observed an hourglass-like pattern in case of *P. ostreatus*, *M. kentingensis*, *A.*
877 *bisporus*, with stage 3 primordia, young fruiting body, and stage 2 primordia having the lowest TAI values, respectively.
878 No consistent pattern was observed in the remaining six species. Abbreviations: VM: vegetative mycelia, HK: hyphal
879 knot, P1: stage 1 primordia, P2: stage 2 primordia, P3: stage 3 primordia, YFB: young fruiting body, FB: fruiting body.
880 Transcriptome Age Index (TAI) for the nine species.

881

882
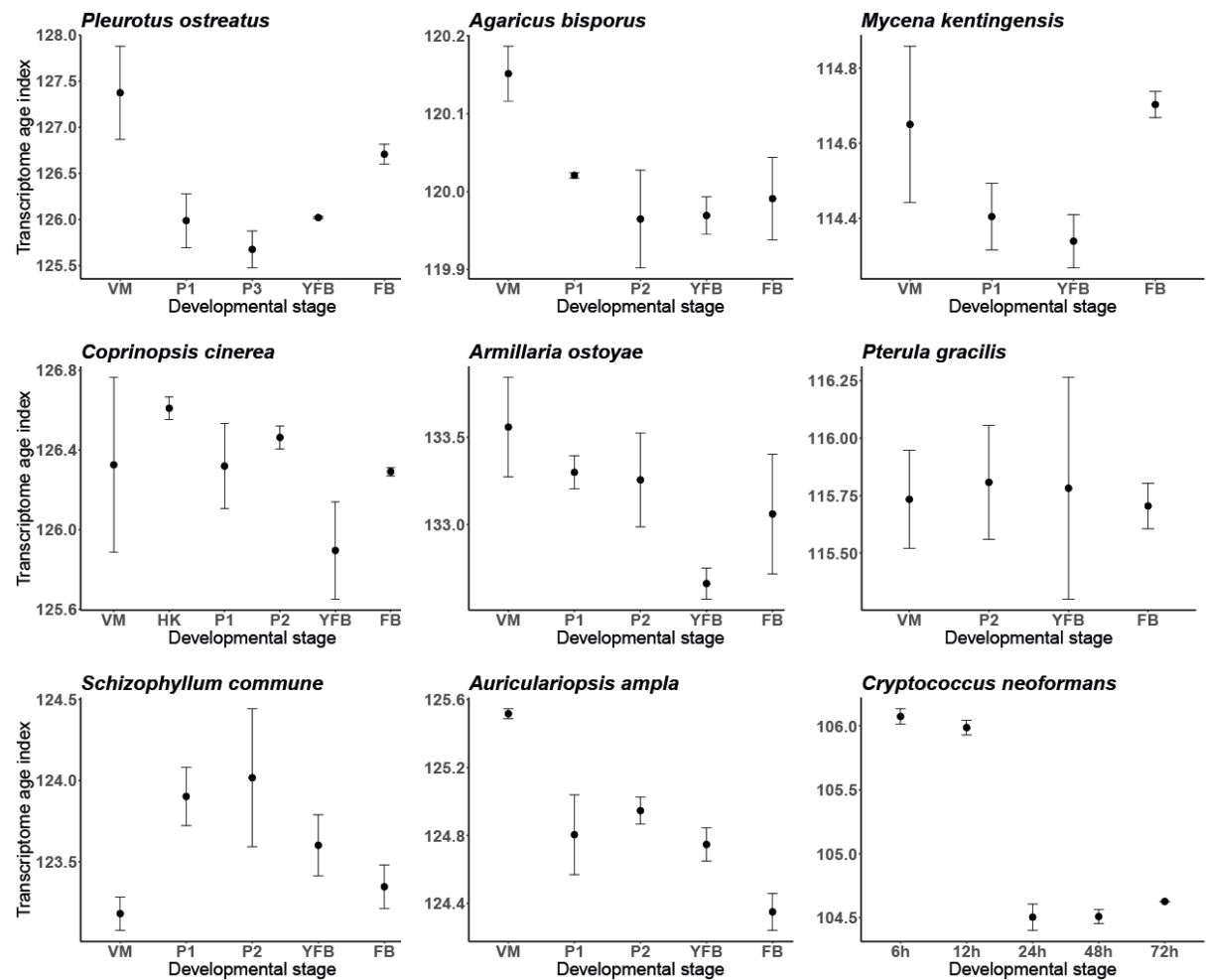
883   **Figure S6**: Developmentally regulated (FBDR) genes occasionally cluster together in genomic 'hotspots'. a) A bar chart
884   summarizing the number of FBDR hotspots detected per genome (total = 153), and the degree of overlap between FBDR
885   hotspots and predicted biosynthetic gene clusters (BGCs). b) A box-and-whisker plot summarizing the distribution of %
886   gene content conservation and the distribution of % FBDR abundance conservation of all 153 hotspots when searched for
887   in genomes other than the one in which they are found. Significance between distributions determined by the Wilcoxon
888   Rank Sum test. c) Scatterplot and linear regression describing relationship between the % gene content conservation and
889   % FBDR abundance conservation of each of the 153 hotspots when searched for in genomes other than the one in which
890   they are found (number of observations = 153 hotspot queries x 8 target genomes). % FBDR abundance conservation may
891   exceed 100% if more FBDR genes are found in target regions as compared with query hotspot. Shaded region around the
892   fitted regression line represents that 95% confidence interval.

893

31
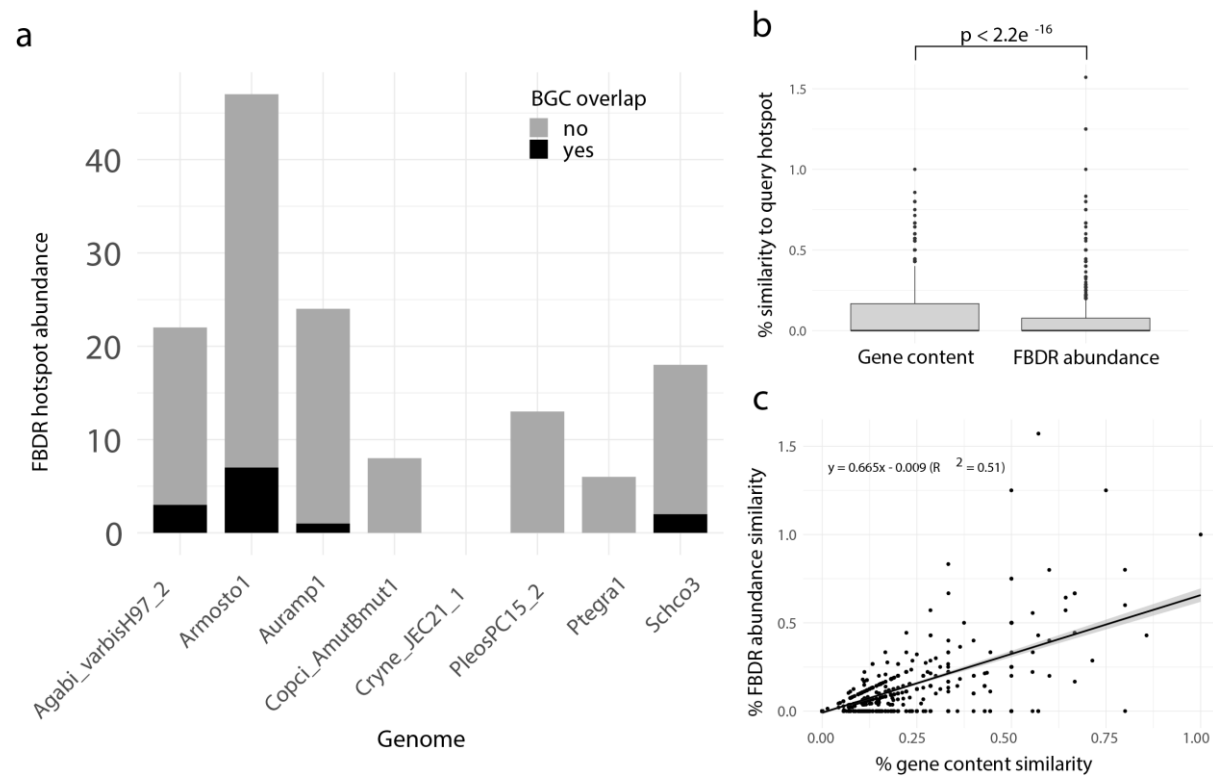
894 **Figure S7**: Principal Component Analysis based on AS ratio. Replicates of stages clustered together and therefore Allele
895 Specific Expression showed a development- and tissue-specific pattern. Abbreviations as follows: 'VM' vegetative
896 mycelium; 'P1' stage 1 primordium; 'P3' stage3 primordium; 'YFB' young fruiting body, 'FB' fruiting body; 'H' cap
897 (entire); 'C' cap trama (only the inner part, without Lamellae, or skin); 'L' lamellae; 'S' stipe; 'V' cuticle; 'D'
898 dedifferentiated tissue of cap.
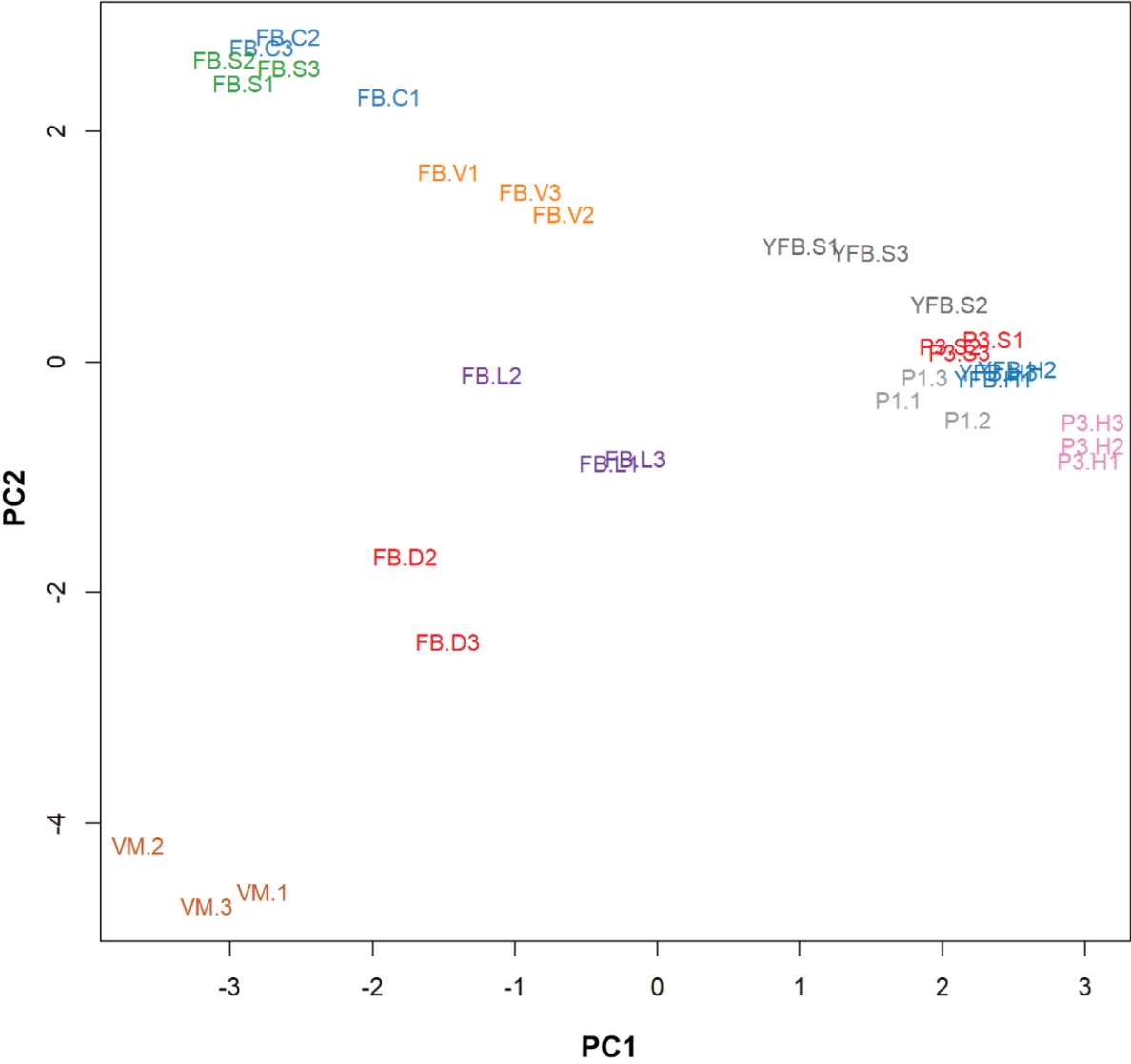
899

Figure S8: Examples for Allele Specific Expression (ASE) patterns during fruiting body formation of *Pleurotus ostreatus*. Gene expressions (log$_2$ transformed FPKM) from the two nuclei are colored with blue (PC9) and red (PC15). *P. ostreatus* gene- and protein-IDs (PleosPC15_2_) are displayed in each plot as a title **a)** a conserved CON6-family sporulation-specific gene. **b)** Mannose-6-phosphate isomerase (IPR016305) **c)** a gene encoding a protein with F-box domain (IPR001810) and Leucine-rich repeat (IPR032675), where expression from PC9 is 'turned off' in mature fruiting bodies. Abbreviations as follows: 'VM' vegetative mycelium; 'P1' stage 1 primordium; 'P3' stage3 primordium; 'YFB' young fruiting body, 'FB' fruiting body; 'H' cap (entire); 'C' cap trama (only the inner part, without Lamellae, or skin); 'L' lamellae; 'S' stipe; 'V' cuticle; 'D' dedifferentiated tissue of cap.

33
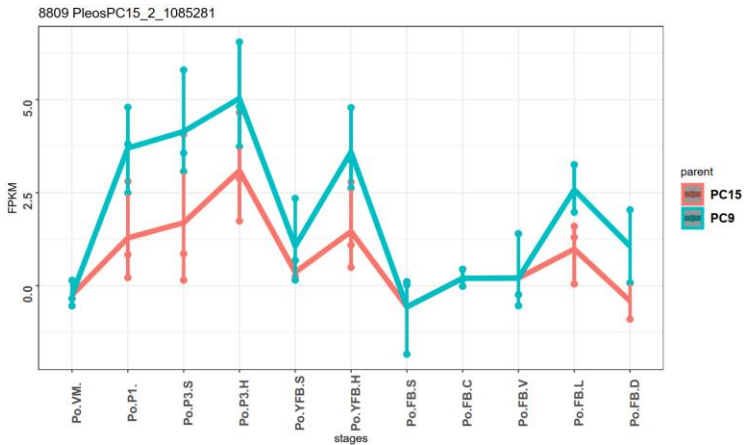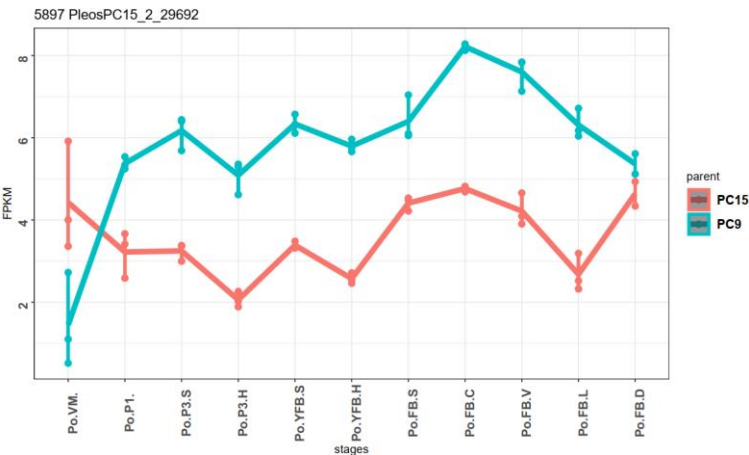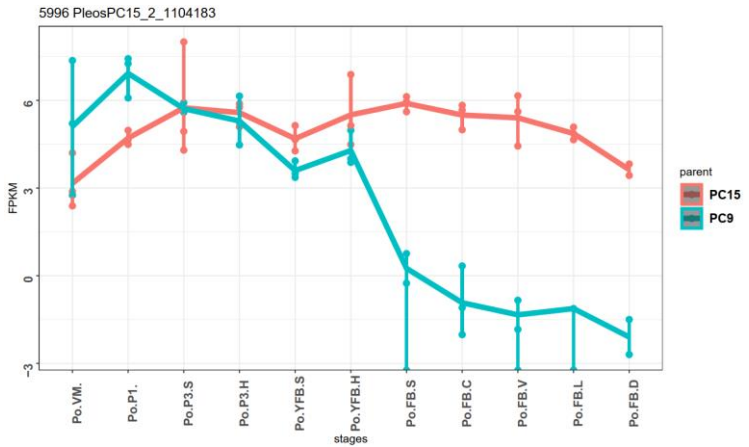
913 **Figure S9:** The Nuclear Read Ratio (NRR, the contribution of nuclei to the total expression) across stages and tissues.
914 Red dots represent the biological replicates separately. A slight dominance of PC9 was observable (mean NRR across
915 samples 0.97; max difference 12.5% Values smaller than 1 mean the dominance of the PC9 nucleus over PC15 while the
916 opposite marks the dominance of PC15. Abbreviations as follows: 'VM' vegetative mycelium; 'P1' stage 1 primordium;
917 'P3' stage3 primordium; 'YFB' young fruiting body, 'FB' fruiting body; 'H' cap (entire); 'C' cap trama (only the inner
918 part, without Lamellae, or skin); 'L' lamellae; 'S' stipe; 'V' cuticle; 'D' dedifferentiated tissue of cap.

919

920
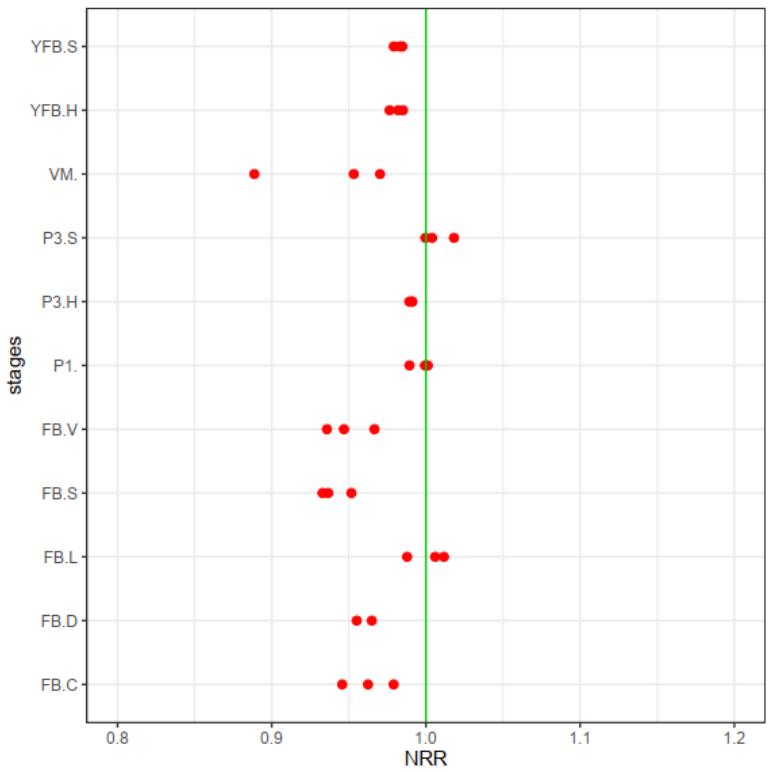
921 **Figure S10:** Chromosomal Read Ratio (CRR, the contribution of nuclei to the expression of scaffolds) across stages and
922 tissues. Red dots represent the biological replicates separately. Only scaffold 12 was consistently biased towards PC9,
923 whereas other scaffolds varied depending on developmental stages and tissue types (CRR min-max=0.62-1.31; max
924 difference 37.2%). Values smaller than 1 mean the dominance of the PC9 nucleus over PC15 while the opposite marks
925 the dominance of PC15. Abbreviations as follows: 'VM' vegetative mycelium; 'P1' stage 1 primordium; 'P3' stage3
926 primordium; 'YFB' young fruiting body, 'FB' fruiting body; 'H' cap (entire); 'C' cap trama (only the inner part, without
927 Lamellae, or skin); 'L' lamellae; 'S' stipe; 'V' cuticle; 'D' dedifferentiated tissue of cap.

928

929

930 **Figure S11**: Gene Ontology (GO) enrichment for ASE genes with minimum two-fold change at least in one stage
931 between the two parental nuclei. KS means the p-value of Kolmogorov-Smirnov test implemented in the R package
932 'topGO'. BP: Biological Process; MF: Molecular Function; CC: Cellular component.

933

934
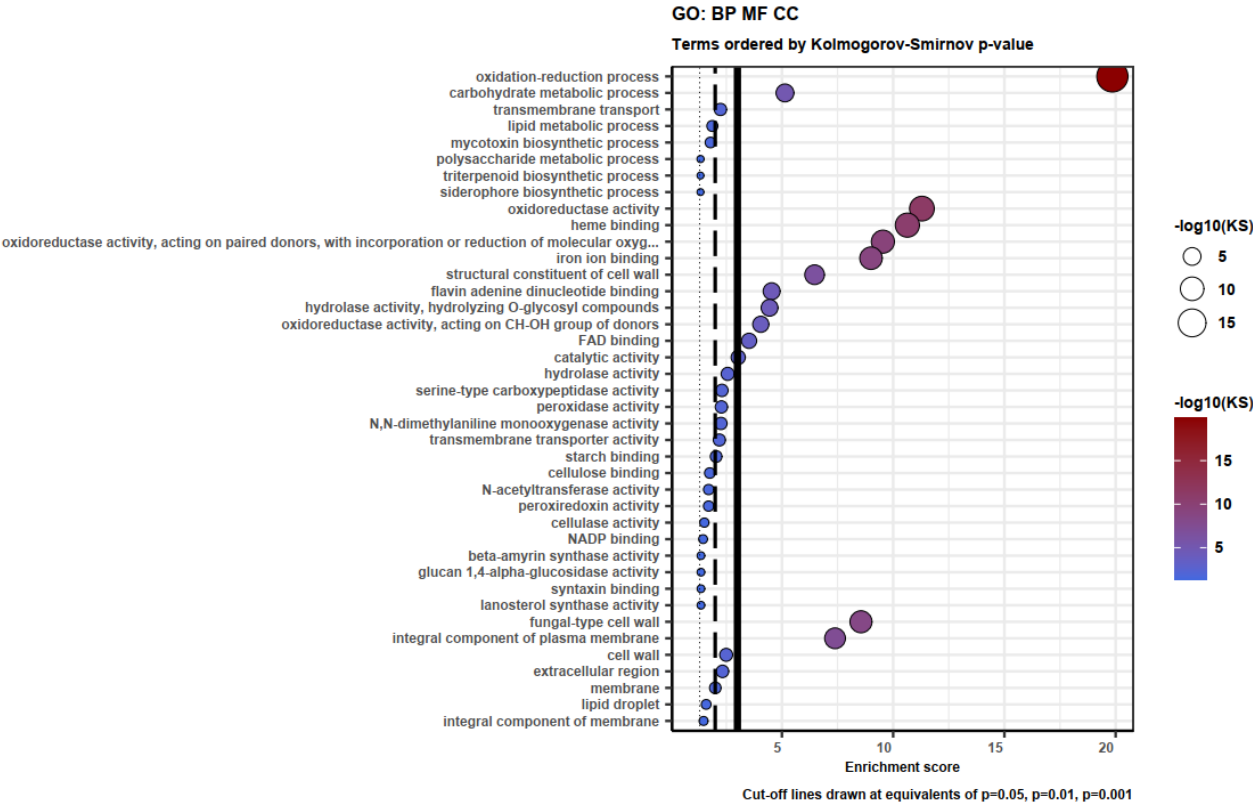
935

936 **Figure S12**: Pipeline of RNA editing and Allele Specific Expression annotation. Abbreviations: VRS Variant Read
937 Support; RS Read Support; RVF Relative Variant Frequency.
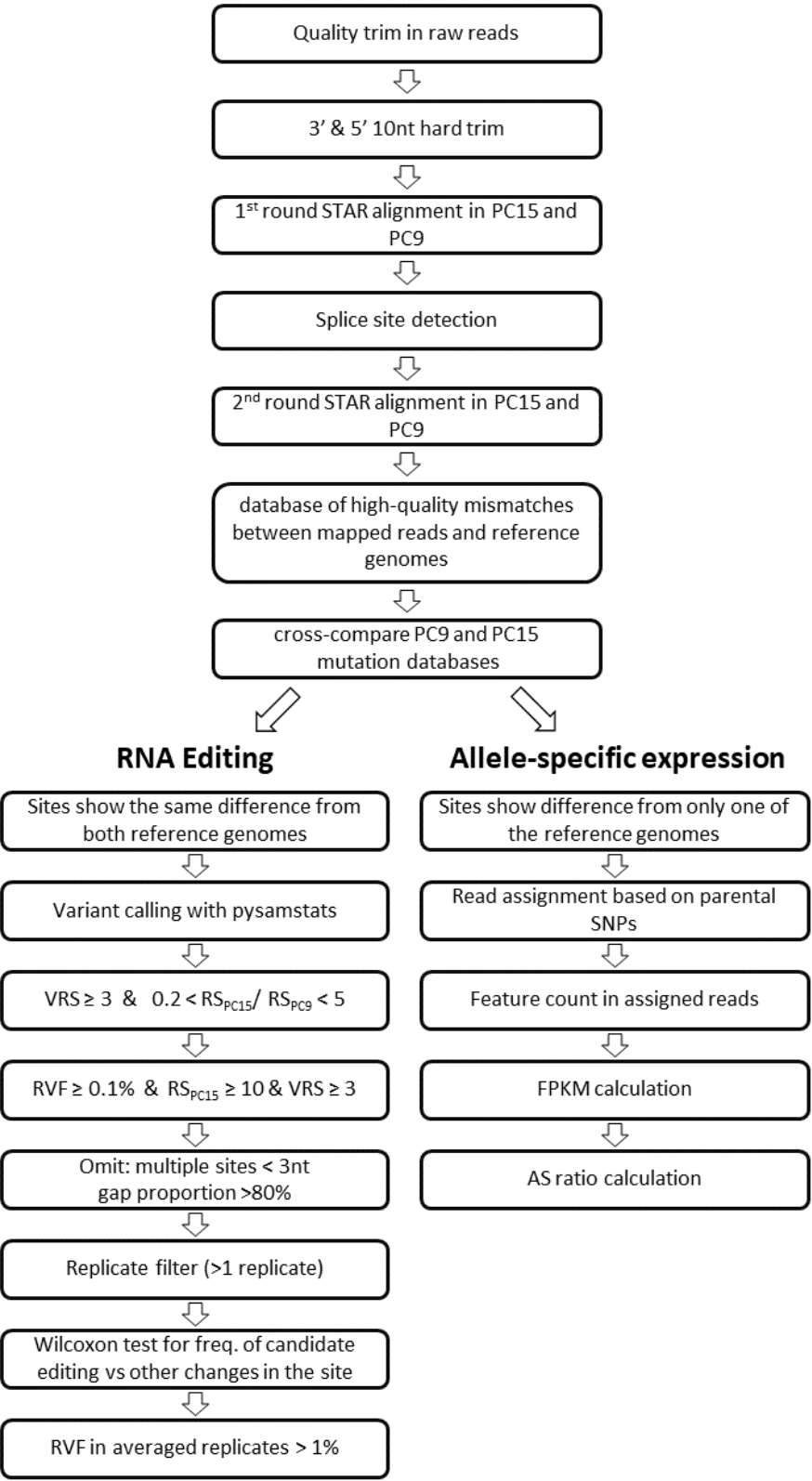
938

939   **Figure S13:** Examples for variants of different types. In a) and b) erroneous read alignment around splice sites causing
940   variants (red arrows) similar to RNA editing. In c) and d) green arrows represent potential RNA editing sites, while
941   yellow arrows represent allele specific SNPs.

942
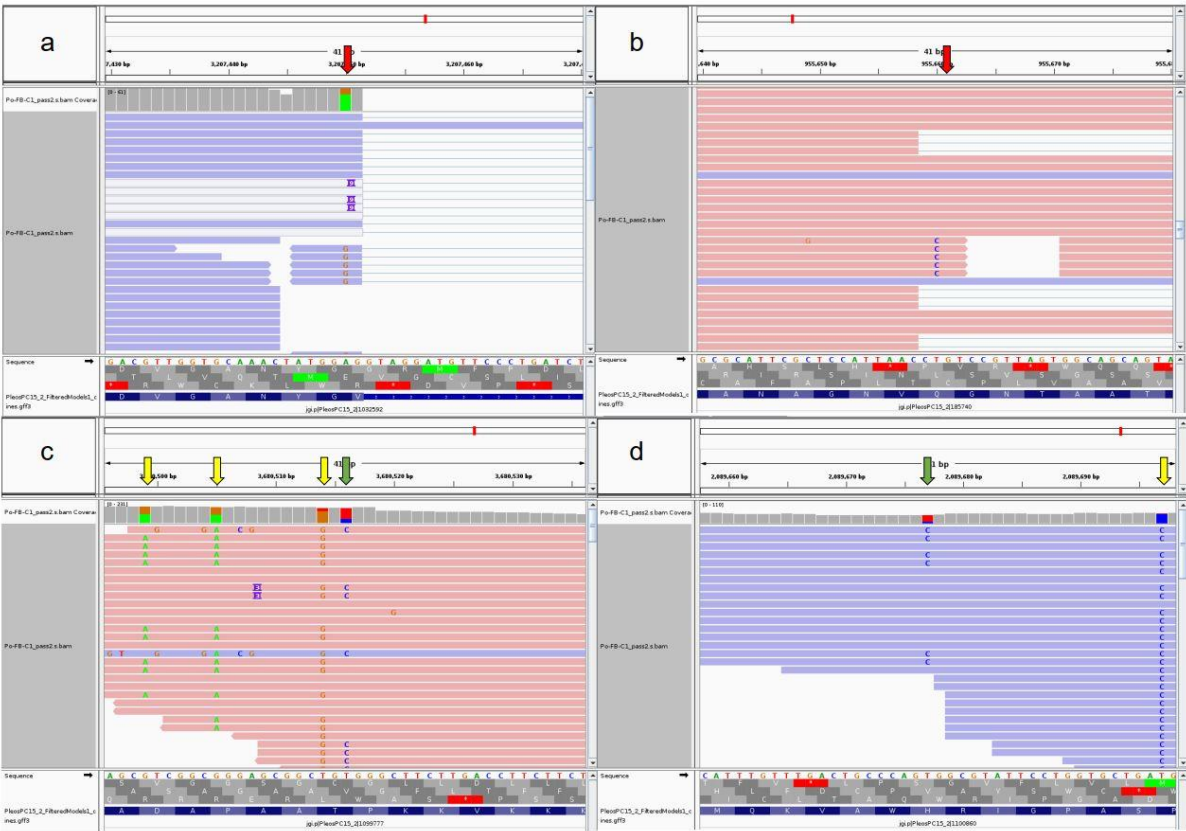
943 **Figure S14**: Sequence motifs surrounding the most frequent candidate RNA editing changes displayed as sequence logos.
944 4th position represents the variants among reads. 1-3 is the upstream 3 positions, while 4-7 is the downstream 3 positions.
945 a) A-to-G b) C-to-A c) C-to-T d) G-to-A e) T-to-C changes.
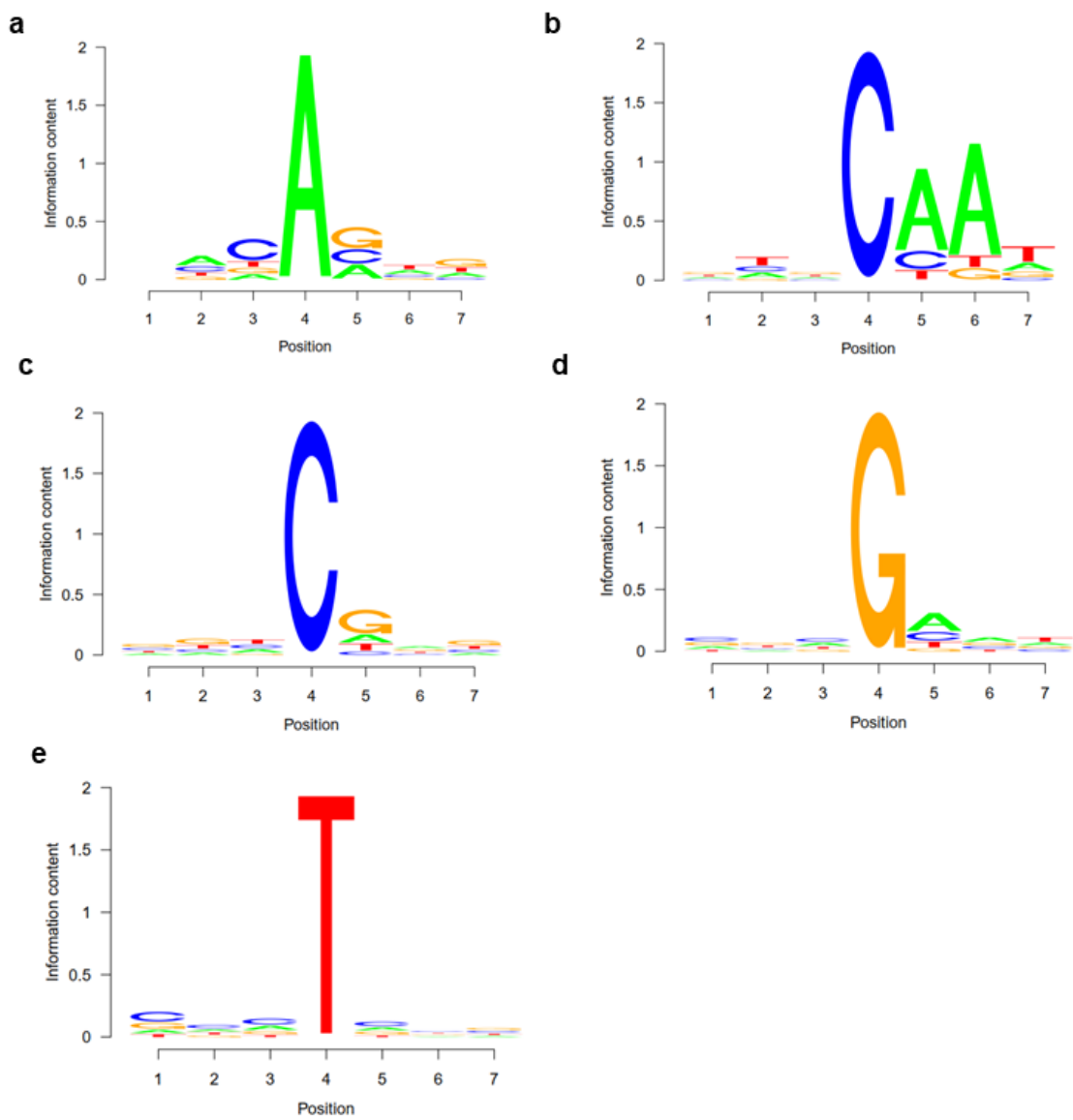
946

947   **Figure S15**: a) Maximum likelihood amino acid distances between PC15 and PC9 proteins (model=WAG). b) dN/dS
948   distribution for the three gene groups under the M0 model in CodeML. Abbreviations: equally expressed genes EE, genes
949   with allele specific expression at least in one stage with two- (S2) or four-fold change (S4). Lines and p-values (<1e-3)
950   represent the pairwise comparison of Nemenyi post-hoc test of Kruskal Wallis test.

951
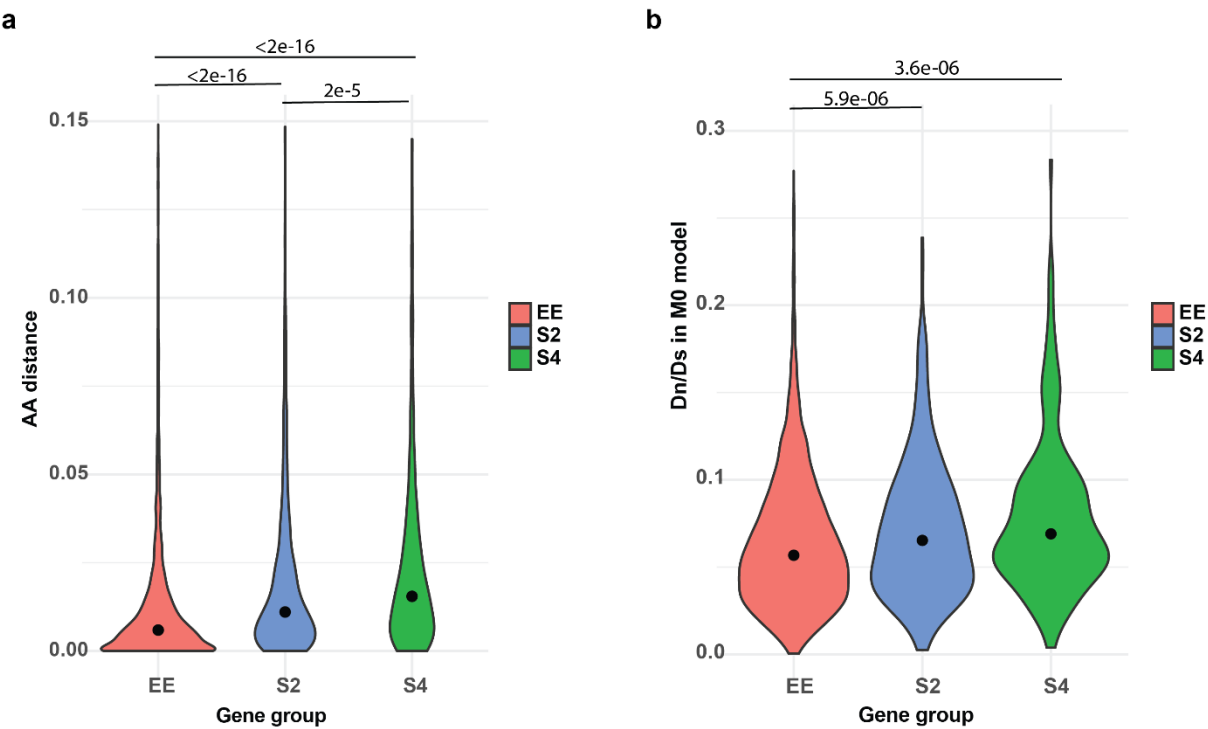
952   **Figure S16**: Proportion of Allele Specific Expression (ASE) shows a significant increasing tendency (Mann-Kendall
953   statistics in the title) across gene ages among developmentally regulated genes (Fold Change >=4). Size of circles
954   represents the number of proteins ($\log_{10}$ transformed).

955
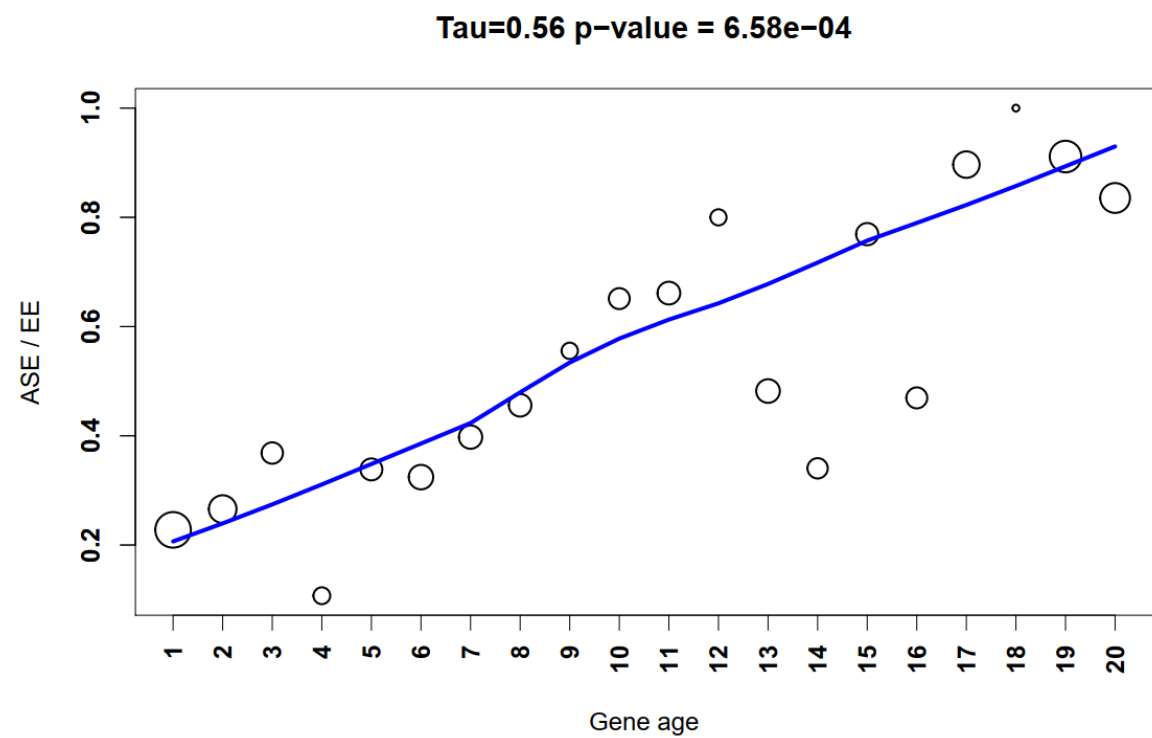
Figure S17: Distribution of genes across gene ages (1 representing oldest and 20 the youngest), broken down by ASE, developmental regulation, and duplication in *Pleurotus ostreatus*. Bars represent proportions of gene numbers relative to the total gene number of a group (equal, S2 or S4). Abbreviations: equal – equally expressed genes; S2 – ASE with two-fold change; S4 –ASE with four-fold change; NDR – non-developmentally regulated gene DR – developmentally regulated gene.
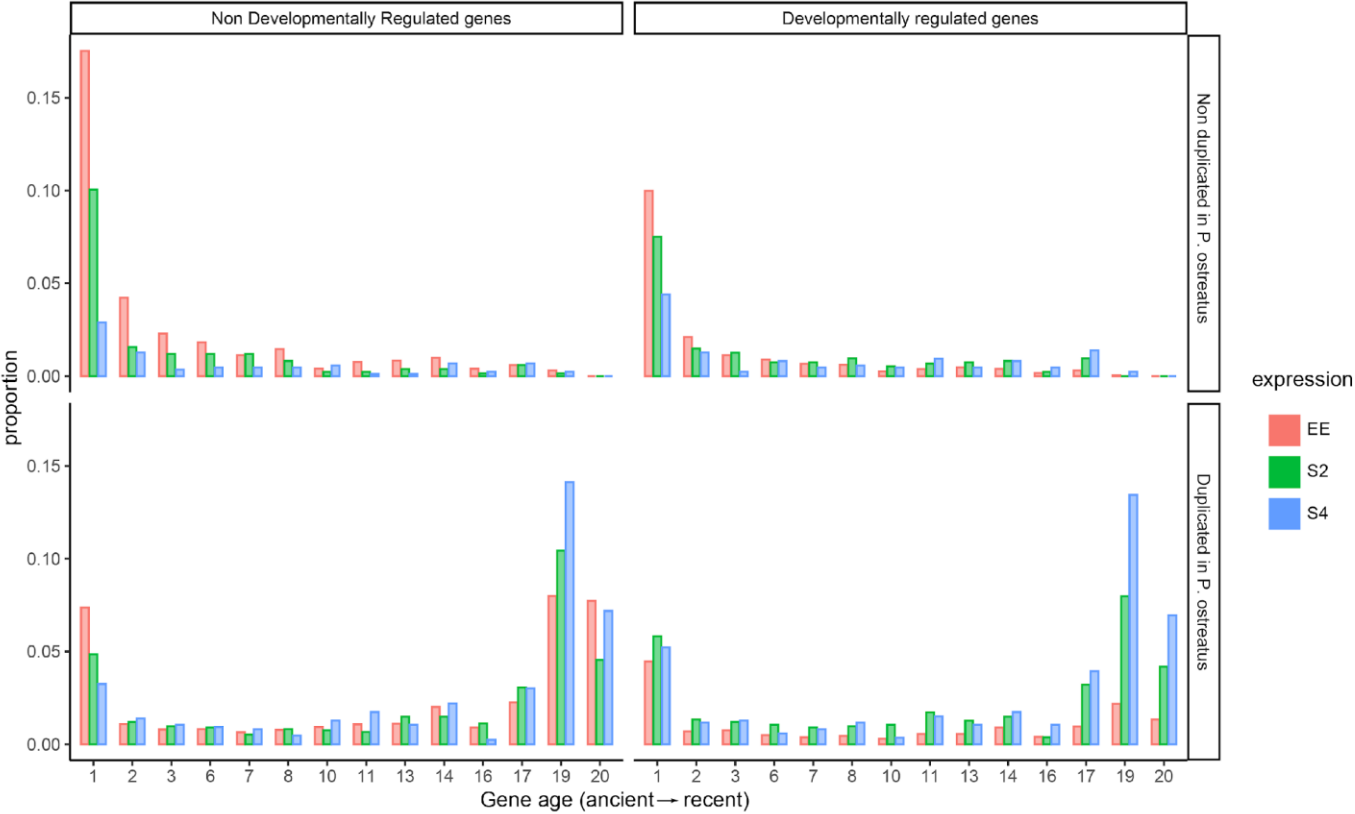
962   **Figure S18**: Pipeline of Natural Antisense Transcripts. Numbers represent the retained transcripts in each filtering step.

963

P. ostreatus   *P. gracilis*

7607	In repeat masked region	3011
7556	Non-structural RNA	3008
2228	Minimal expression filter	777
2086	UTR filter	763
2043	avg FPKM >= 2 of min one stage/tissue	763
939	Non-coding	312

964

43

965
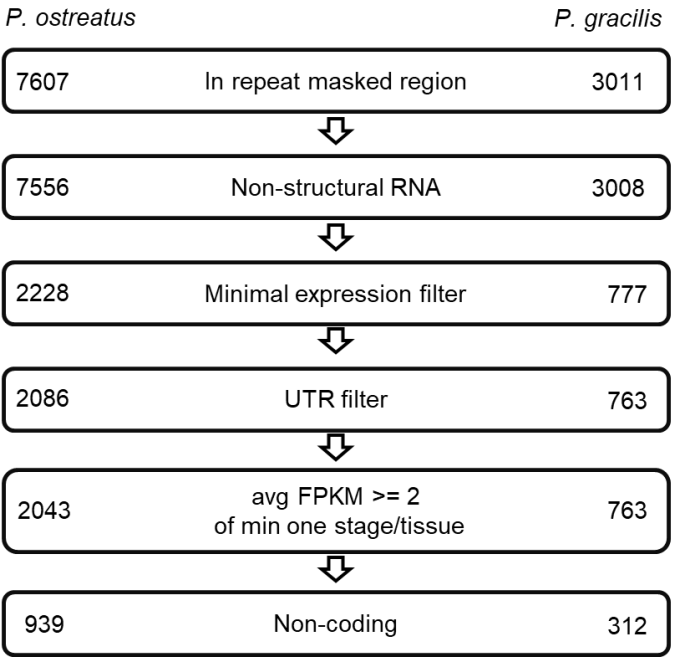
Figure S19: Length (a/b) and exon (c/d) number distribution of natural antisense transcripts in *Pleurotus ostreatus* (a/c) and *Pterula gracilis* (b/d). NATs were divided into putatively coding and noncoding categories using the default settings of CPC2 (Kang et al., 2017)
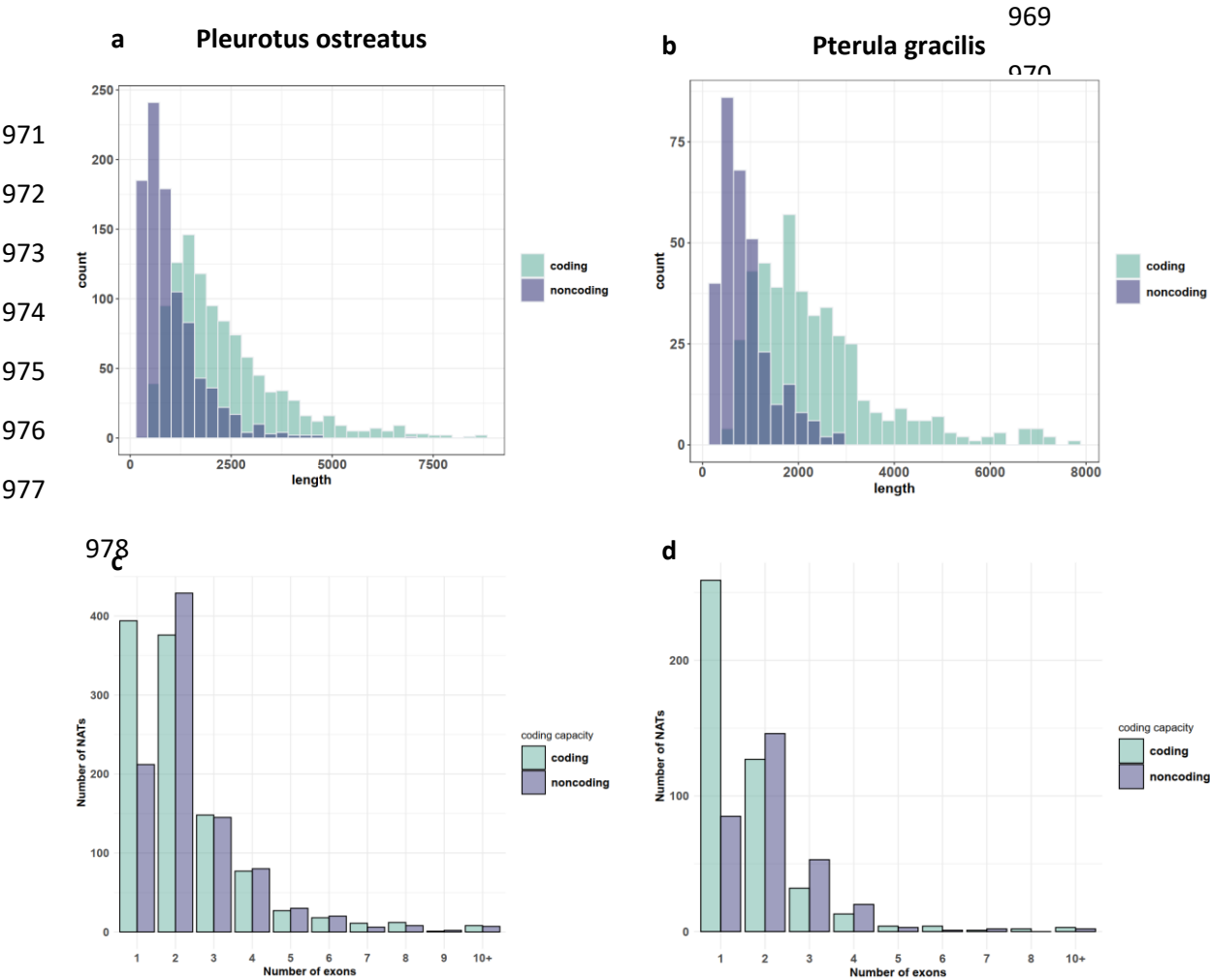
980 **Figure S20**: Principal Component Analysis (PCA) plot based on the expression of Natural Antisense Transcripts detected

981 in a) *Pleurotus ostreatus* and b) *Pterula gracilis*. Abbreviations as follows: 'VM' vegetative mycelium; 'P1' stage 1

982 primordium; 'P3' stage3 primordium; 'YFB' young fruiting body, 'FB' fruiting body; 'H' cap (entire); 'C' cap trama

983 (only the inner part, without Lamellae, or skin); 'L' lamellae; 'S' stipe; 'V' cuticle; 'D' dedifferentiated tissue of cap.
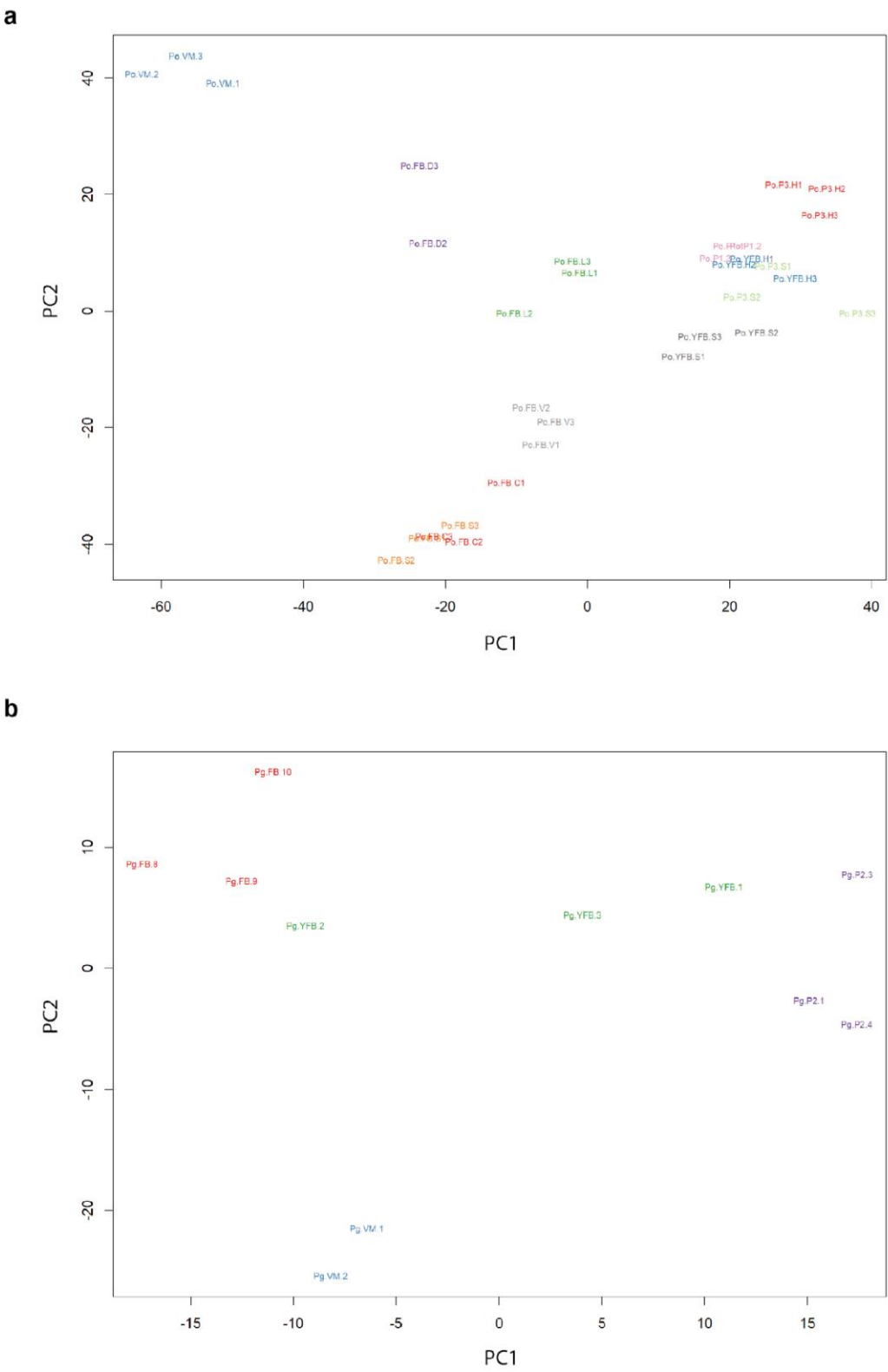

984

985 **Figure S21:** Conservation of sense genes and their antisense transcripts (NAT) in *Pterula gracilis*. a) similarity of sense
986 transcripts measured with –log10(e-value) from MMSeq2 search b) mapping score of antisense transcripts based on
987 Minimap2. Warmer color represents a higher similarity according to the scales

988
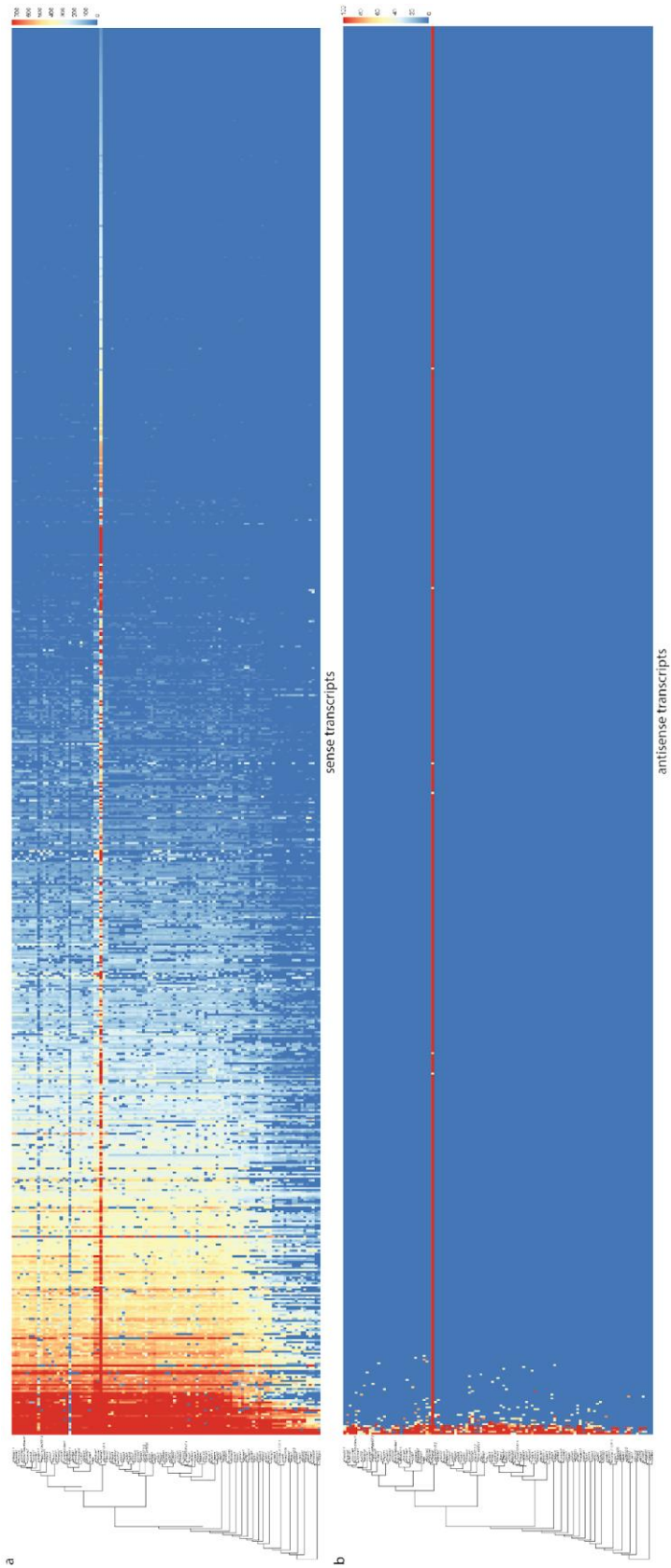
989 **Figure S22**: Expression pattern of 263 sense transcripts and their antisense transcripts which showed significant positive
990 correlation (Pearson r ≥ 0.7, p < 0.05) in *Pleurotus ostreatus*. Abbreviations as follows: 'VM' vegetative mycelium; 'P1'
991 stage 1 primordium; 'P3' stage3 primordium; 'YFB' young fruiting body, 'FB' fruiting body; 'H' cap (entire); 'C' cap
992 trama (only the inner part, without Lamellae, or skin); 'L' lamellae; 'S' stipe; 'V' cuticle; 'D' dedifferentiated tissue of
993 cap.

994
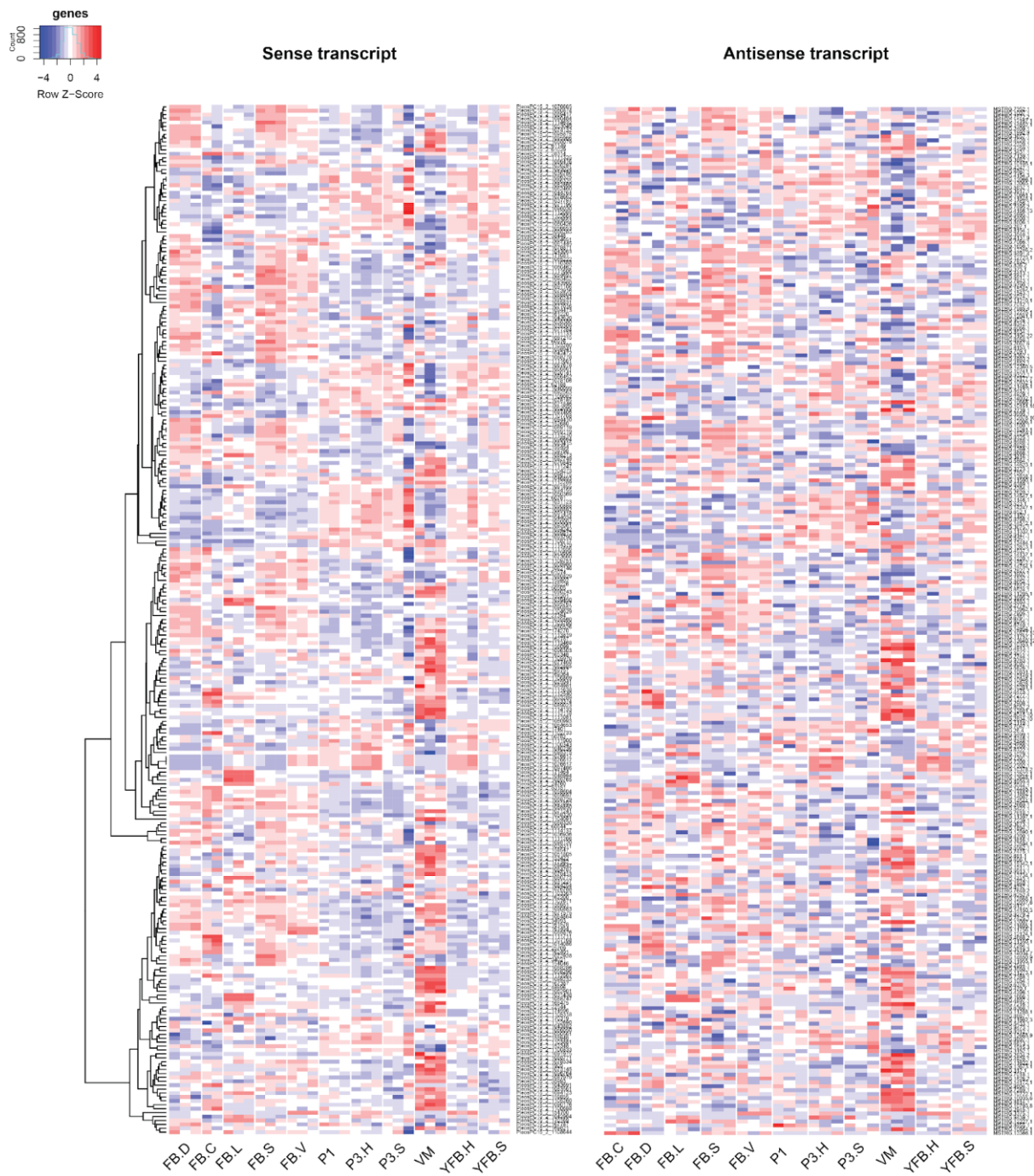
995 **Figure S23:** Permutation test for the number of a) negative (r<-0.7, P<0.05) and b) positive (r>0.7, P<0.05) correlations
996 among the expression of NATs and random genes. Red line represents the observed number of significant correlations.

997

1006
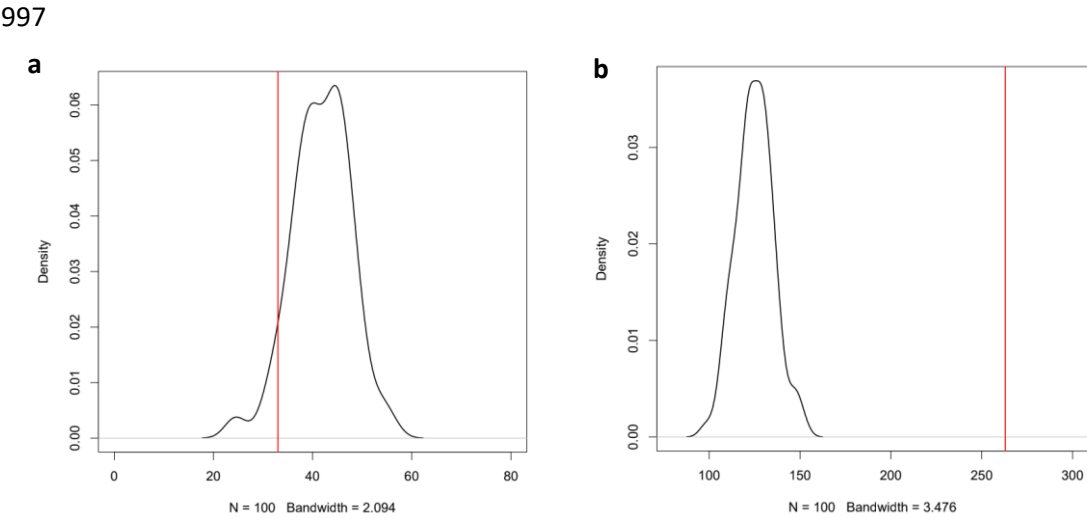
1007 **Figure S24:** Expression pattern of 33 sense transcripts and their antisense transcripts which showed significant negative
1008 correlation (Pearson r ≤ -0.7 p<0.05) in *Pleurotus ostreatus*. Abbreviations as follows: 'VM' vegetative mycelium; 'P1'
1009 stage 1 primordium; 'P3' stage3 primordium; 'YFB' young fruiting body, 'FB' fruiting body; 'H' cap (entire); 'C' cap
1010 trama (only the inner part, without Lamellae, or skin); 'L' lamellae; 'S' stipe; 'V' cuticle; 'D' dedifferentiated tissue of
1011 cap.

1012

1013

48
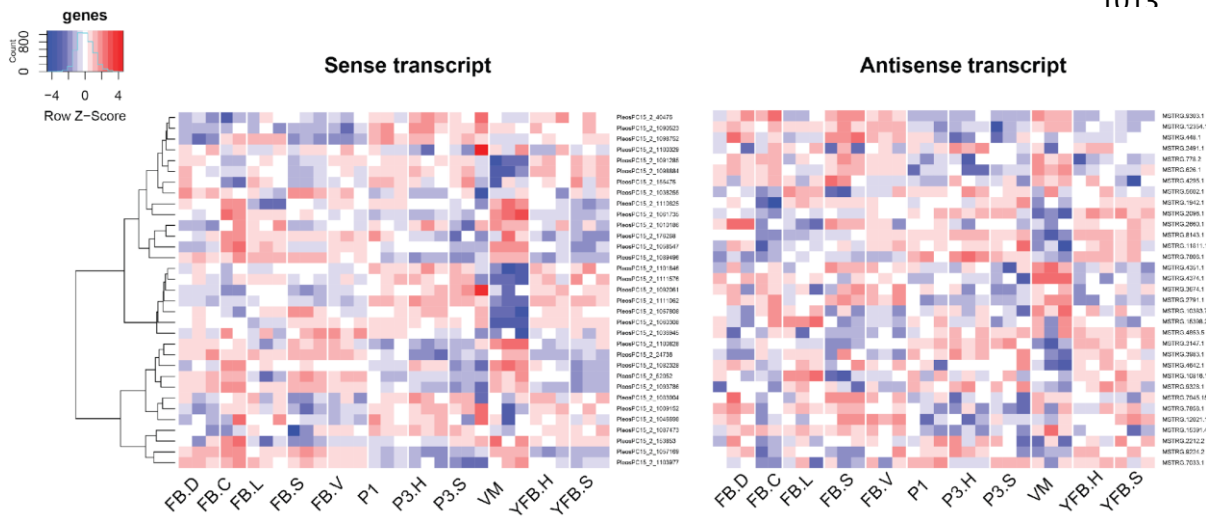
1014 **Figure S25**: Gene Ontology (GO) enrichment for genes which have Natural Antisense Transcripts a) in *Pleurotus*
1015 *ostreatus* and b) in *Pterula gracilis.* KS means the p-value of Kolmogorov-Smirnov test implemented in the R package
1016 'topGO'. BP: Biological Process; MF: Molecular Function; CC: Cellular component.

1017
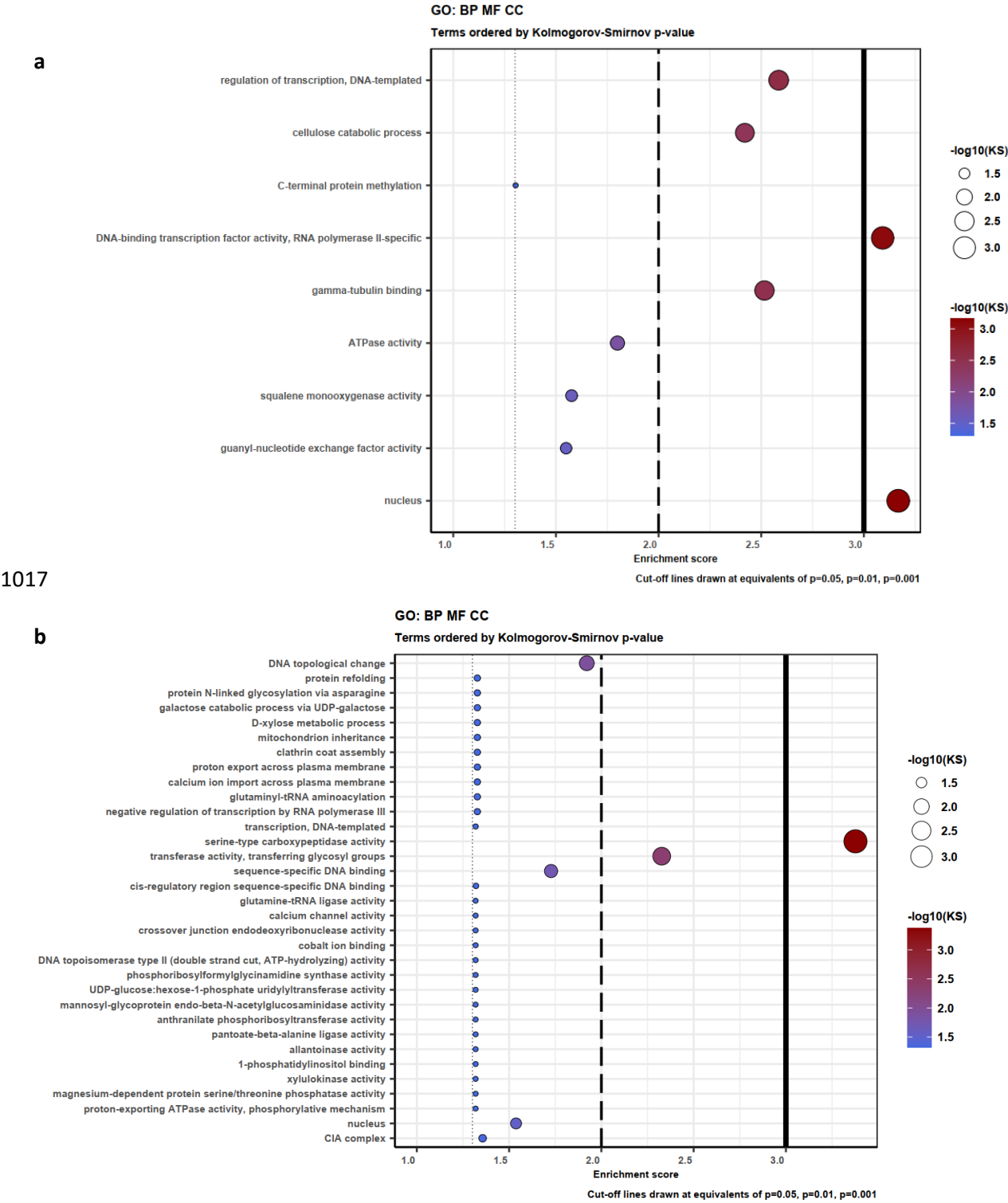
Figure S26: Proportion of Developmentally regulated (DR > 4 FC) genes in different gene ages. P-values and odds ratio above bars comes from Fisher exact test, added only when significant (p<0.05).
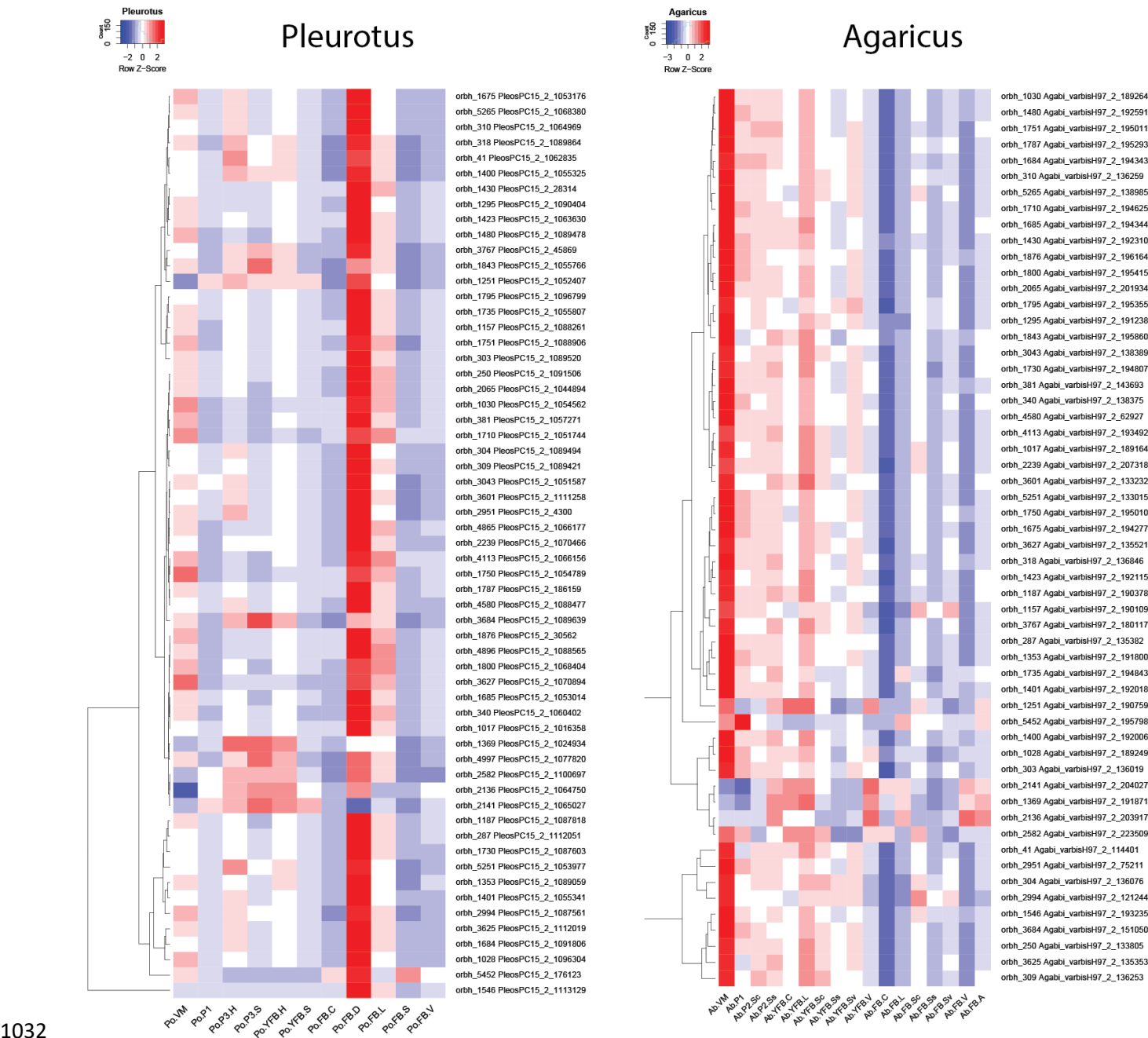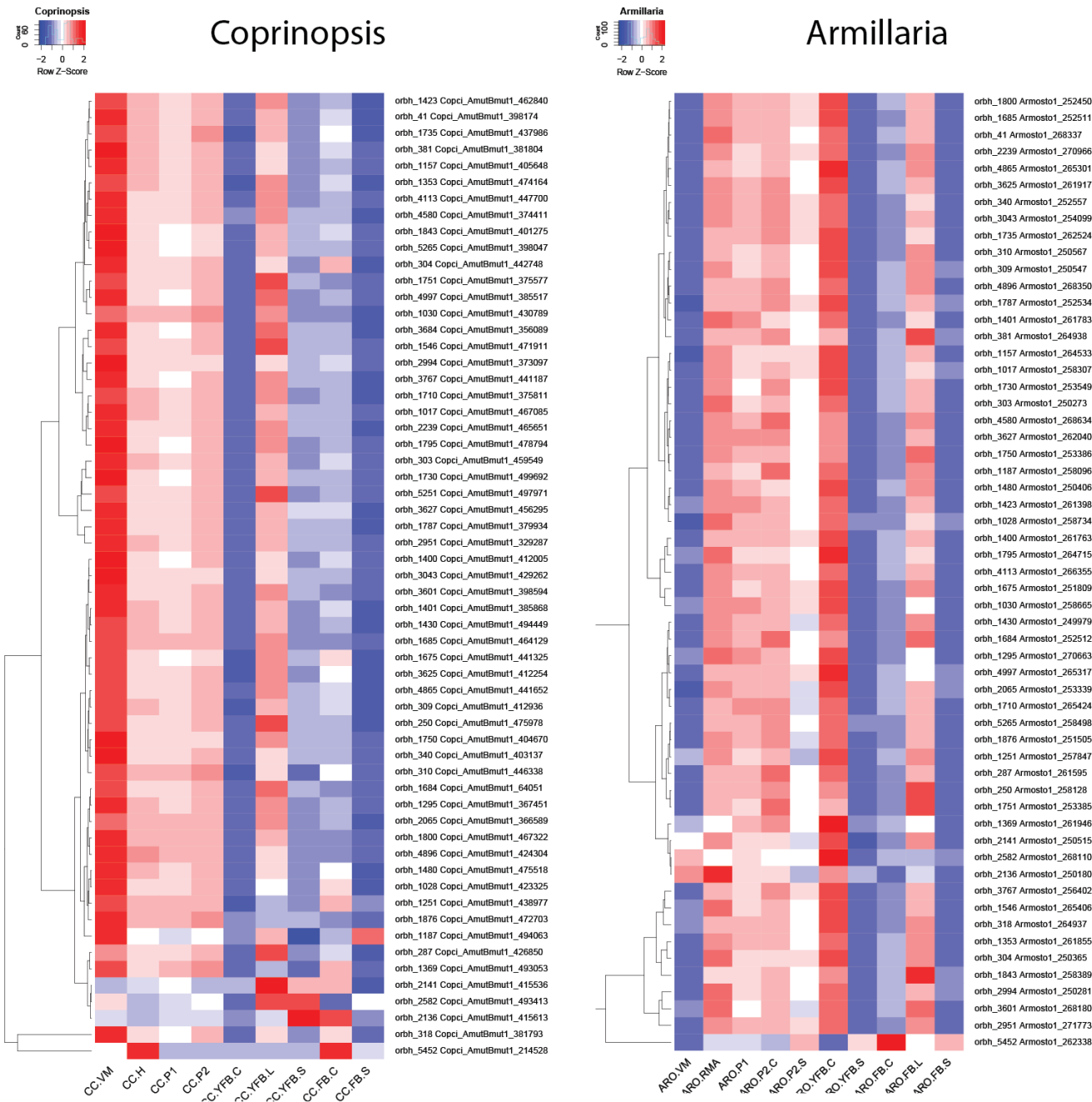
1022
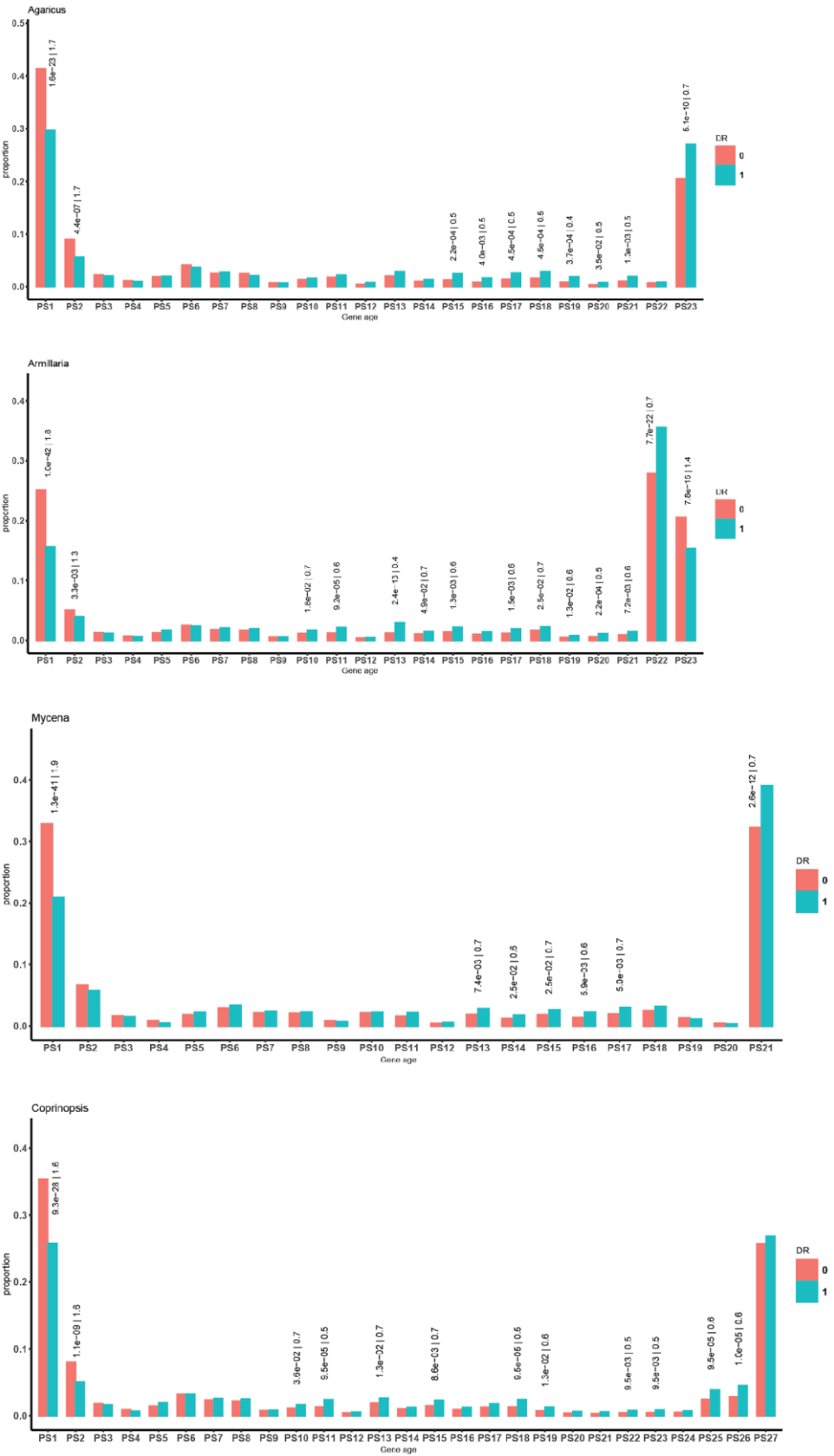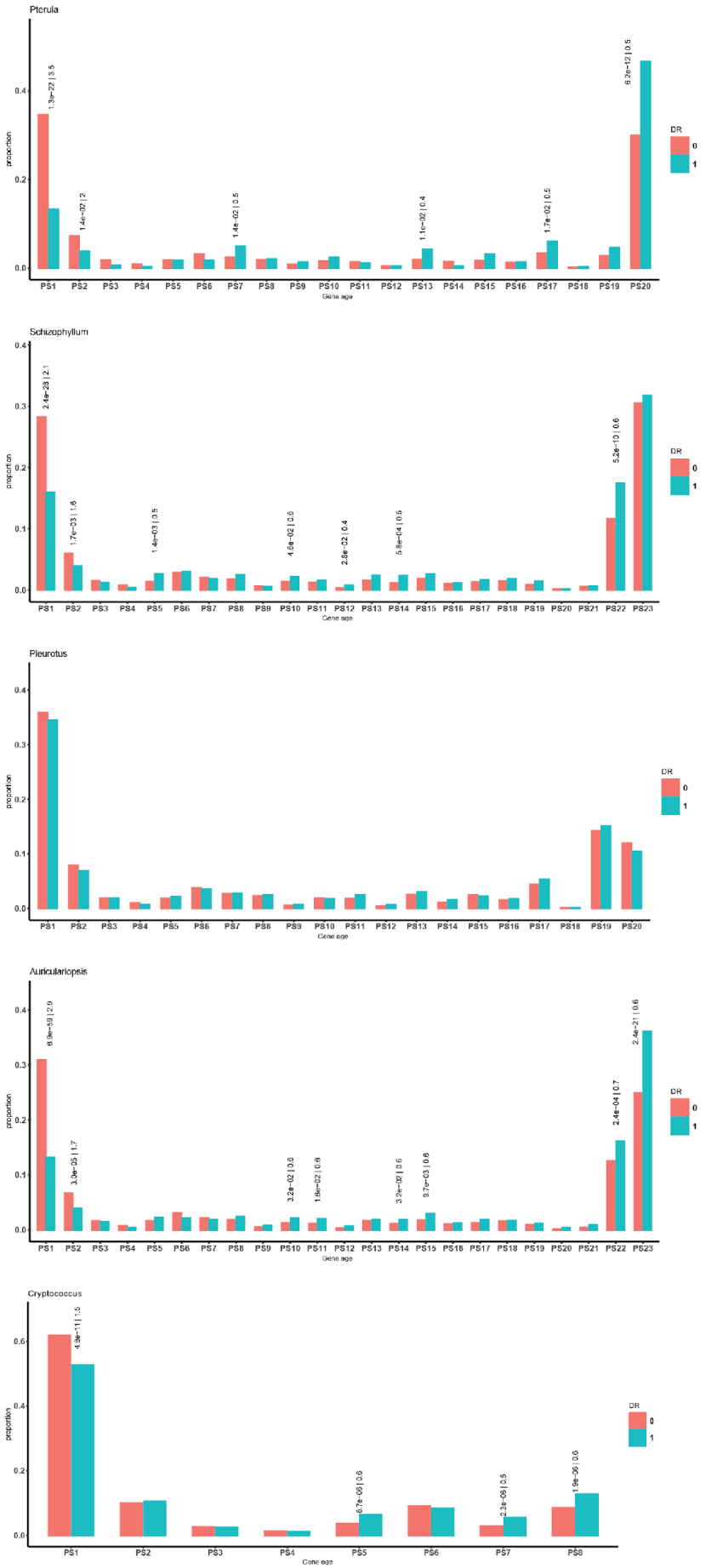
1023   **Figure S27**: Expression of meiotic genes in the nine species. Abbreviations as follows: 'VM' vegetative mycelium; 'P1'
1024   stage 1 primordium; 'P3' stage3 primordium; 'YFB' young fruiting body, 'FB' fruiting body; 'H' cap (entire); 'C' cap
1025   trama (only the inner part, without Lamellae, or skin); 'L' lamellae; 'S' stipe; 'V' cuticle; 'D' dedifferentiated tissue of
1026   cap 'A' annulus. For stage details see Table S10.
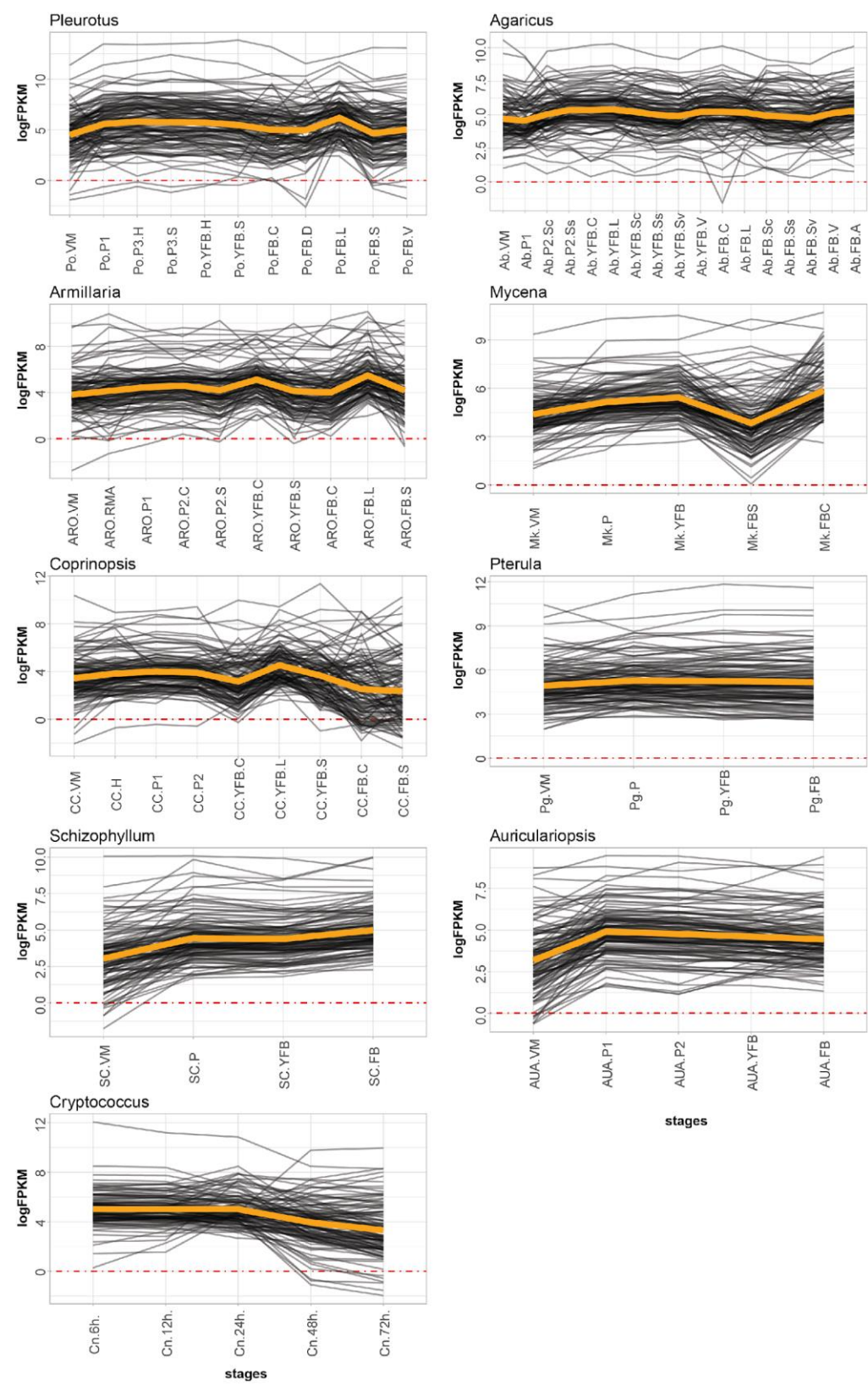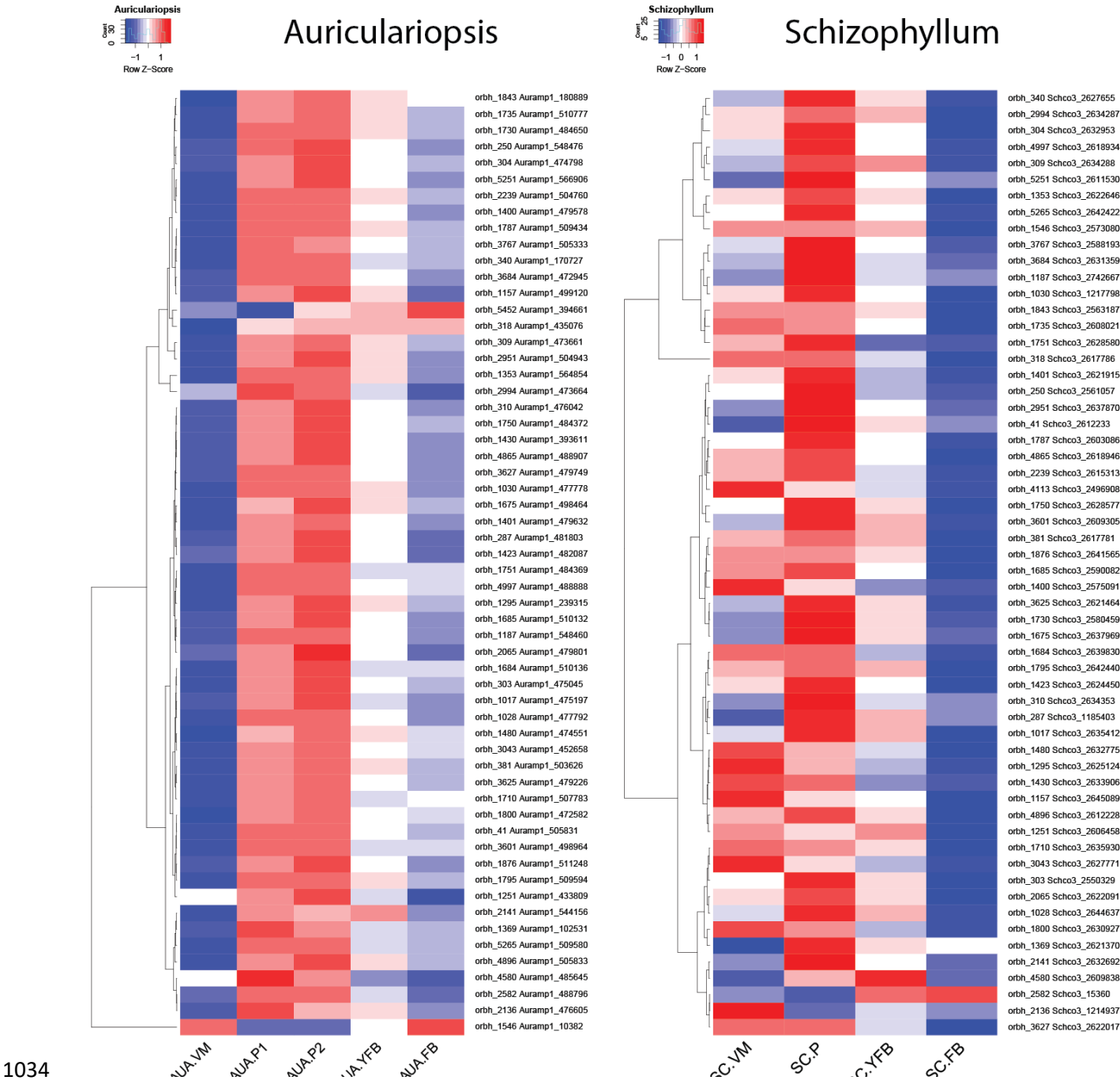

1027

Figure S28: Expression of ribosomal proteins in the nine species. Abbreviations as follows: 'VM' vegetative mycelium; 'P1' stage 1 primordium; 'P3' stage3 primordium; 'YFB' young fruiting body, 'FB' fruiting body; 'H' cap (entire); 'C' cap trama (only the inner part, without Lamellae, or skin); 'L' lamellae; 'S' stipe; 'V' cuticle; 'D' dedifferentiated tissue of cap 'A' annulus. For stage details see Table S10.

1033

1034

1036   **Figure S29**: Species tree with the number of relative gene ages (red). For deciphering species IDs see Table S11.

1037

1038 **Captions for Table S1 to S12**

1039 **Table S1. (separate file).** Mapping statistics for *Pleurotus ostreatus* and *Pterula gracilis*

1040 **Table S2. (separate file).** Metadata of the 138 FBDR hotspots

1041 **Table S3. (separate file).** Mapped reads to the parental reference genomes and distribution of reads according to parental
1042 assignment

1043 **Table S4. (separate file).** Averaged AS ratio among replicates of 4943 genes, which showed imbalance at least one
1044 sample.

1045 **Table S5. (separate file).** InterPro domain enrichment analysis for genes with Allele Specific Expression (S2 and S4)
1046 among all IPR annotated genes.

1047 **Table S6 (separate file).** Gene Ontology enrichment for genes with Allele Specific Expression.

1048 **Table S7 (separate file).** Detected potential RNA editing sites

1049 **Table S8 (separate file).** Conserved 1:1 ortholog groups.

1050 **Table S9 (separate file).** Putative defense related ortholog groups.

1051 **Table S10 (separate file).** Species which were used for transcriptomic analysis

1052 **Table S11 (separate file).** Species, which were used for the species tree estimation and phylostratigraphy

1053 **Table S12 (separate file).** Gene Ontology enrichment for CM-specific and Shared orthologs